Summer 2016

Mixing dynamics in municipal water storage tanks

Pramod Narayan Bangalore

Department:

MIXING DYNAMICS IN MUNICIPAL WATER STORAGE TANKS

by

PRAMOD NARAYAN BANGALORE

A THESIS

Presented to the Graduate Faculty of the

MISSOURI UNIVERSITY OF SCIENCE AND TECHNOLOGY

In Partial Fulfillment of the Requirements for the Degree

MASTER OF SCIENCE

in

MECHANICAL ENGINEERING

2016

Approved by

Dr. Kelly Homan, Advisor
Dr. Kakkattukuzhy M. Isaac
Dr. Yanzhi Zhang

ABSTRACT

The purpose of this study is to investigate the effects of different control variables on mixing in municipal water storage tanks using Computational Fluid Dynamics(CFD) solutions with ANSYS FLUENT for isothermal, positively and negatively buoyant inflow conditions. Poor mixing of old water and new water leads to dead zone formation, which when introduced in the distribution system can cause major water quality issues. Data for this study was generated using Multiphase CFD flow modeling technique using Volume of Fluid (VOF) approach with species transport. The vessel was considered to be mixed when Coefficient of Variation (COV) dropped below 0.10.

Results of isothermal flows show that for unity aspect ratio vessels, increase in momentum to eight times the baseline value cause a reduction of 67.7% reduction in the COV maximum value. With sufficient momentum, even tall vessels were found to mix. Positively buoyant inflow conditions are therefore uniformly desirable for mixing. Buoyancy was found to be a more dominant source of mixing than momentum. Negatively buoyant solutions indicate a very high dependance of mixing on buoyancy and hence are found to be undesirable to achieve uniform mixing. Results show that with increase in negative buoyancy effects, even at high velocities, the vessel was unmixed. At lower jet momentum and higher buoyancy effects, deadzones occupied more than 50% of the tank volume. Higher aspect ratio vessels are especially prone to stratification and poor mixing was generally observed with negatively buoyant inflows. Overall results reveal that some tanks which did not get mixed during the filling process got mixed in the hold cycle (inflow shutoff). A sufficient settling time is necessary after the fill duration to achieve the highest possible degree of mixing for a tank with a given momentum, aspect ratio and buoyancy.

ACKNOWLEDGMENTS

My research journey over the past two years has been an enriching experience, one which helped me to become a better person, both personally and technically. This research work would not have been possible without the support and help from so many people.

I would like to express my heartfelt gratitude to Dr. K.O. Homan, who has not only been my adviser, but also has been my mentor and guiding force throughout this journey. His support and guidance was pivotal to the completion of my thesis and without whom, this work would not have been possible. I consider myself to be extremely fortunate to work under him. He has always been very understanding towards me and I truly appreciate his sincere concern for my well being. I have also truly enjoyed all the personal discussions that I had with him. Words are insufficient to fully exress my thanks to him.

I am also thankful to the esteemed members of my committee, Dr. K.M. Isaac and Dr. Yanzhi Zhang for their support and encouragement towards this work. The courses that I took under Dr. Isaac really helped my understanding of Fluid dynamics. Dr. Zhang's course was very helpful to me to gain knowledge about application of numerical methods.

I want to thank Mohammed Al-Yasiri for his constant motivation and help. I also thank my lab friend Ganesh Ravi Shanker for his help and encouragement.

I would like to thank my parents S Lakshminarayan and Bharathi Narayan and my brother, Rohit Narayan for their continous support and encouragement over the last two years. I would also like to express my gratitude to my extended family in US for all their help and support.

Lastly, I want to sincerely thank my spiritual guru Sri. Dr. K.S. Narayanacharya who has been a tremendous influence in my life.

TABLE OF CONTENTS

Page

LIST OF ILLUSTRATIONS

Figure Page

LIST OF TABLES

NOMENCLATURE

Roman

$\vec{g}$	Acceleration due to gravity, m/s^2
$\hat{D}$	Tank width, m
$\hat{H}$	Tank height, m
h	Perpendicular distance between the jet and the wall parallel to it, m
k	Turbulent Kinetic Energy, m^2/s^2
Q	Volumetric Flow rate, m^3/s
$\hat{t}$	Time, s
$\hat{u}$	Dimensional velocity
t	Dimensionless Flowtime
$\hat{u}$	dimensional velocity, m/s

Greek

$\hat{\psi}$	Dimensional Streamfunction
$\hat{\varepsilon}$	Dimensional kinetic energy, kJ/s
μ	Dynamic Viscosity, kg/ms
ψ	Dimensionless Streamfunction

ρ Density, kg/m^3

ε_o Dimensionless dissipation with fixed scale

ρ_{a} Density of Air

ϵ Turbulent Kinetic Energy dissipation rate, m^2/s^3

Subscripts

ρ_∞ Fluid density at a reference state, kg/m^3

ρ_f Density of feed water, kg/m^3

ρ_t Initial density of tank water, kg/m^3

$\vec{J}_i$ turbulent thermal conductivity

A_c Cross sectional area, m^2

b_o Half inlet jet width, m

$\hat{d}_{j,o}$ Baseline jet diameter, m

E_k Dimensionless Instantaneous Kinetic Energy

E_k Dimensionless kinetic energy

E'_k Dimensionless Instantaneous Kinetic Energy along a horizontal plane

$E_{k,o}$ Dimensionless Kinetic energy with fixed scale

Fr_j Jet Froude number

$\hat{H}_o$ Initial Free surface height, m

k_t diffusion flux of species j

$\hat{L}_s$ Length scale, m

l_m Length scale for a plane jet, m

$\hat{t}_s$ Time scale, s

T_∞ Operating or reference temperature, K

T_i Inlet jet temperature, K

T_l Local fluid temperature, K

T_o Tank fluid temperature, K

$\hat{U}_j$ Jet velocity, m/s

$\hat{u}_s$ Velocity scale, m/s

$\hat{u}_{j,o}$ Baseline jet velocity, m/s

u_m Velocity along the centerline axis, m/s

U_o Uniform Velocity in the jet, m/s

u_j Jet velocity

1. INTRODUCTION

Water Storage tanks can be categorized into ground storage and elevated storage tanks. Ground storage tanks can be below the ground or can be constructed above grade in the distribution systems. These reservoirs or tanks can be either covered or uncovered. There are two types of elevated storage tanks: namely, elevated steel tanks and standpipes. Standpipes are tall cyclindrical tanks with a high height to depth ratio. They are mainly used for emergency storage and for pressure equalization in the distribution system. Only a portion of the storage volume in a standpipe that is above the level required to maintain system pressure is considered to be useful storage. Most standpipes have a common inlet and outlet and generally operates on a fill draw cycle. Elevated storage tanks have elliptical or spherical shape and are usually constructed on a single pedestral. These tanks usually have better mixing characteristics than standpipes.

Water utilities are faced with challenges with respect to maintaining water quality that conforms to increasingly strict standards set by EPA. Excessive water age is perhaps the most important factor that impacts water quality. Standpipes are more susceptible to stratification because of the high height to depth ratio [Grayman and Rossman, 2004, Kennedy et al., 1993]. Martel et al. [2002] recommends allowing the water level to fluctuate more widely than the targeted withdrawal of 60% of volume in one day and then refilling it the next day. They indicate that that even withdrawal of 20% of the volume in a standpipe and an immediate refill it could leave a major volume of storage stagnant or poorly mixed for long periods of time.

In the first part of this research work, CFD simulations of filling cycle in water storage tanks for non-buoyant flows have been performed for tanks with different aspect

ratios, jet velocities and jet diameters to cover a wide range of water storage tanks in operation today. Different parameters are utilitized to characterize the level of mixing in the tank and recommendations are made to achieve optimal mixing for a given tank. In the second part of the research, CFD simulatons for buoyant flows have been performed to cover a wide range of temperature differences chosen according to seasonal changes.

2. LITERATURE REVIEW

Water storage tanks are utilized for storage, equalizing water demands and for maintaining pressure in distribution systems. There are many sources that can cause water quality problems. Quality issues in water storage facilities can be classified into microbiological, chemical or physical. Poor practices in water distribution system have the potential to have devastating consequences on public health. Some examples of how storage facilities have been the main cause of disease outbreaks have been discussed in the white paper by EPA AWWA [2002]. A detailed discussion of the water quality issues that have direct consequences on public health have also been discussed in the paper. With over 400, 000 finished water storage facilities in USA, water quality problems continue to affect many utilities. Martel et al. [2002] gives a description of the problems causing water quality issues and also provides a stepwise guide to mitigate the water quality problems.

Many experimental studies have been conducted on water storage tanks [Boulos et al., 1996, Grayman and Clark, 1993, Grayman et al., 2000, Kennedy et al., 1993, Mahmood, 2005, Rossman and Grayman, 1999] to investigate water quality issues with particular emphasis on detention times. Grayman and Clark [1993] developed a 3 compartment hydraulic storage tank model based on hydrodynamic and statistical models to predict the variations in tracer concentration over time and also for modeling the age of water. Good agreement was observed between the predicted and actual results based on field sampling data obtained from two tanks in the Cherry Hills- Brushy plains network. Boulos et al. [1996] conducted extensive sampling of a reservoir with emphasis on understanding dynamics of hydraulic mixing and free chlorine residual concentration variation in the reservoir. The analysis of flouride concentration during the startup period of flouride feed were higher

than the theoretically predicted concentrations using the continuously stirred tank reactor (CSTR) model that indicated the presence of short circuiting between reservoir inlet and outlet. The CSTR model represents a tank under fill/draw cycle and assumes that the contents of the tank are instantaneously mixed resulting in a completely mixed tank with constant concentration at any time. The author recommended regular field sampling for effective management of the distribution systems. Kennedy et al. [1993] studied the influent and effluent chlorine concentrations, temperature and water levels for three different tanks (standpipe, ground storage tank and an elevated tank) due to contrasting geometries. The study was conducted to determine the effect of tank geometry and volumetric change on mixing characteristics and water quality. No effect of inlet/outlet location was investigated during this work. It was found that while tank geometry had little effect on mixing behavior, tank operation was found to have a significant impact on mixing. The author recommended that volumetric change between fill and draw cycles should be maximized for effective mixing and elevated tanks should be used for store water in distribution systems. Standpipes were found to be the least desirable tank design with respect to effluent water quality. Rossman and Grayman [1999] conducted experiments on scale model cyclindrical tanks under fill draw conditions with seven conductivity probes placed in the tanks to measure the salinity of salt used as a tracer. A statistic known as Coefficient of Variation (COV) based on the mean and standard deviation of the conductivities measured along the probe locations was defined for measuring mixing time. Thirty experiments were conducted with no buoyancy effects and the Okita formula [Okita and Oyama, 1963] for mixing was modified based on the experimental results. Good agreement was found with the application of this formula to a full sized reservoir. The results are applicable, however, only for cyclindrical tanks with aspect ratios (H/D) less than 1.0. Empirical relationships were derived for minimum volume required for good mixing and for avoiding stratification in tanks. Tian and

Roberts [2008a] used 3D laser induced fluorescence (3DLIF) technique for measurements of the tracer concentrations of the entire tank. Experiments were conducted on a variety of tank geometries with different inlet orientations. This is perhaps the most detailed study of experiments conducted in a laboratory on mixing. Tian and Roberts [2008b] included the effects of buoyancy in the experiments.

CFD has become widely used in the water industry as an evaluation tool of jet mixing in storage tanks. Hoffman [1996] used commercial CFD software package FLUENT to analyze mixing of an inhibitor into an existing storage tank with the help of jets. Only one half of the domain was modeled and the simulation results were not compared with experimental results. Jayanti [2001] used the commercial code CFX to study the hydrodynamics of mixing in cyclindrical tank with a single jet inlet. No volume change in the tank was considered with the use of a large outlet provided at the top from where fluid was taken out at a flowrate equivalent to the inlet flow rate. A steady state velocity field was established first and then tracer was introduced in to the tank. The resulting transients were monitored to characterize the degree of mixing. The author investigated the effects of vessel shape, injection period, length of the jet, vessel height and calculation scheme on mixing. The conclusion was that the optimal shape for a vessel to achieve good mixing is dependent on the parameters specific to the particular problem under consideration. A key factor for reducing the mixing time was the elimination of deadzones in the vessel. Another interesting observation by the author is that the mixing time is not determined uniquely by consistently applying the 95% homogeneity criterion and depends on how and where the concentration is measured. Patwardhan [2002] computed CFD simulation for jet mixed tanks and validated the CFD results with detailed experimental results. The results showed that there was good agreement between the CFD and experimental results for calculation of mixing time, but the concentration profiles at various locations in the tank tested were

not predicted well. No buoyancy effects were considered and constant volume flow was assumed. Tracer concentration data was captured at four probe locations in the domain. Wasewar and Sarathi [2008] have given an excellent summary of all the expermental correlations of jet mixing in tanks. Different parameters investigated include jet velocity, jet angle, location of jet and aspect ratio. Marek [2007] presented the results of 3D URANS-simulations of mixing processes in storage tanks. The numerical results were validated by comparison with experimental results. Mahmood [2005] performed CFD simulations for different storage tank geometries (standpipes, ground tanks and elevated tanks) with and without the inclusion of temperature difference between inlet and tank. The CFD results were validated based on field measurements of temperature variation and chlorine residuals. Limiter information regarding details of CFD simulation such as boundary conditions, constant or variable volume were provided.

A limitation in the majority of the experimental studies with the exception of Tian and Roberts [2008a,b] is that only a limited number of sampling points were used for measurement of data and its subsequent analysis. This reveals only very limited insight into the complex tracer concentration, velocity flow fields and deadzones formed in the tank, each of which siginificantly impacts the water quality. Also the applicability of different mixing time correlations proposed from experimental data is limited over a wide range of tanks because of its dependence on experimental constants or difference in experimental protocols or not being representive of the actual water storage tank operation where there is an increase in water level.

Although CFD has been used in the past to study the mixing patterns in storage tanks, there are some shortfalls that have not been addressed. Almost in all of the CFD simulations, a constant volume has been asssumed in the simulations i.e whatever mass inventory is put in through the inlet is being taken out through the outlet. This is not representative of the

reality where the flow field is unsteady because of the rise in water level during the fill cycle. Published CFD simulations have not taken this into account. Also the simulations have not been performed for the complete fill cycle. Another important gap in the existing work is that only a limited number of probes are defined in the domain to capture tracer concentration variation which is used for characterizing the level of mixing. This does not take into account any dead zones formed and hence can provide a misleading picture about level of mixing. Also most of the geometries simulated in the literature have an aspect ratio of less than one. Higher aspect ratio tank simulations are very limited. Most of the CFD simulations on water storage tanks in literature do not consider the temperature difference between the inlet and the tank. The buoyancy forces (positive and negative buoyancy) created due to density differenes is found to significantly impact mixing as reported by [Grayman and Rossman, 2004, Kennedy et al., 1993, Tian and Roberts, 2008b]. Even a temperature difference of 1 °C has been found to impact mixing as observed by these authors in their experimental work.

The objective of the present work is to address some of the deficiences in the previous CFD work. Simulations are carried out for tanks with aspect ratios of 1.25, 2.4 and 5 to understand the impact of higher aspect ratio on mixing. Multiphase phase modeling using the Volume of Fluid approach has been used for tracking the free surface between water and air and a time dependent solution is computed for all the cases. Assuming the volumetric flow rate to be constant, a number of cases have been run with different jet velocities and diameter to understand the impact of momentum on mixing. Also buoyancy effects due to temperature differences have also been taken into account and a number of cases have been run with different temperatures to analyze the impact of positive and negative buoyancy on mixing.

3. ISOTHERMAL FLOW SIMULATIONS

The design and operation of water storage tanks in distribution systems play a significant role in the quality of water being supplied to consumers from utilities. Some of the significant factors that affect the water quality include the aspect ratio of tanks, location of the inlet, width of the tank, volume change during the filling process, duration of the filling cycle, inlet flowrate etc. A numerical study of the mixing patterns that are setup in the filling process has been made in this study and also to identify the control variables that affect the water quality through mixing.

Simulation of Isothermal Filling processes is a first step in this work as it helps to generate results for baseline jet behavior. The baseline results have been analyzed to understand the mixing processes and are used for comparison with non isothermal solutions in the subsequent chapter.For the Isothermal simulations, it is assumed that there is no temperature difference between the jet inlet and the tank. Hence buoyancy effects are not considered and constant density is used for the water and the air that is displaced during the filling process. Results are computed for a number of cases identified by keeping the volumetric flow rate constant and changing the inlet jet diameter and the aspect ratio of the tanks.

As the name suggests, multiphase flow is one which contains more than one phase. The phases can be gas, solid and liquid or it can also be a combination of phases. Multiphase flows can be classified into four categories: gas-liquid or liquid-liquid flows; gas-solid flows; liquid-solid flow; and three phase flows. The Multiphase Flow modeling technique using the Volume of Fluid approach is used for tracking of the free surface of water as the volume changes with the progression of the filling cycle. Species transport was utilized to study

and visualize the level of mixing of old water with the incoming fresh water and to identify zones of stratification. Different Parameters such as Coefficient of Variation, Kinetic Energy, Tracer concentration, Jet behavior etc. are utilized to characterize the flowfield and the level of mixing in the vessel and make recommendations to achieve uniform mixing inside the tank. As the water enters the tank, jet flow occurs and the ambient water get entrained into the jet thus creating entrainment zones. Mixing in the water storage tank is accomplished through the development of a turbulent jet. Mixing a fluid requires a source on energy and this source is provided through the inflow.

3.1. PROBLEM FORMULATION

The commercial CFD software package ANSYS Fluent was used for the simulations. A schematic of the geometry used for the CFD simulations Figure 3.1. The domain of interest is a two dimensional rectangular tank with a dimensional width and height of $\hat{D}$ and $\hat{H}$ respectively. The dimensional inlet pipe length is chosen to be equal to twice the dimensional jet diameter $\hat{d_{\mathrm{j}}}$. In this work, although the domain is two dimensional, from convention, the inlet width is referred to as jet diameter. The position of the initial free surface height is $\hat{H}_{\mathrm{o}}$ whose position is a variable that changes during the filling process. During the filling process, water enters the vessel through the inlet with a uniform velocity $\hat{U}_{\mathrm{j}}$ m/s and air is pushed out of the tank through the outlet vent at a volumetric flow rate which matches the water entering through the inlet, so as to satisfy conservation of mass.

In ANSYS Fluent, the governing differential equations are solved for the conservation of mass and momentum and any applicable scalar equations such as turbulence and species transport. Fluent uses a control-volume-based technique that involves the division of the geometry into discrete control volumes using a computational grid and integration of the governing equations on the individual control volumes to construct algebraic equations

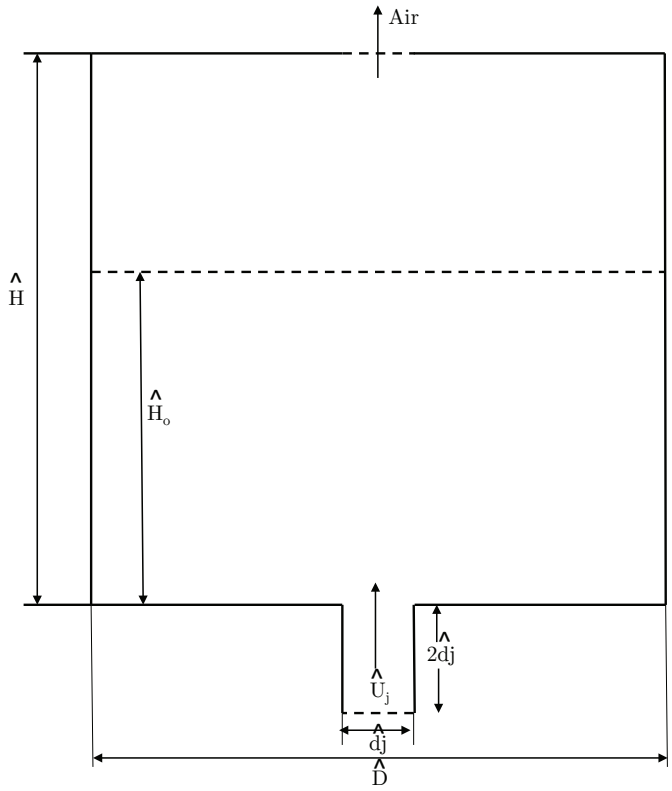

Figure 3.1. Problem Schematic with a common inlet/outlet. Water enters the tank through the common inlet and causes a change in the position in the free surface which signifies an increase in volume.

for the discrete dependent variables such as velocities, pressures, temperatures etc. The discretized equations are linearized and the solutions of the linear equations are used to update the values of the dependent variables ANSYS [2013a]. In a CFD solution, the flow variables are solved only at each cell centers. The values at other locations are obtained through interpolation of the face values calculated at the cell centers.

3.1.1. Fundamental Governing Equations. The governing equations solved for a Multiphase Flow CFD simulation using Volume of Fluid (VOF) method along with species transport are continuity, momentum, species transport and volume fraction equations. In

addition to these equations, turbulence model is used for calculation of turbulent quantities in case of turbulent flows. The continuity equation for an incompressible fluid in vector form is given by

$$\nabla \cdot \hat{\mathbf{u}} = 0 \tag{3.1}$$

where $\vec{u}$ is the velocity vector

The two dimensional momentum equation for a newtonian fluid with constant viscosity and density in vector form is given by

$$\rho \frac{D\hat{\mathbf{u}}}{Dt} = -\nabla \hat{p} + \mu \nabla^2 \hat{u} \tag{3.2}$$

where $\hat{p}$ is dimensional static pressure, ρ is the dimensional density and $\hat{u}$ is the dimensional velocity.

The dimensional x and y components of the Navier - Stokes equation of motion assuming no body force are given by

$$\rho\left(\frac{\partial \hat{u}}{\partial \hat{t}} + \hat{u}\frac{\partial \hat{u}}{\partial \hat{x}} + \hat{v}\frac{\partial \hat{u}}{\partial \hat{y}}\right) = -\frac{\partial \hat{p}}{\partial \hat{x}} + \mu\left(\frac{\partial^2 \hat{u}}{\partial \hat{x}^2} + \frac{\partial^2 \hat{u}}{\partial \hat{y}^2}\right) \tag{3.3}$$

$$\rho\left(\frac{\partial \hat{v}}{\partial \hat{t}} + \hat{u}\frac{\partial \hat{v}}{\partial \hat{x}} + \hat{v}\frac{\partial \hat{v}}{\partial \hat{y}}\right) = -\frac{\partial \hat{p}}{\partial \hat{y}} + \mu\left(\frac{\partial^2 \hat{v}}{\partial \hat{x}^2} + \frac{\partial^2 \hat{v}}{\partial \hat{y}^2}\right) \tag{3.4}$$

Volume of Fluid (VOF) is one of the methods using the Euler-Euler approaches in Multiphase modeling. In an Euler-Euler approach, the volume fractions of different phases are assumed to be continuous functions of space and time and their sum is always equal to one. VOF is a surface tracking technique used for tracking of the interface between the two phases which are immiscible. This approach is especially suitable in our case as there is no interaction between water and air and it represents a case of stratified flow in which

regions of water and air are well defined at the start and throughout the fill cycle.The Air phase is modeled because the VOF approach does not allow for regions where no fluid is present and also to make the simulation more representative of the actual tank operation. The properties and variables in any given cell are represented completely by either one of the unique phases or by a mixture of one or more phases. The field variables and properties are shared by different phases and represent the volume-averaged values with the condition that the volume fraction of each of the phases is known at each cell location. VOF is most suitable for stratified or free surface flows where tracking of the interface between two immiscible fluids is required. This approach tracks the volume fraction of each of the fluids defined through the domain. A modified version of the High Resolution Interface Capturing (HRIC) scheme is used to capture the interface between water and air. Modified HRIC scheme consists of a nonlinear combination of upwind and downward differencing while providing improved accuracy over the QUICK and second order schemes and being less computationally expensive ANSYS [2013a].

The interface tracking is done by the solution of the continuity equation for the volume fraction of the secondary phase which in this case is defined to be air. The volume fraction equation for the q^{th} phase assuming no mass transfer between phases and no mass source is given by

$$\frac{1}{\rho_{\text{q}}}\left[\frac{\partial\left(\alpha_{\text{q}}\rho_{\text{q}}\right)}{\partial t}+\nabla\cdot\left(\alpha_{\text{q}}\rho_{\text{q}}\vec{v_{\text{q}}}\right)\right]=0 \tag{3.5}$$

where α_{q} is the volume fraction of q^{th} phase and ρ_{q} is the density of q^{th} phase.

The volume fraction equation was solved using implicit time discretization in the present study. The volume fraction equation is solved only for the secondary phase with the volume fraction of the primary phase computed by the following equation.

$$\sum_{q=1}^{n} \alpha_{\mathrm{q}} = 1 \tag{3.6}$$

A Species Transport equation is used to define a tracer which has the same properties as that of water. The tracer corresponds to a marker for old water present in the tank before the start of the filling cycle. During the course of the filling cycle, the concentration profiles of the tracer are studied to understand the mixing patterns in the tank and also to identify dead zones in the tank, if any, where there is no mixing observed. The tracer concentration predicted for the entire domain is used to calculate a parameter called the Coefficient of Variation(COV) which is used to characterize the level of mixing [Rossman and Grayman, 1999].ANSYS Fluent predicts for each phase,the local mass fraction of each species defined through the solution of a convection-diffusion equation for the species ANSYS [2013a].

In the present work, it is assumed that there is no chemical reaction between the species and that there is no creation by addition either from the dispersed phase or from any user defined sources. In addition, it is also assumed that there is no mass transfer between species from phase 1 to phase 2. The tracer concentration of each species when applied to a multiphase mixture is calculated by ANSYS [2013a]

$$\frac{\partial \left(\alpha^{\mathrm{q}} \rho^{\mathrm{q}} Y_i^q\right)}{\partial t} + \nabla \cdot \left(\alpha^{\mathrm{q}} \rho^{\mathrm{q}} \vec{v^q} Y_i^q\right) = -\nabla \cdot \vec{J_i^q} \alpha^{\mathrm{q}} \tag{3.7}$$

where α^q is the volume fraction for phase q, $\vec{J_i^q}$ is the diffusion flux of i^{th} species in the q^{th} phase and Y_i^q is the local mass fraction of i^{th} species in the q^{th} phase.

3.1.2. Simulation Setup and Save Strategy. All the simulations corresponds to a Reynolds number Re equal to an order of magnitude 10^5. So the flow is highly turbulent. As it not feasible to resolve the turbulent scales using the direct numerical simulation(DNlS) because of computing resources requirements, we have elected to solve the Reynolds Av-

eraged Navier Stokes(RANS) equations. In the present work, the Realizable $k-\epsilon$ model [Tsan-Hsing Shih, 1994] was used to close the turbulent transport equations. This model solves two additional transport equations viz. turbulent kinetic energy k and dissipation rate ϵ and uses the eddy viscosity approach to model the Reynolds Stresses. Standard wall functions were used for the near wall treatment. For the VOF scheme, the implicit formulation was used to discretize the volume fraction action. Two phases (water and air) are defined in the simulation with water phase containing the mixture of water and tracer.Water was defined to be the primary phase and the secondary phase was modeled as air. No interactions such as surface tension force were included between the phases. A Modified HRIC scheme was selected as the interpolation scheme for the volume fraction equation.

The properties of the tracer were defined to be similar to that of water and no reactions were enabled for the species. The mass diffusivity value is given a value of 10^{-10} m^2/s. ANSYS Fluent uses the constant-dilute-approximation (Fick's law) to model mass diffusion due to concentration gradients. The turbulent diffusion coefficient normally overwhelms the laminar diffusion coefficient, so a constant value for laminar diffusion constant in most cases is acceptable.

The most important field variables data like velocities, turbulence quantities, streamfunction, tracer mass fraction, volume fraction etc were saved for the entire domain every 100 timesteps. These data henceforth will be referred to as low frequency data and were used for calculation of Coefficient of Variation, kinetic energy, streamfunction and for generation of contour plots used in the analysis. To conduct a tracer monitoring study [Grayman et al., 2000] that would help us to study the motion and mixing patterns of the tracer in the tank and to study the variations of velocities along the tank height, it was required to define monitors that would capture the tracer mass fraction, horizontal and vertical velocities at every time step. These data henceforth will be referred to as high frequency data. Several horizontal

line monitors with length equal to the tank width were defined at equally spaced distances along the tank height. Images were saved directly from Fluent and later processed using an open source tool FFMPEG. To judge convergence for this transient problem, the scaled residuals were set to 10^{-4} for the continuity equation and 10^{-5} for the other equations. The under relaxation factors remain unchanged for the majority of the cases.

3.1.3. Boundary and Initial Conditions. The inlet is specified as a velocity inlet with turbulent intensity and hydraulic diameter quantities specified for turbulence. The mass fraction of the tracer is set to zero at the inlet. This means that only fresh water is pumped in through the inlet and no tracer is introduced through the inlet. An outlet vent is provided at the top of tank for the air to escape through during the filling cycle. The walls are specified to be impermeable boundaries with no slip.

The initial conditions for the simulation are as follows. The turbulent kinetic energy k and dissipation rate ϵ for the initial condition were calculated using the empirical relationships provided in the Fluent manual [ANSYS, 2013b]. Also for all the cases run, it was assumed that the tank was initially 60% full and that there was a 30% change in volume during the filling cycle. The reason for choosing a 30% change in volume during the fill cycle is because of the guidelines given by EPA [AWWA, 2002] on daily water turnover rate. Also as an initial condition, tracer has been patched with the water so as to have a uniform distribution of tracer and water for 60% volume of the tank volume before the start of the fill cycle. The initial dimensional free surface height, $\hat{H}_{\mathrm{o}}$, at the start of the filling cycle corresponds to the initial 60% volume. The remaining 40% of the tank volume is patched with air as an initial condition. The simulation was started with a very small timestep size and as the flow developed, the timestep size was increased by an order of magnitude till the fixed timestep size could be used. The fixed timestep size of 0.15 and 0.10 was chosen based on the Courant number calculation in the jet region.

3.1.4. Non Dimensionalization. In this section, the governing equations are non-dimensionalized by selection of scales for velocity, length and time. In addition to choosing the scales, analytical expressions for mean tracer concentration, dimensionless free surface height, kinetic energy and streamfunction are also derived and compared with CFD predicted solution. The velocity, length and time scales are referred to by $\hat{u}_s$, $\hat{L}_s$ and $\hat{t}_s$ respectively.

The velocity scale for non dimensionalization is chosen to be $\hat{U}_j$ so that the velocity limits are always between zero and unity. The length scale for non dimensionalization is chosen to be $\hat{D}$, the width of the tank . The time scale $\hat{t_s}$ for non dimensionalization is taken to be the ratio of volume of the tank to the volumetric flow rate *i.e.* $\hat{V}/\hat{Q}$. The problem with this time scale is that it will be different for different tank aspect ratios. Substituting the volume term, we obtain $\hat{t}_s = ((\hat{D^2} \cdot (\hat{H}/\hat{D}) \cdot \hat{Z})/\hat{Q})$. Assuming that the ratio $(\hat{H}/\hat{D})$ is equal to one, then we would obtained the expression for the time scale as $\hat{t_s} = ((\hat{D}^2\hat{Z})/\hat{Q})$. This time scale is more appropriate since we are changing $(\hat{H}/\hat{D})$ in the simulations while keeping the volumetric flow rate as constant. The term $\hat{t}_s$ represents the time required to fill a volume equal to $\hat{D}^2 \cdot \hat{Z}$ *i.e.* time required to fill a volume corresponding to the volume of unity aspect ratio tanks. Non dimensionalization is done to reduce the number of dependent variables.

Following the selection of the scales for non dimensionalization, we have the following dimensionless quantities,

$$d_j = (\hat{d}_j/\hat{D}) \Rightarrow \text{Jet width to vessel diameter ratio}$$

$$H = (\hat{H}/\hat{D}) \Rightarrow \text{Vessel aspect ratio}$$

$$H_{\mathrm{o}} = (\hat{H}_{\mathrm{o}}/\hat{D}) \Rightarrow \text{Initial free surface height}$$

$$H_{\mathrm{f}} = (\hat{H}_{\mathrm{f}}/\hat{D}) \Rightarrow \text{Final free surface height}$$

$$t = ((\hat{u}_j\hat{d}_j)/\hat{D}^2)\hat{t} \Rightarrow \text{dimensionless Flowtime}$$

$$\psi = (\hat{\psi})/(\rho\hat{u}_j\hat{D}) \Rightarrow \text{dimensionless Streamfunction}$$

Eqns (3.3) and (3.4) show the x and y components of the Navier-Stokes equation for momentum. Since the scales for non dimensionalization are chosen above, Eqn (3.3) can be non-dimensionalized. Substituting the dimensional parameters as a product of the nondimensional parameter and the scale of non-dimensionalization, we get

$$\left(\frac{u_s}{t_s}\frac{\partial u}{\partial t} + \frac{u_s^2}{L_s^2}\left(u\frac{\partial u}{\partial x} + v\frac{\partial u}{\partial y}\right)\right) = \left(\frac{\mu}{\rho}\frac{u_s}{L_s^2}\right)\left(\frac{\partial^2 u}{\partial x^2} + \frac{\partial^2 u}{\partial y^2}\right) \tag{3.8}$$

Rearranging the terms and cancelling the common terms in LHS and RHS, we get

$$\left(\frac{\partial u}{\partial t}\right) + \left(\frac{t_s u_s}{L_s}\left(u\frac{\partial u}{\partial x} + v\frac{\partial u}{\partial y}\right)\right) = \left(\frac{\nu t_s}{L_s^2}\right)\left(\frac{\partial^2 u}{\partial x^2} + \frac{\partial^2 u}{\partial y^2}\right) \tag{3.9}$$

In the above equation, let the terms $\left((t_s u_s)/L_s\right)$ on the LHS be represented by A and $\left((\nu t_s)/L_s^2\right)$ on the RHS be represented by B. Both the terms A and B are dimensionless values. Considering term A, we have

$$\left(\frac{t_s u_s}{L_s}\right) = \left(\frac{\hat{u}_j}{\hat{D}}\frac{\hat{D}^2\hat{Z}}{\hat{u}_j\hat{Z}\hat{d}_j}\right) \tag{3.10}$$

Cancelling the terms, we get

$$\left(\frac{t_s u_s}{L_s}\right) = \frac{1}{d_j} \tag{3.11}$$

where d_j is the dimensionless jet diameter

Considering term B,

$$\left(\frac{\nu t_s}{L_s^2}\right) = \left(\frac{\nu}{\hat{D}^2}\right)\left(\frac{\hat{D}^2 \hat{Z}}{\hat{u}_j \hat{d}_j \hat{Z}}\right) \tag{3.12}$$

This simplifies to

$$\left(\frac{\nu t_s}{L_s^2}\right) = \left(\frac{1}{Re_j}\right) \tag{3.13}$$

Thus, the solution is completely specified by d_j, H_o and Re. Writing the mass balance equation, we have the LHS representing the volume change due to inflow and RHS representing the volume added to the tank for a fill duration of $\Delta\hat{t}_{\mathrm{f}}$,

$$(\hat{H}_f - \hat{H}_o)\hat{D}\hat{Z} = (\hat{U}_j \hat{d}_j)\Delta\hat{t}_f \hat{Z} \tag{3.14}$$

$$\frac{\hat{H}_f}{\hat{D}} - \frac{\hat{H}_o}{\hat{D}} = \left(\frac{\hat{U}_j \hat{d}_j \Delta\hat{t}_f}{\hat{D}^2}\right) \tag{3.15}$$

$$H_f - H_o = (\hat{U}_j \hat{d}_j)\left(\frac{\hat{t}_s \Delta t_f}{\hat{D}^2}\right) \tag{3.16}$$

Substituting for expression for time scale, we get

$$(\Delta t_f) = H_f - H_o \tag{3.17}$$

The theoretical expression for calculating the free surface height is given by,

$$\hat{H}_f = \hat{H}_o + \frac{\hat{Q}\hat{t}}{\hat{A}_c} \tag{3.18}$$

$$\hat{H}_f = \hat{H}_o + (\hat{U}_j \hat{d}_j \hat{t} \hat{Z})/(\hat{D}\hat{Z}) \tag{3.19}$$

Substituting the expression for the time, we get

$$H_f = H_o + t \tag{3.20}$$

Since as an initial condition, the initial volume in the tank is filled with tracer concentration of $\phi = 1$, we have

$$\begin{aligned} \bar{\phi}\hat{H}_f \hat{D}\hat{Z} &= \hat{H}_o \hat{D}\hat{Z} \\ &= \frac{\hat{H}_o}{\hat{H}_f} \\ &= \frac{\hat{H}_o}{\hat{H}_o + \frac{\hat{u}_j \hat{d}_j \hat{t}}{\hat{D}}} \\ &= \frac{1}{(1 + \frac{\hat{u}_j \hat{d}_j \hat{t}}{teD\hat{H}_o})} \\ &= \frac{1}{(1 + \frac{\hat{u}_j \hat{d}_j \hat{t}_s t}{\hat{D}\hat{H}_o})} \end{aligned} \tag{3.21}$$

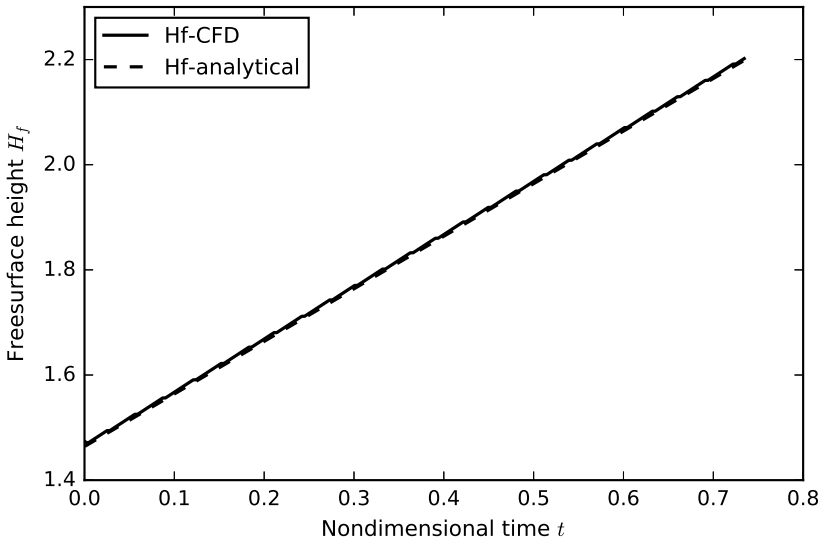

Figure 3.2. Comparison of CFD results with the analytical expression for calculating the free surface height

Substituting for timescale

$$\bar{\phi} = \frac{1}{\left(1 + \frac{\hat{u}_j \hat{d}_j}{\hat{D}\hat{H}_o} \frac{\hat{D}^2}{\hat{u}_j \hat{d}_j} t\right)}$$

$$\bar{\phi} = \frac{1}{1 + \frac{t}{H_o}} \tag{3.22}$$

The above two analytical expressions for calculating the free surface height and average tracer concentration was compared with the CFD results to verify the accuracy of the results. Figures 3.2 and 3.3 shows the comparison between CFD obtained results and the analytical results for calculating the free surface height and average tracer concentration respectively. As seen from the figures, excellent agreement has been observed between theoretical and analytical results.

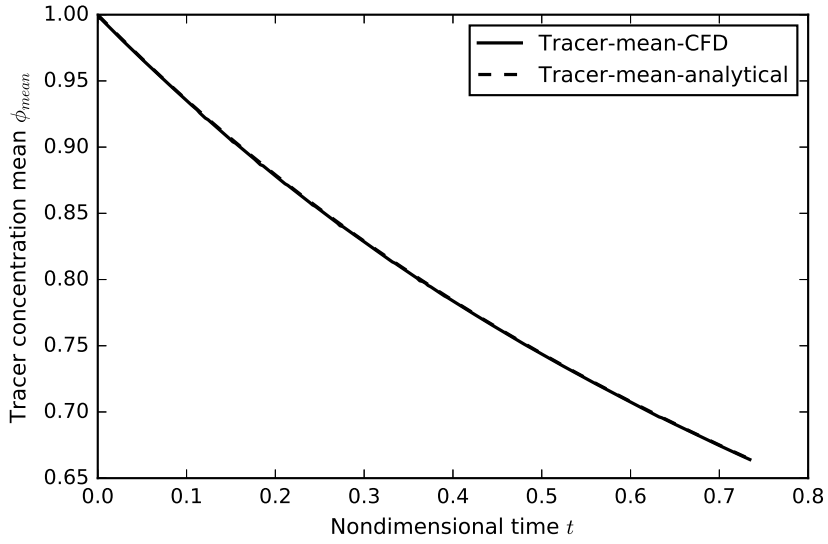

Figure 3.3. Comparison of CFD results with the analytical expression for calculating the average tracer concentration

3.1.5. Kinetic Energy Formulation. Writing the kinetic energy balance for the filling process, we have the following equation

$$\frac{\partial}{\partial t}\int_V \rho((1/2)\hat{u}\cdot\hat{u})\,\mathrm{d}V = \frac{(\dot{m}\hat{u}_j^2)}{2} - \hat{\varepsilon} = \frac{(\rho\dot{V}\hat{u}_j^2)}{2} - \hat{\varepsilon} \tag{3.23}$$

Defining total kinetic energy, $\hat{E}_k$, as

$$\hat{E}_k = \int_V \rho\frac{1}{2}\hat{u}\cdot\hat{u}\,\mathrm{d}V \tag{3.24}$$

Integrating along the volume and non dimensionalizing the terms using the scales defined, we get

$$\frac{\hat{E}_k}{\frac{1}{2}\rho\hat{u}_j^2\hat{D}\hat{Z}} = \int_0^{H_f}\int_0^1 u\cdot u\,\mathrm{d}x\mathrm{d}y$$
$$\frac{\hat{E}_k}{\frac{1}{2}\rho\hat{u}_j^2\hat{D}^2\hat{Z}} = E_k$$
$$\hat{E}_k = E_k\frac{\rho}{2}\hat{u}_j^2\hat{D}\hat{Z}^2 \tag{3.25}$$

Substituting the expression for $\hat{E}_k$ back in the energy balance, we get

$$\frac{\partial}{\partial t}(E_k\frac{1}{2}\rho\hat{u}_j^2\hat{D}\hat{Z}) = \frac{\rho}{2}V^{\bullet}\hat{u}_j^2 - \hat{\varepsilon}$$
$$\frac{((\rho\hat{u}_j^2\hat{D}^2\hat{Z}))}{(2\hat{t}_s)}\frac{\partial}{\partial t}E_k = \frac{\rho}{2}V^{\bullet}\hat{u}_j^2 - \hat{\varepsilon}$$
$$\frac{\partial E_k}{\partial t} = \frac{(\rho 2V^{\bullet}\hat{u}_j^2 2\hat{t}_s)}{(2\rho\hat{u}_j^2\hat{D}^2\hat{Z})} - \frac{(2\hat{\varepsilon})}{(\rho\hat{u}_j^2\hat{D}^2\hat{Z})} \tag{3.26}$$

Substituting for timescale

$$\frac{\partial E_k}{\partial t} = 1 - \frac{\varepsilon}{(1/2\rho\hat{u}_j^2V^{\bullet})} \tag{3.27}$$
$$\frac{\partial E_k}{\partial t} = 1 - \frac{\varepsilon}{(1/2\rho\hat{u}_j^2\hat{u}_j\hat{d}_j)}$$

Thus, for the filling cycle

$$\frac{\partial E_k}{\partial t} = 1 - \varepsilon \tag{3.28}$$

At the point of inflow shutoff

$$\frac{\partial E_k}{\partial t} = -\varepsilon \tag{3.29}$$

For all the simulations carried out, the inlet flow rate is assumed to be constant and variations in jet velocities is obtained by changing the jet diameter. Hence $\hat{u}_{j,o}\hat{d}_{j,o} = \hat{u}_j\hat{d}_j$, *i.e.* $\hat{u}_j = \hat{u}_{j,o}\hat{d}_{j,o}/\hat{d}_j$. The previous formulation of kinetic energy used a sliding scale i.e it was proportional to the jet velocity at the momentum of the specific case being studied. An alternative fixed scale is formulated for kinetic energy that is useful for comparison of kinetic energy between cases with different jet velocities. The Kinetic energy for cases with different jet velocities is scaled according to the baseline jet velocity. Since the volumetric flowrate is constant, we have

$$\begin{aligned} \hat{u}_j &= \hat{u}_{j,o}\frac{d_{j,o}}{d_j} \\ \hat{u}_j^2 &= \hat{u}_{j,o}^2\left(\frac{d_{j,o}}{d_j}\right)^2 \end{aligned} \tag{3.30}$$

Substituting this velocity in the kinetic energy formulation, we have

$$E_k = \frac{\hat{E}_k}{\frac{\rho}{2}\hat{u}_{j,o}^2\hat{D}^2\hat{Z}} \cdot \left(\frac{d_{j,o}}{d_j}\right)^2$$

from the definition of dimensionless kinetic energy

$$E_k = E_{k,o} \cdot \left(\frac{d_{j,o}}{d_j}\right)^2 \tag{3.31}$$

$$E_{k,o} = E_k \cdot \left(\frac{d_{j,o}}{d_j}\right)^2 \tag{3.32}$$

Similarly for dissipation

$$\varepsilon_o = \varepsilon\left(\frac{d_{j,o}}{d_j}\right)^2 \tag{3.33}$$

Rewriting the kinetic energy balance

$$\frac{\partial E_{k,o}}{\partial t} = (\frac{d_{j,o}}{d_j}\Big)^2 - \varepsilon_o \tag{3.34}$$

The local kinetic energy per unit mass is defined as

$$\hat{e}_k = \frac{1}{2}\hat{u}\cdot\hat{u} \tag{3.35}$$

We note

$$\begin{aligned} \hat{u} &= u(x,y)\hat{i} + v(x,y)\hat{j} \\ \frac{\hat{e}_k}{\frac{1}{2}\hat{u}_j^2} &= \left(\frac{\hat{u}}{\hat{u}_j}\right)\cdot\left(\frac{\hat{u}}{\hat{u}_j}\right) \\ e_k &= \Big(u\cdot u\Big) \end{aligned} \tag{3.36}$$

Integrating along a horizontal plane

$$\hat{E}_k' = \int_0^{\hat{D}}\int_0^{\hat{Z}} \frac{\rho}{2}\Big(\hat{u}\cdot\hat{u}\Big)\,\mathrm{d}\hat{x}\mathrm{d}\hat{z} \tag{3.37}$$

After non-dimensionalization

$$\hat{E}'_k = (\rho \hat{Z} \hat{D}) \int_0^1 \hat{u}_j^2 \Big(\hat{u} \cdot \hat{u} \Big) \, \mathrm{d}x$$
$$\frac{\hat{E}'_k}{\frac{1}{2}(\rho \hat{Z} \hat{D} \hat{u}_j^2)} = \int_0^1 \Big(\hat{u} \cdot \hat{u} \Big) \, \mathrm{d}x \tag{3.38}$$

Instantaneous Kinetic Energy along a horizontal plane

$$E'_k = \int_0^1 \Big(\hat{u} \cdot \hat{u} \Big) \, \mathrm{d}x \tag{3.39}$$

Integration over y axis gives the instantaneous kinetic energy over the domain

$$E_k = \int_0^{H_f} {E_k}' \, \mathrm{d}y \tag{3.40}$$

Average specific kinetic energy for the domain can be defined by

$$e_k = \frac{E_k}{H_f} \tag{3.41}$$

3.1.6. Solution Methodology. ANSYS Fluent version 15.0 was used for performing the simulations. The geometry for the simulation is as shown in Figure 3.1. The two-dimensional precision solver was enabled for all the runs for improved accuracy and reduced round off error. For all the simulations in this work, two phases were defined using the multiphase modeling approach *i.e.* phase 1 corresponding to a mixture of water and tracer and phase 2 corresponding to air. A time dependent solution was computed for all the cases. The justification for doing a time dependent solution is as follows. The domain of interest has a single inlet/outlet from where water is pumped in or pumped out based on

whether it is a fill or draw cycle. Since in the filling process, mass inventory is continuously being added to the tank and there is not outflow, the level of the water goes up. The flow field is highly transient and dependent on the duration of the filling cycle. The recirculation zones formed as the result of the inflow are also time dependent and significantly impact the mixing seen in the results. The pressure based segregated solver scheme was used where the individual governing equations are solved sequentially. In this method, the conservation of mass of the velocity field is achieved by solving a pressure correction equation. The velocity field corrected by the pressure always satisfies the continuity equation ANSYS [2013a]. The Pressure-Implicit with Splitting of Operators (PISO) scheme for the pressure-velocity coupling, part of the $SIMPLE$ family of algorithms [Patankar, 1980] is chosen in the simulation. PISO is based on the higher degree of the approximate relation between the corrections for pressure and velocity. The two corrections it uses are the neighbor correction and skewness correction. PISO is recommended for transient calculations as it allows for increased values of the under relaxation factors without loss of the stability [ANSYS, 2013a]. Second order Upwind scheme of spatial discretization is used for all scalar equations including momentum, turbulent kinetic energy, turbulent dissipation rate and species transport. A bounded second order implicit method was used for temporal discretization. Gradients are used for constructing values of a scalar variable at the cell values and for computing secondary diffusion terms and velocity derivatives. The Least Squares Cell-Based method was used to calculate the gradients to discretize the convection and diffusion terms in the flow conservation equations [ANSYS, 2013a]. The high performance computing facility at Missouri S&T was used almost exclusively for the simulations.

3.1.7. Grid Resolution and CFD Validation. Although ANSYS Fluent code has been validated for different models many times [Das and Basu, 2010], it is critical to validate

the calculation methodology specific to our simulation results to demonstrate the numerical accuracy of the simulation. This would involve comparison of the CFD simulation results with experimental results and/or analytical results pertaining to tank mixing. Unfortunately, there are no experimental results of mixing in tanks available for a one-on-one comparison with CFD results. Wasewar and Sarathi [2008] validated their CFD solutions by comparing the velocity profile of a free turbulent jet computed by CFD with the analytical solution of Davies [1972] and by comparison of CFD mixing times with the experimental results. Jayanti [2001] validated his CFD results by comparing the CFD simulation results of a turbulent jet issuing into an infinite domain with the analytical solution of Schlichting [2000]. In the second step of validation, the CFD mixing times for cylindrical tanks were compared with mixing times calculated by correlations. However, neither of these authors used their actual CFD results for validation of their solution. In the present work, a two step validation approach has been adopted to demonstrate grid convergence and to validate the CFD solution. In the first step, the analytical solution for a plane turbulent free jet reported by Rajaratnam [1976] is compared with the actual CFD solution for two jet velocities. In the next step, the Coefficient of Variation is computed for 3 different grid sizes corresponding to a case where $1/dj$ is equal to 25 with an aspect ratio of 2.40 to demonstrate grid convergence.

3.1.8. Plane Turbulent Free Jet Solution. Rajaratnam [1976] has compared the experimental results on plane turbulent jets reported by different authors and has provided a generalized equation for jet velocity decay along the centerline axis for a plane turbulent free jet. The equation is of the form

$$\frac{u_m}{U_o} = \frac{3.78}{\sqrt{\bar{y}/b_o}} \tag{3.42}$$

where b_o is the half-inlet jet width, U_o is the uniform velocity in the jet and $\bar{y}$ is the centerline axis distance.

The solution for the centerline jet decay obtained from the above equation is compared with CFD cases for two jet velocities with varying aspect ratios. Aspect ratio refers to the ratio of vessel height to the width. Figure 3.4 represents the comparison of the analytical jet solution with the CFD jet solutions obtained for cases with constant jet velocity of 0.944 m/s and aspect ratios equal to 1.25, 2.4 and 5.0 respectively. Strictly the analytical solution is only valid for a plane turbulent jet issuing into an *infinite* domain where as in the CFD computations, the jet is issued into a finite domain bounded by walls as shown in Figure 3.1. It is observed that the velocity profiles calculated from CFD agrees very well with that predicted by the analytical solution. There is a systematic deviation from the theoretical curve observed at axial distances of 60, 100 and 110 jet diameters corresponding to aspect ratios of 1.25, 2.4 and 5 respectively. This appears to be a limitation of the theory as similar deviation is observed in the experimental data for plane turbulent free jets as reported in Rajaratnam [1976]. An even better agreement between the theoretical and the CFD predicted velocity profiles is seen in Figure 3.5 which corresponds to a velocity of 1.888 m/s. Although the CFD solutions involved the jet issuing into a finite domain, there is very good agreement between the theoretical and CFD predicted velocity profiles as seen from the two figures.

3.1.9. Grid Convergence. The Coefficient of Variation is a statistical measure which provides a relative measure of the dispersion within a sample of values. This parameter has been often used in the literature [Rossman and Grayman, 1999, Tian and Roberts, 2008a] to define the mixing time. Mixing time was defined as the time when the COV fell below some critical value usually taken as 0.05. For the present study, COV is defined as the ratio of the standard deviation of the tracer concentration to the mean tracer

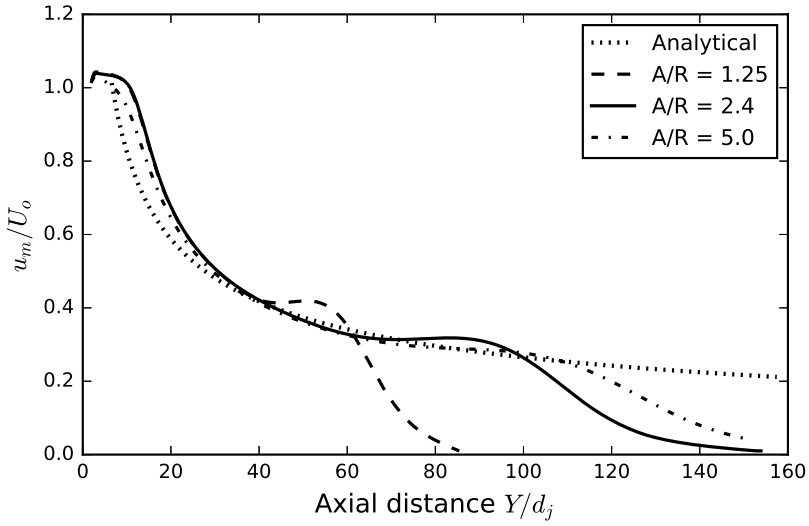

Figure 3.4. Decay of centerline jet velocity along the centerline axis. Here the centerline jet velocity is non dimensionalized by the uniform velocity of the jet and axial distance is scaled by the jet diameter. CFD jet solution is calculated from the case with jet velocity of 0.944 m/s and varying aspect ratio.

concentration. Here tracer concentration is measured for the entire domain of the interest, *i.e.* the concentration of the tracer is captured at all the nodes in the domain during the simulation. For demonstrating grid convergence, COV is computed for three cases with each case corresponding to a different grid size. An overlay showing the variation of COV with the non dimensional time *t* for the three grid sizes is shown in the Figure 3.6. From the figure, it is clear that there is deviation in the COV calculated for the 1e5 nodes grid compared with 2e5 nodes grid and 1.5e5 nodes grid solutions although the deviation is less than 10%. The COV variation profiles for 1.5e5 node grid and 2.0e5 node grid indicates that the CFD solution is independent of the grid size.

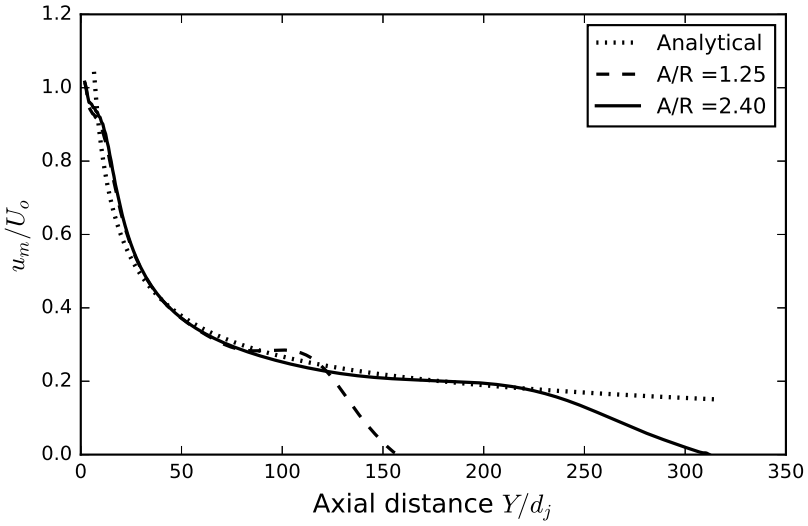

Figure 3.5. Decay of centerline jet velocity along the centerline axis. Here the centerline jet velocity is non dimensionalized by the uniform velocity of the jet and axial distance is scaled by the jet diameter. CFD jet solution is calculated from cases with jet velocity of 1.89 m/s and varying aspect ratio.

3.2. RESULTS AND DISCUSSION

The described CFD model simulates the filling process of a two-dimensional rectangular water storage tank which is initially filled with old water,represented by a tracer, and for which new water is pumped in through the inlet. The tracer is useful to visualize the movement of the new water through the flow domain. Typical inlet flow rates range from 0.1524 ft/s to 0.9144 ft/s and the aspect ratio of the tanks range from 2 to 5. For the isothermal simulations, there was no density difference between the inflow and the tank contents. Different cases was chosen based on the combination of increased momentum given by 2M,4M *and* 8M where M refers to the baseline case momentum and aspect ratios of 1.25, 2.4 and 5 respectively. The jet Reynolds number $\mathrm{Re_j}$ is constant for all the cases and

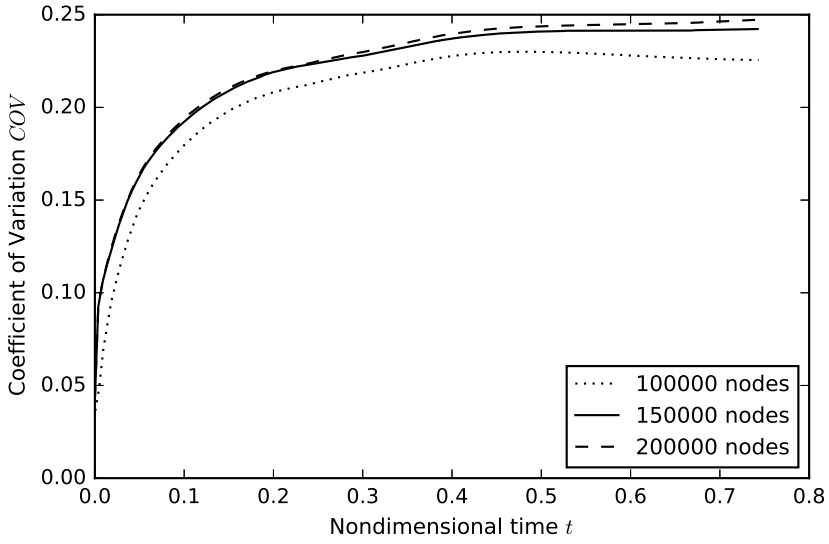

Figure 3.6. Coefficient of Variation computed for the case ($1/d_{\mathrm{j}} = 25$) for three grid sizes

equal to 2.88×10^5 which characterizes the flow to be highly turbulent. Table 3.1 shows the values of the initial free surface height H_o, final free surface height H_f and the duration of filling cycle Δt_f for different combinations of $1/d_j$. The parameters corresponding to $1/d_j = 25$ represents the baseline case. These parameters were chosen based on It is given below,

$$\hat{d}_{j,o} = 1.219\mathrm{m} \tag{3.43}$$

$$\hat{u}_{j,o} = 0.236\mathrm{m/s} \tag{3.44}$$

$$\hat{H} = 73.152\mathrm{m} \tag{3.45}$$

$$\hat{D} = 30.480\mathrm{m} \tag{3.46}$$

3.2.1. Impact of Momentum for Near Unity Aspect Ratio Tanks. In this section, cases corresponding to $1/d_j$ equal to 25, 100 and 200 with an aspect ratio of 1.25 are

Table 3.1. Isothermal Filling Cases with chosen control variables, Reynolds Number Re = constant

$(1/d_j)$	H_o	H_f	Δt_f=H_f-H_o	Aspect Ratio
25	0.83	1.19	0.36	1.25
	1.49	2.23	0.74	2.4
	3.05	4.85	1.80	5.0
50	1.46	2.20	0.73	2.4
100	0.76	1.14	0.38	1.25
	1.46	2.20	0.73	2.4
	3.01	4.77	1.76	5.0
200	0.76	1.13	0.38	1.25
	1.46	2.20	0.74	2.4

analyzed with different parameters. The momentum for these cases are represented by M, 4M and 8M respectively. Here M refers to the momentum at the baseline jet velocity. The impact of momentum on mixing is studied for this baseline comparison. Coefficient of Variation(COV) has been used in the literature [Patwardhan, 2002, Rossman and Grayman, 1999, Tian and Roberts, 2008a] to characterize mixing in the tanks. The tank was considered to be mixed when the COV fell below a certain value which usually was taken to be 0.05 or 0.10. [Patwardhan, 2002, Rossman and Grayman, 1999] placed probes at arbitrary locations in the tank to measure the tracer concentrations and for calculating the mixing time.

In the present study, COV was calculated from the low frequency data for the entire domain to get an accurate measure of mixing as deadzones if any, in the tank affected the COV value. Jayanti [2001] found a significant difference in the mixing time calculations depending on where the mixing criterion was applied *i.e.* whether the criterion was applied for the entire domain or when it was applied for the two conductance probes located at arbitrary positions in the tank. Thus, mixing time is strongly dependent on where and how the tracer concentration is measured.

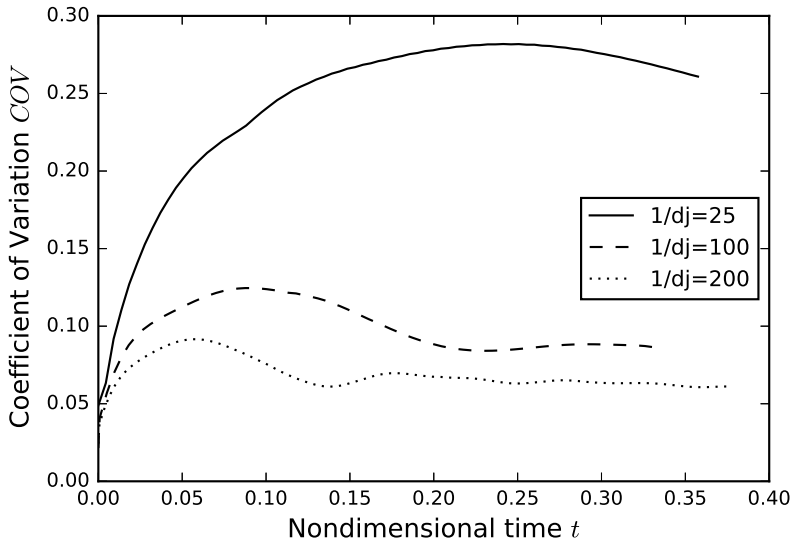

Figure 3.7. Coefficient of Variation *COV* for jet velocities corresponding to 0.236m/s, 0.944m/s and 1.888m/s with aspect ratio of 1.25

The recirculation zones setup in the *unmixed* case do not extend to the bottom of the tank. So a dead zone of high tracer concentration is formed at the bottom of the tank that is responsible for the high COV values. Figure 3.8 shows the tracer concentration contour plot at the end of the fill cycle for the unmixed case. From this figure, it is seen that there is a region of high concentration of tracer at the tank bottom, thus pointing to stratification and poor mixing. In contrast, Figures 3.9 and 3.10 shows the tracer contour plot for cases with momentum 4M and 8M respectively. These tanks are considered to be well mixed where a uniform concentration of tracer is observed in the tank. Hence we can see that, just by increasing the momentum by four times the baseline momentum while preserving a constant volumetric flow rate, optimal mixing can be achieved in the tank with the same aspect ratio. It is to be noted that the impact of increasing the momentum from 4M to 8M is not as high as increasing the momentum from M to 4M.

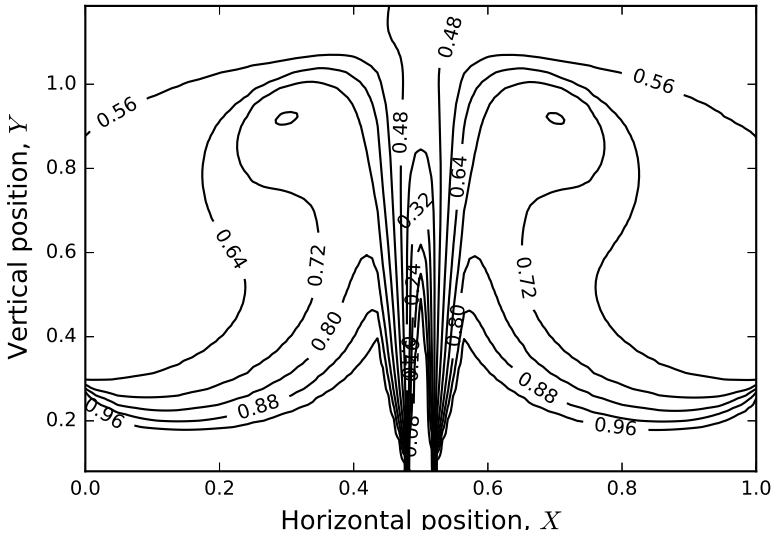

Figure 3.8. Tracer contour line plot at the end of fill cycle for case with $1/d_j = 25$ at baseline jet momentum. The labels indicate the mass fraction of the tracer. The presence of a deadzone region is clearly observed at the tank bottom with region of high tracer concentration.

Figure 3.11 shows the streamline contour plot for the unmixed case. Here it can be seen that the recirculation zone formed by the entrainment layers created by the inlet jet do not extend till the tank bottom.

Tracer studies are conducted to study the motion of the tracer and the mixing patterns. They provide information regarding the level of mixing in the fill process and detention time of the water in the tank [Grayman et al., 2000]. In the present work, tracer concentration data along a number of horizontal surface monitors defined at equal distances along the height of tank are saved during the simulation and analyzed for mixing behavior. The height of each monitor from the tank bottom is equal to Y_im with all the monitors equally spaced. The height of each monitor is non dimensionalized by the tank width D measured in meters. For a tank that is "*well mixed*", we expect the tracer concentration to

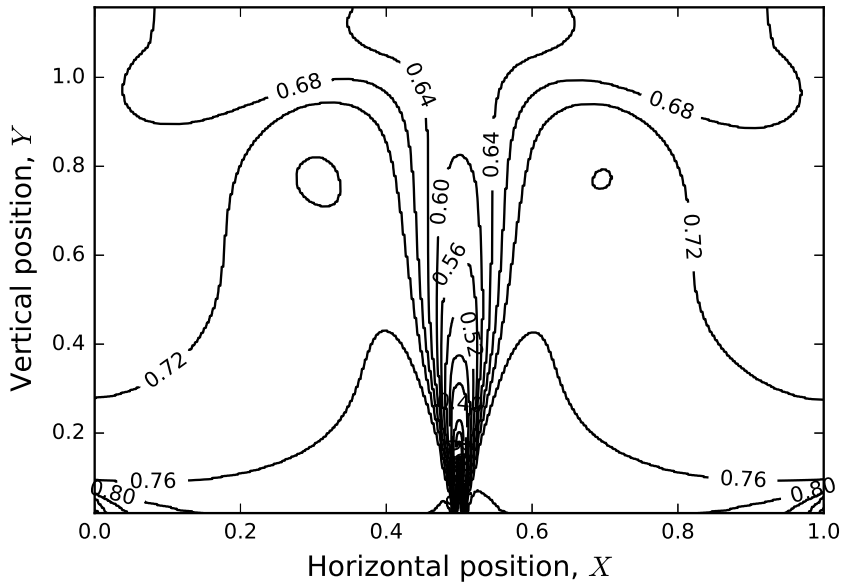

Figure 3.9. Tracer contour line plot at the end of fill cycle for case with $1/d_j = 100$ corresponding to 4M momentum. The labels indicate the mass fraction of the tracer. No presence of any dead zone as the tank is well mixed

converge along all the monitors. Figures 3.12, 3.13 and 3.14 shows the variation of tracer concentration along different monitors for cases where $1/d_j = 25, 100$ *and* 200 respectively. Maximum deviation in the tracer concentration between monitors is observed in Figure 3.12 as expected. No convergence of tracer is observed. The differences in monitors $y = 0.22$, 0.44 and 1.09 point to stratification. In comparison, very good convergence of tracer concentration between monitors is seen in Figures 3.13 and 3.14 consistent with the cases 4M and 8M being well mixed.

Using the kinetic energy formulation with the fixed scale, the instantaneous dimensionless kinetic energy for the three cases is computed and plotted in Figure 3.15 showing the variation with time t. The average of the kinetic energy for the three cases are calculated to be 0.0262, 0.15 and 0.35 respectively. This shows that for the tank to be mixed in the

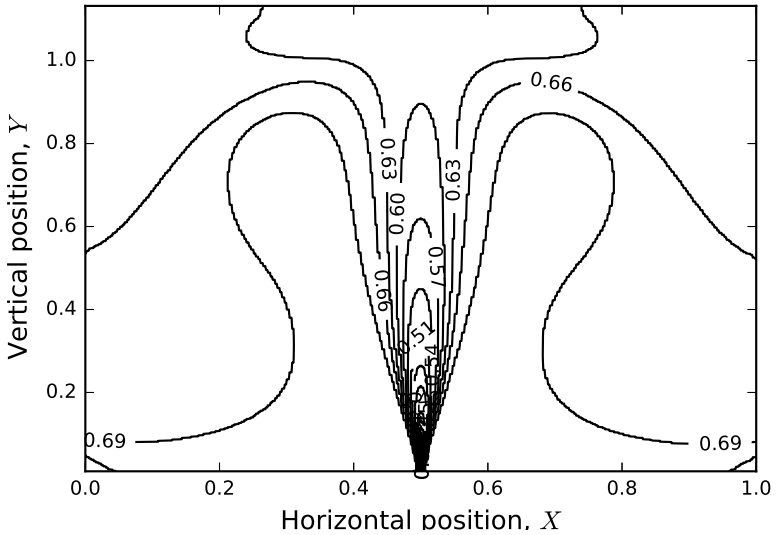

Figure 3.10. Tracer contour line plot at the end of fill cycle for case with $1/d_j = 200$ corresponding to 8M momentum. The labels indicate the mass fraction of the tracer. No presence of any dead zone as the tank is well mixed with uniform tracer concentration seen through the entire tank.

fill cycle, the inlet momentum should be sufficient so that the average kinetic energy is the tank is equal to atleast 0.15. From the Figure, the kinetic energy rises to a peak and then asymptotes for the case with momentum M since the kinetic energy of the jet is not sufficient to stir the tank contents. The peak value occurs when the jet hits the free surface and as it spreads towards the wall, there is a dip in the kinetic energy values till the recirculation zone spreads towards the tank base. Thereafter we see an increase in the kinetic energy for cases with momentum 4M and 8M as the kinetic energy is sufficient to stir the entire tank contents.

3.2.2. Higher Aspect Ratio. In this section, the impact of aspect ratio on mixing at constant momentum is studied. All the cases studied in this set have momentum M corresponding to the baseline jet velocity. Three sets of cases at different aspect ratios cor-

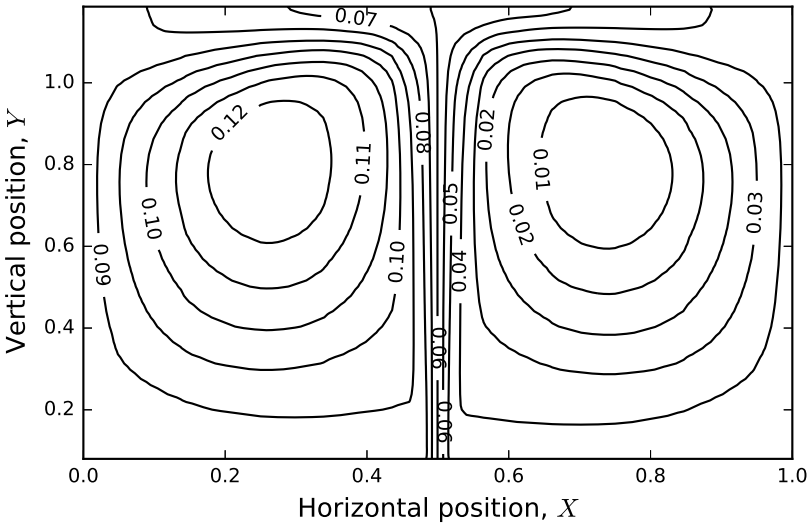

Figure 3.11. Streamline contour line plot at the end of fill cycle for case with $1/d_j = 25$ at baseline jet momentum. The labels indicate the streamfunction values. The recirculation zones do not extend till the bottom of the tank.

responding to $1/d_j = 25$, 100 and 200 are analyzed separately. In the first set corresponding to $1/d_j = 25$, three cases were run with aspect ratios of 1.25, 2.4 and 5. Each of the cases display a unique characteristic behavior for Coefficient of Variation (COV) calculations as seen in Figure 3.16. The curve corresponding to aspect ratio 1.25 reaches a peak in COV value and then drops whereas for an aspect ratio 2.4, the COV reaches a peak and becomes asymptotic. The COV curve corresponding to aspect ratio 5 is a linear increasing curve beyond $t = 0.8$ till the end of the fill cycle. None of these are *mixed* at the end of the filling process. With the definition of mixing time as the time when the COV drops below 0.10, the COV values for these cases are much higher than the mixed value. Case with aspect ratio 1.25 has been discussed in the previous section. Tank with an aspect ratio 2.4 is unmixed and shows a similar behavior to that of aspect ratio 1.25 tank. Here also a a dead

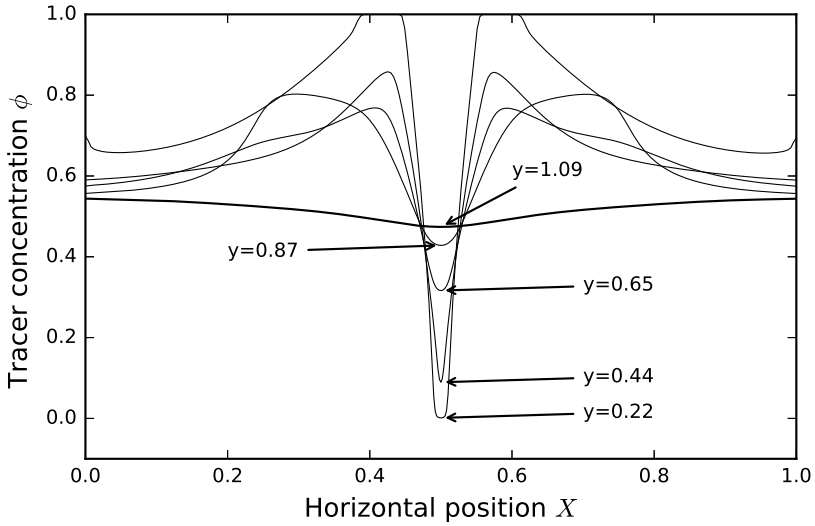

Figure 3.12. Tracer concentration variation along horizontal monitors defined at distances equal to $y = \hat{Y}_i/\hat{D}$ for the case $1/d_j = 25$.

zone is formed at the bottom of the tank that is preventing the tank to be mixed. Again the jet momentum is not sufficient stir up the tank contents.

As seen from the COV plot, the COV value keeps on increasing with the progression of the fill cycle for the tank with aspect ratio of 5. This clearly points to the formation of deadzone whose size keeps on increasing. It is important to analyze the factors causing the tank to stratify as many tanks in the United States have a high aspect ratio. Tanks with aspect ratio greater than 2 often serve as standpipes. These tanks are generally susceptible to stratification and should be analyzed for mixing problems. In this case, the jet driven recirculation zones are limited by the height at which the jet momentum can sustain mixing *i.e.* only a finite region of tank is mixed by the inlet jet and mixing above this region takes place only due to molecular diffusion which is extremely slow and ineffective. The jet does not have sufficient momentum to reach the free surface and the entrainment layers that

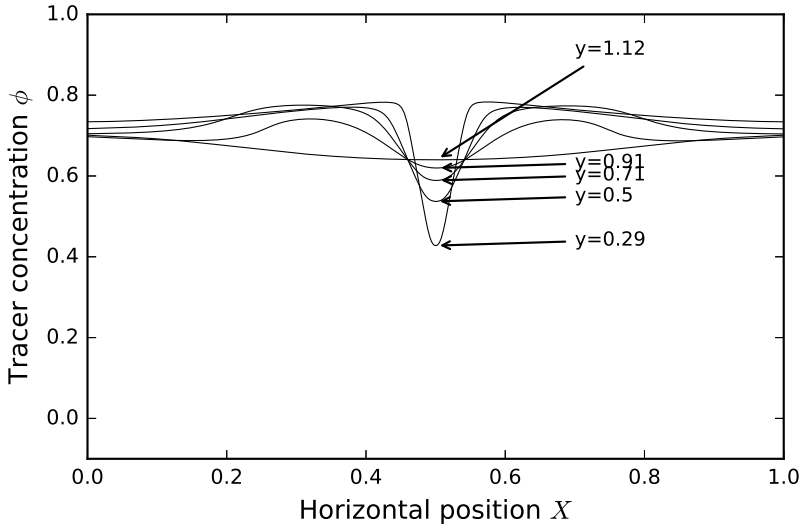

Figure 3.13. Tracer concentration variation along horizontal monitors defined at distances equal to $y = \hat{Y}_i/\hat{D}$ for the case $1/d_j = 100$

setup the recirculation zones are confined only to a fraction of the tank. As a result, mixing does not take place from the top (free surface) to the bottom as it happens in other cases with different momentum and aspect ratio. Instead, mixing takes place from the bottom to the top with the majority of the mixing above the maximum rise height happening due to molecular diffusion. Figures 3.17 shows the tracer contour plot at t = 0.62. It is clear from the plots that the maximum height that the jet could penetrate and mix was already achieved by time t = 0.62. This means that the fill process beyond this time would only displace a finite volume of water above the maximum height until the end of the fill cycle *i.e.* further filling process will not cause any difference in mixing.

The streamline contour plot shown in Figure 3.18 shows that the extent of the recirculation zone is limited to only the bottom portion of the tank. It has already been established that the entrainment layers created by the inlet jet is a dominant source of mixing.

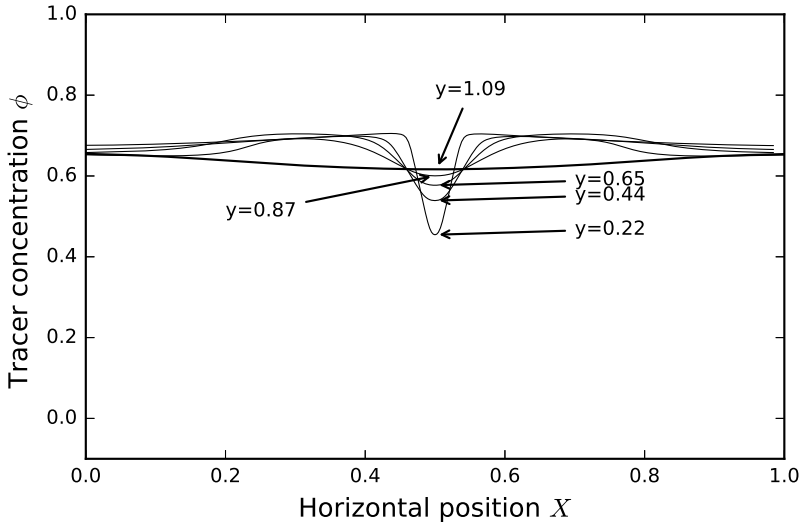

Figure 3.14. Tracer concentration variation along horizontal monitors defined at distances equal to $y = \hat{Y}_i/\hat{D}$ for the case $1/d_j = 200$

The figure corresponds to the end of the fill cycle *i.e.* at $t = 1.8$. From the Figure, it is clear that the strong recirculation zone setup due to the entrainment of the ambient fluid by the turbulent jet is a source of mixing only towards the bottom of the tank.

Figure 3.19 shows the tracer contour plot at the end of the fill cycle. A region of high tracer concentration is observed in the top portion of the tank which is a deadzone with low velocity. This region is an impediment for mixing. For this case, seven horizontal monitors at equal distances were defined for saving tracer concentration and velocity data at every time step. It is important to analyze the decay of velocity along the height of the tank as it is another parameter that can be used to revel the level of mixing in the tank. A plot of decay of vertical velocity along 7 different monitors is shown in Figure 3.20. The y values in the graph corresponds to the height at which each monitor is defined from the tank bottom. There is no variation in the vertical velocity at all for monitors at $y = 3.08,\ 3.75$ *and* 4.41

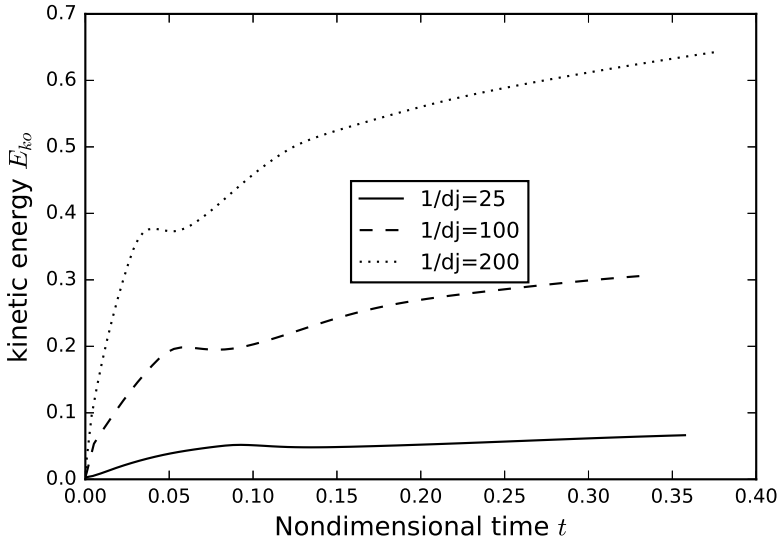

Figure 3.15. Kinetic energy variation using fixed scale

with the velocity values close to zero. Only a very low velocity variation is observed at y = 2.41. This clearly points out that a region of low velocity exists in the tank that is not being mixed by the inlet jet. In this region, mixing takes place by molecular diffusion which is extremely ineffecient and slow.

The next step in the analysis is the tracer study that shows the convergence of tracer concentration along different monitors. It's already been established that the tank with aspect ratio of 5 is unmixed with the help of tracer, streamline contour and vertical velocity decay plots.The level of stratification can be shown with the help of tracer concentration convergence plot. As shown in Figure 3.21, there is no convergence of the tracer concentration among monitors located at y = 3.08, 3.75 *and* 4.41 although we can see that the lower part of the tank is *well mixed* from convergence of tracer at lower part of the tank.

The instantaneous kinetic energy is calculated on a per unit height basis (non dimensionalized) at six flow times for the aspect ratio 5 tank is shown in Figure 3.22. From

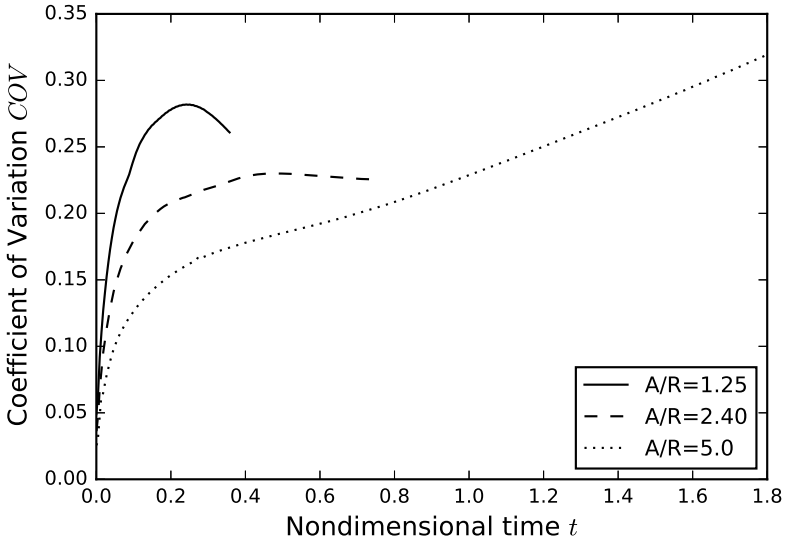

Figure 3.16. Coefficient of Variation for different aspect ratio (A/R) at constant momentum M

the figure, we can make the following observations. The maximum kinetic energy E'_k at time 0.03, 0.38, and 0.74 are equal to 0.12, 0.07, *and* 0.05 respectively. The maximum kinetic energy E'_k remains constant from time $t = 0.74$ till the end of the fill cycle. Between time $t = 0.38$ and 0.74, the jet reaches the maximum height during which its momentum can sustain induced mixing. Notably, the height at which the kinetic energy E'_k maximum corresponds to the jet having achieved the maximum height. From the figure, it can also be seen that the kinetic energy reduces to almost zero at higher free surface height. This corrorborates what was seen in the vertical velocity decay and the streamline plots that the jet induced kinetic energy is concentrated in the bottom half of the tank and whatever mixing that takes place beyond the maximum height is only by molecular diffusion.

As a comparison, the instantaneous kinetic energy per unit height is calculated for cases with aspect ratio 5.0 and 1.25 and plotted in Figures 3.23 and 3.24. In Figure 3.23,

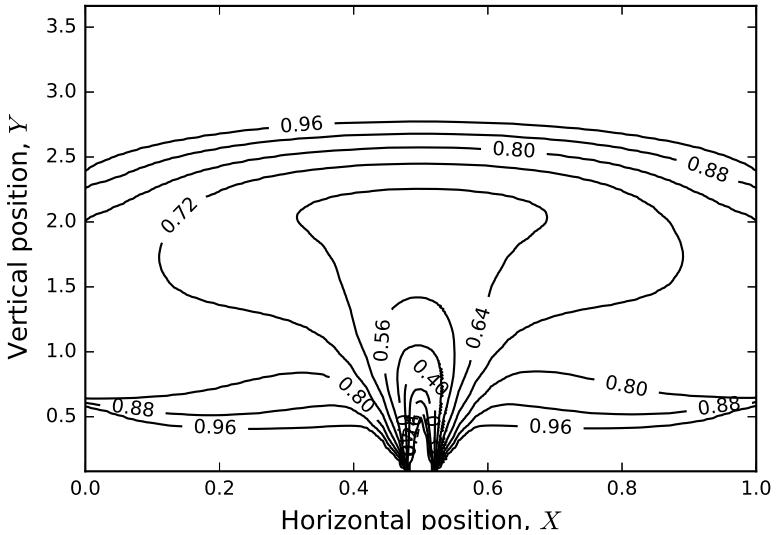

Figure 3.17. Tracer contour line at time $t = 0.62$ for the case with baseline momentum M and aspect ratio equal to 5. Note the maximum rise height of the jet corresponds to a free surface height between 2.3 and 2.5.

the maximum kinetic energy E'_k location in the tank is constant and corresponds to half of the final free surface height. We see variations in the kinetic energy at higher free surface height in the plots which shows that jet induced mixing is present near surface height.

The average specific kinetic energy e_k is plotted for the three cases as shown in Figure 3.25. From the figure, it is seen that e_k is highest for aspect ratio of 1.25 and lowest for aspect ratio of 5.0. This is because e_k is volume averaged kinetic energy and for this case, it is more appropriate for comparison since it gives an averaged value at any instant in time that is available for mixing.

The second set corresponds to $1/d_j = 100$ with 3 cases run at aspect ratios of 1.25, 2.4 and 5. All the cases run in this set have a momentum equal to $4M$ where M corresponds to the baseline jet velocity. All the tanks are *mixed* as seen in the COV plot shown in Figure

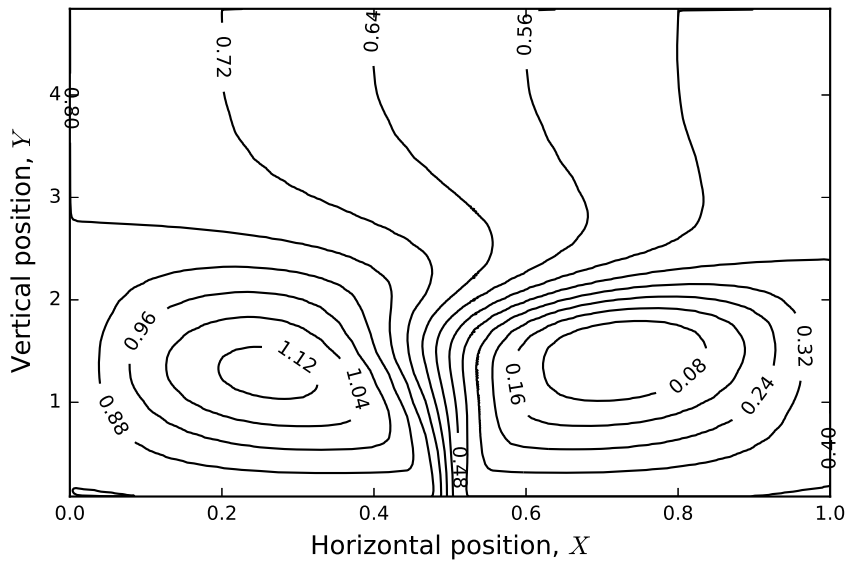

Figure 3.18. Stream line contour plot at t = 1.8 (fill cycle end) for the case with baseline momentum M and aspect ratio equal to 5.

3.26. The COV plot for the aspect ratio 5 tank increases and then drops below 0.1. This case displays a unique behavior that will be discussed below.

The inlet jet deviates from its neutral position during the fill process and hits the right wall creating a small recirculation zone at the bottom right of the tank. Figure 3.27 shows the formation of three recirculation zones at t = 0.31 just before the jet hits the right wall. It can be observed that there is one dominant zone that is going to be responsible for mixing. Once the jet hits the right wall, it is directed towards the free surface by the wall. As the jet moves towards the free surface, the tank gets mixed by the dominant recirculation zone whose size increases with the progression of the fill cycle. At the end of the fill cycle, the aspect ratio of this dominant recirculation zone is four. Figure 3.28 shows the streamline plot at the end of the fill cycle at t = 1.75. From the plot, we can infer that the dominant recirculation was mainly responsible for mixing of the tank after the jet deviated

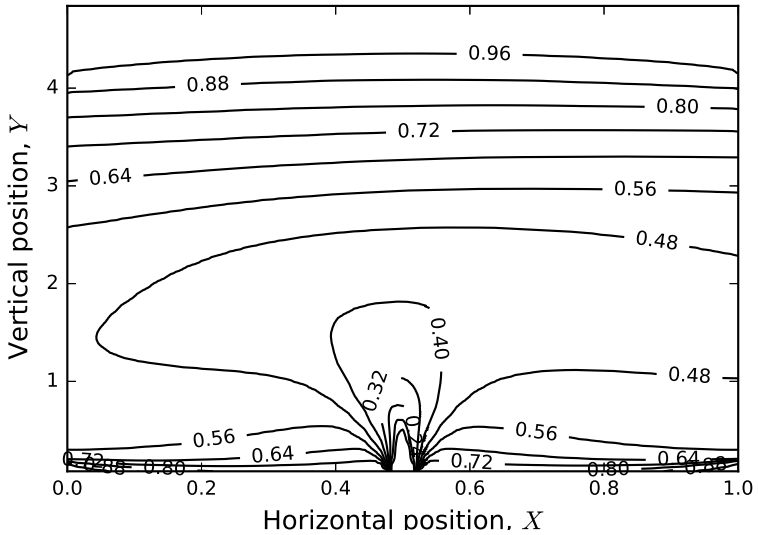

Figure 3.19. Tracer contour line at time t = 1.80 (fill cycle end) for the case with baseline momentum M and aspect ratio equal to 5.

from its neutral position. It can also be inferred that there is no significant impact on mixing because of the deviation of the jet.

An important observation is to be made here. In the previous section, the mixing for the aspect ratio 5 tank that was unmixed was discussed. In this section also, a similar tank with momentum 4M that was $well - mixed$ was discussed. Even though the jet deviated from its neutral position, it had minimal effect on mixing as there was optimal mixing of old water and new water in the tank at fill cycle end. An increase of momentum to four times the baseline momentum caused the tank to mix. So from these two cases, we can identify that inlet momentum is a key factor in mixing. With sufficient momentum even tanks with higher aspect ratio can be mixed. Sometimes there might be a limitation in increasing the momentum, like low pump capacity or insufficient distribution pressure to get an increase in flowrate etc. The other alternative to get higher momentum is by increasing the inlet jet

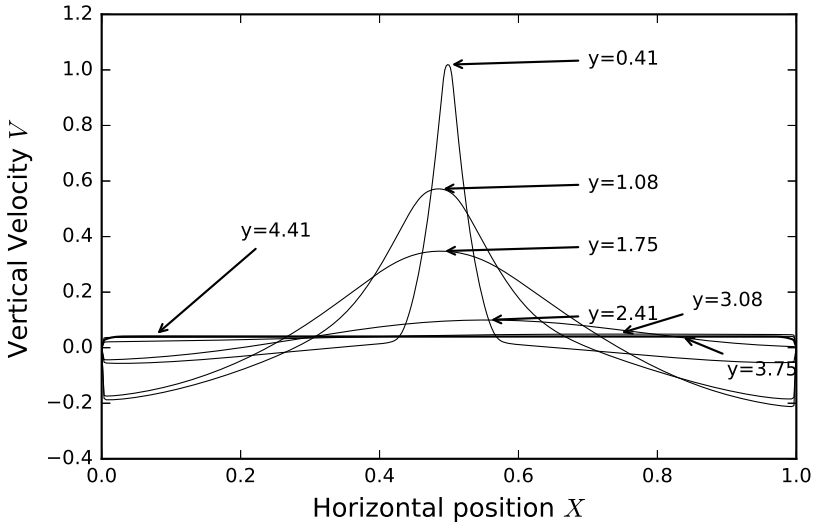

Figure 3.20. Decay of vertical velocity along the tank height for tank with aspect ratio of 5.0. Velocity is non dimensionalized by the jet velocity. Each curve corresponds to a surface monitor

velocity with reduced jet diameter as we have done in this study. This remedy is easier to implement by the water utilities without any major design changes or cost.

The third set corresponds to $1/d_j = 200$ with two cases run at aspect ratios of 1.25 and 2.4. The momentum for this set can be represented by 8M where M refers to the baseline momentum. Both the cases are $well-mixed$ at the end of the fill cycle. The jet momentum is sufficient to stir up the entire tank contents. The tank with aspect ratio 2.4 deviates from the neutral position similar to the case discussed above, there is a dominant recirculation zone that is mainly responsible for mixing. Before the jet deviates, the tank is well mixed. Figure 3.29 shows the COV plot for these two cases. The COV maximum values is less than the mixing criterion. Also it was observed that there was very good convergence of the tracer concentration along horizontal monitors which is mixing.

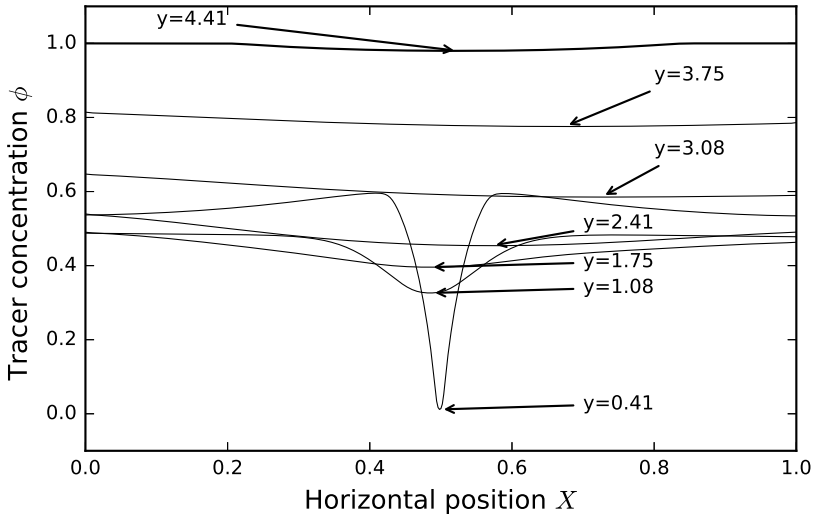

Figure 3.21. Tracer concentration variation along horizontal monitors defined at distances equal to $y = \hat{Y}_i/\hat{D}$ for the case $1/d_j = 25$ with aspect ratio 5.

3.2.3. Inflow Cessation. We have studied how the mixing happens during the fill cycle with the help of different parameters. It has been reported that majority of the mixing happens during the fill cycle [Grayman and Rossman, 2004]. However, Tian and Roberts [2008a] reports that mixing can occur before or after the inflow stops. Although the author does not mention anything about the source of mixing once the inflow is shut off, the objective of this section is to understand the level of mixing occurring after the inflow is shut off and the source of this mixing. Once the fill cycle CFD simulation was completed (when volume change or volume increase from 60 to 90% was achieved), the inflow was shutoff. In terms of CFD setup, the boundary conditions for the inlet jet was changed from velocity inlet to wall. No other changes were made in the simulation setup. Hereafter the simulation conducted after the inflow is shut off will be referred to as the hold cycle. For all the cases, the hold cycle was conducted for a sufficiently long time until the residual

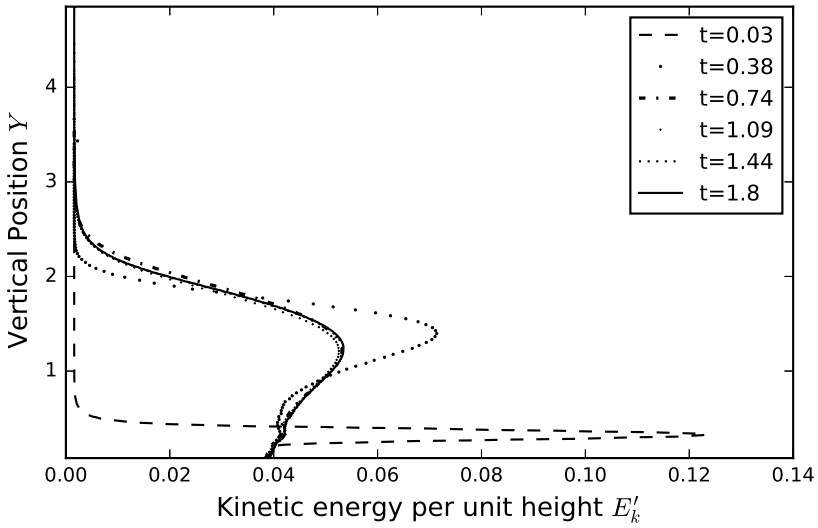

Figure 3.22. Instantaneous Kinetic energy per unit height at six flow times for the case $1/d_j = 25$ with aspect ratio 5.

kinetic energy in the tank at the end of the fill cycle was dissipated. To summarize from the previous sections, there were three cases that did not mix during the fill cycle according to our mixing criterion. These three cases correspond to $1/d_j = 25$ with an aspect ratio of 1.25, 2.4 and 5. As seen from these cases, the jet momentum was not sufficient to mix the tank contents during the fill cycle resulting in the formation of dead zones. For the other cases which were already mixed in the fill cycle, we can expect the COV to drop further in the hold cycle thereby signifying even better mixing. The key factor for significant mixing to happen in the hold cycle is the amount of residual kinetic energy available in the tank at the end of the fill cycle.

The cases that did not mix during the fill cycle will be analyzed to check if the hold cycle allows for tank to become mixed. Figure 3.30 shows the COV overlay for fill and hold cycle for the three cases being discussed. It can be observed from the plot that, for the

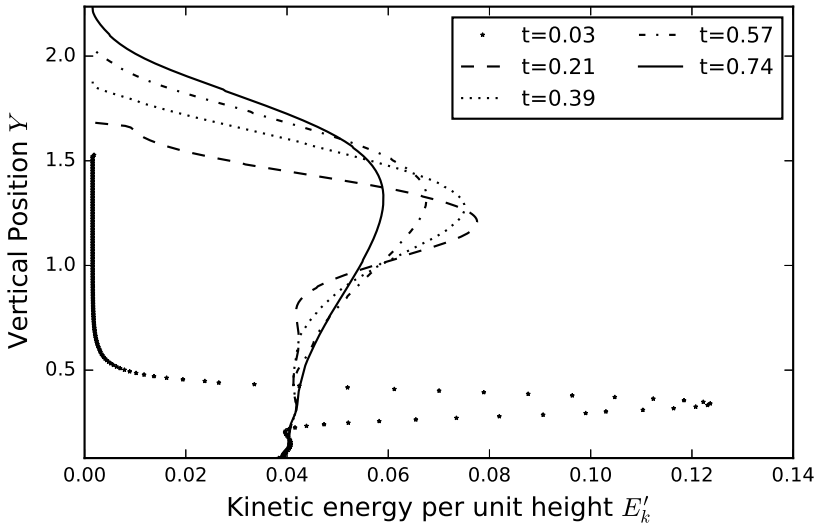

Figure 3.23. Instantaneous Kinetic energy per unit height at five flow times for the case $1/d_j = 25$ with aspect ratio 2.4.

case with an aspect ratio 1.25, the Coefficient of Variation drops to below 0.1 during the hold cycle which implies that the tank has now mixed according to our mixing criterion. The COV minimum values for cases with aspect ratio 1.25, 2.4 and 5.0 are 0.049, 0.176 and 0.2936 respectively. This shows that the tank which was unmixed during the filling process is $well - mixed$ at the end of hold cycle because of the residual kinetic energy. The COV values at the end of the fill cycle for the three cases are 0.261, 0.225 and 0.312 respectively. From this, we observe a 81.23% drop in the COV value between the fill and hold cycle for the aspect ratio 1.25 tank. The two other tanks with higher aspect ratios, however do not become mixed during the hold cycle, since their COV values still above 0.1. We do see a 21.78% drop in COV value for the aspect ratio 2.4 tank during the hold cyle. The deadzone that was formed in the fill cycle is not fully dissipated in the hold cycle for this tank. For the aspect ratio 5 tank, the COV value reduction between fill and hold cycle

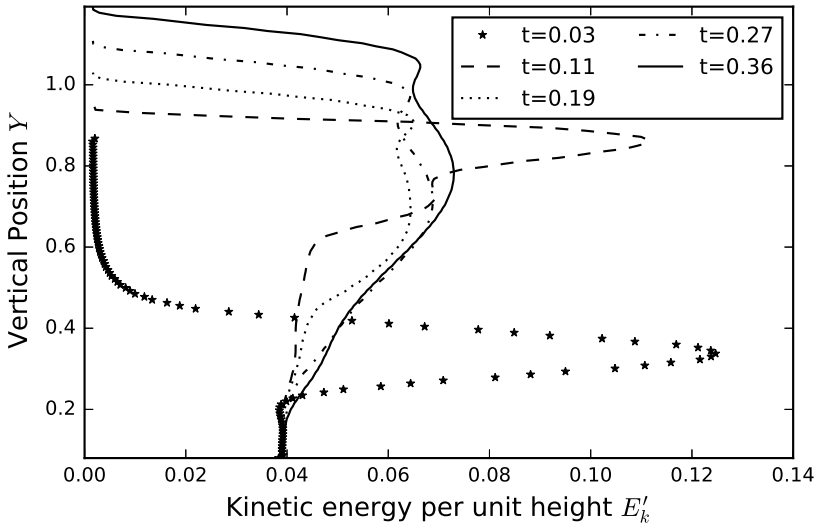

Figure 3.24. Instantaneous Kinetic energy per unit height at five flow times for the case $1/d_j = 25$ with aspect ratio 1.25.

is only 5.9%, consistent with the tank still being stratified. This behavior is expected for this tank since the inlet jet did not have sufficient momentum to reach the free surface could therfore sustain mixing only for a fraction of the tank. Since mixing beyond the maximum rise height happened due to the extremely slow mechanism of molecular diffusion, we do not expect any improvement in the mixing as no residual kinetic energy could be present in the deadzone region. The region below the deadzone is $well-mixed$ during the hold cycle. The average specific kinetic energy is plotted along with dissipation to see the decay in the hold cycle in Figure 3.31. From the Figure, it can be seen that all of the residual energy that was present at the end of the fill cycle has been dissipated. So no further mixing can be expected in the tank. Hence we can infer that, for vessels with aspect ratio of 2.4 and above, mixing cannot be achieved with baseline momentum.

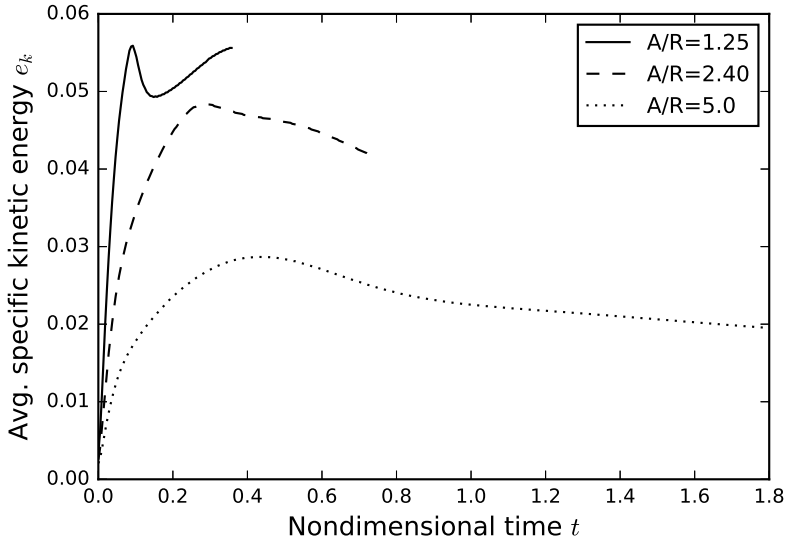

Figure 3.25. Avg. specific kinetic energy for the case $1/d_j = 25$ with aspect ratio of 1.25, 2.4 and 5.

Some important observations can be made here. We have seen that there is scope for significant mixing to take place even after the inflow is shut off. As in the case of the tank with aspect ratio 1.25, there was sufficient residual kinetic energy in the tank at the end of the filling process that could extend the recirculation zone to the bottom thereby mixing the deadzones created in the fill cycle. One also observes that for higher aspect ratio tanks with low inlet jet momentum, the residual kinetic energy is not sufficient to overcome deadzones in the tank and cause complete mixing. This is especially true for tanks with highest aspect ratio of 5. The essential observation is that the residual kinetic energy can be a significant source of mixing after the inflow is shutoff. Even for cases which were *mixed* during the filling process itself, a significant drop in COV was still observed during the hold cycle.

3.2.4. Variable Fill Duration. In this section, CFD simulation results for variable filling times are examined. From the guideline on water turnover rate provided by AWWA

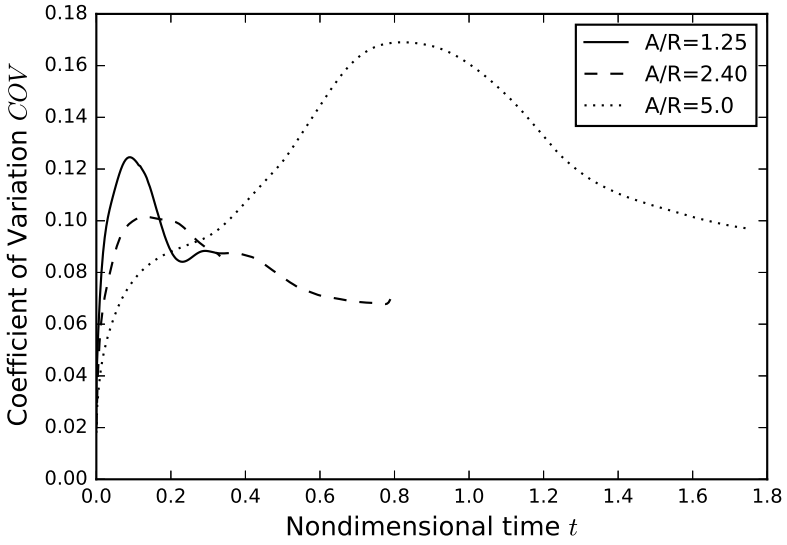

Figure 3.26. Coefficient of Variation for different aspect ratio (A/R) at constant momentum 4M.

[2002], the average recommended daily turnover rate is 30%. In the previous sections, it was assumed that during the fill cycle, there was a volume change/increase of 30%. Kennedy et al. [1993] recommends that that storage reservoirs should be designed to ensure maximum volumetric change to avoid stratification. This is especially true for standpipes which have have aspect ratios greater than two. To avoid stratification in standpipes, the tank operation should be designed to ensure maximum volumetric change occurs during fill and draw cycles especially during periods of low flow. The duration of the fill cycle is highly dependent on demand. If the demand is low during the draw cycle, it will impact the duration for the next fill cycle.

The objective is to examine the effect of different filling times on mixing. Here Two cases that were not mixed in the complete fill cycle are chosen for further analysis. Since all the other cases were mixed at the end of fill and hold cycle, they are not discussed here.

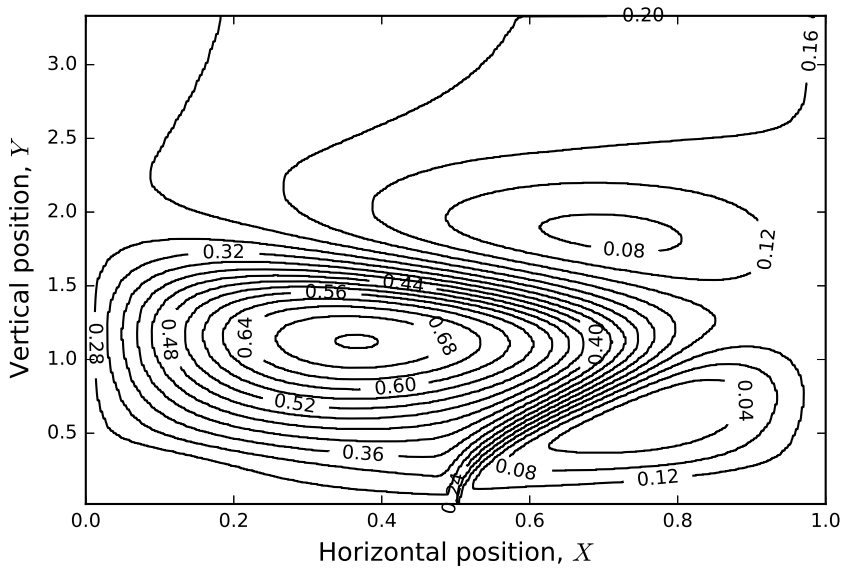

Figure 3.27. Streamline contour plot at t 0.31 for aspect ratio 5 at constant momentum 4M. The stream function values are scaled by a factor of 10. Three recirculation zones are observed

Figure 3.32 shows the overlay of average specific kinetic energy, e_k and COV plot at different fill durations for data corresponding to the case with an aspect ratio of 2.4 at the baseline jet velocity. Two cases were run with flow durations equal to 20% and 60% of the complete fill time. As observed earlier, this case did not mix during the fill and hold cycle. Observing the plot corresponding to 20% fill time, we see that the COV drops below 0.1. The fill duration was $1/5th$ of the complete fill cycle. The reason for the tank to mix during the hold cycle is that only a low volume of water was added through the inflow and the inlet jet momentum was sufficient to mix this new water with the old water so as to achieve a uniform distribution of old and new water. The average kinetic energy for the 20% fill time reaches a peak in the fill cycle and drops exponentially during the hold cycle. This shows that the kinetic energy in the tank is sufficient to spread the recirculation zone through the

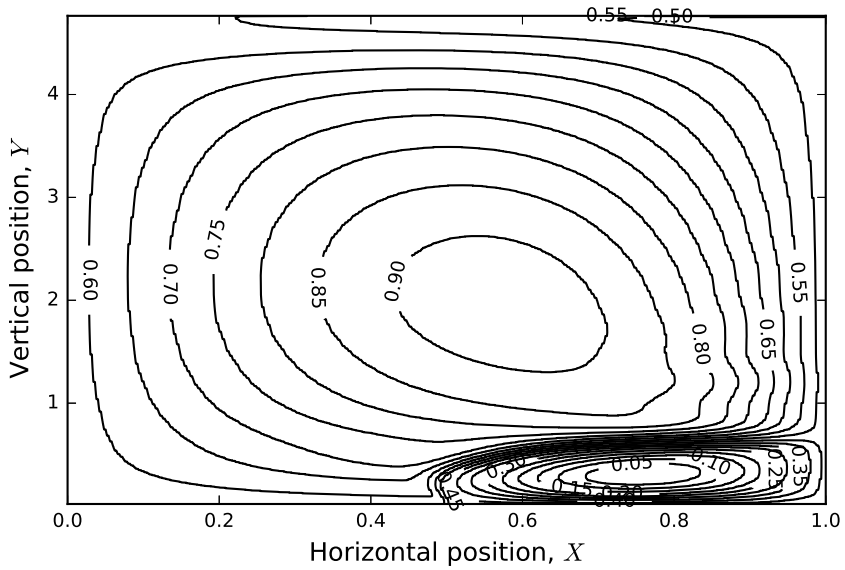

Figure 3.28. Streamline contour plot at t 1.75 for aspect ratio 5 at constant momentum 4M. The stream function values are scaled by a factor of 10.

entire tank. The COV plot corresponding to 60% fill time also drops to a value of 0.108 during the hold cycle that is very close to the mixing criterion. Hence we can consider this tank to be also *mixed*. No further drop in the COV value is expected as the kinetic energy has dissipated completely.

Figure 3.33 shows the COV overlay for 40% fill time and 100% fill time for the tank with aspect ratio 5 at baseline jet momentum. As discussed in the previous sections, the tank remained *unmixed* at the end of the hold cycle. However, the COV value drops to 0.13 during the hold cycle indicating the behavior of the tank tank is close to the *mixed* condition. This behavior is markedly different from the complete fill duration cycle behavior observed earlier. The reason is that the size of the dead zone formed in the tank is smaller since the increase in free surface height is proportionate to the fill duration. If less volume of water is added in the fill cycle, then the momentum required for mixing also reduces proportionately.

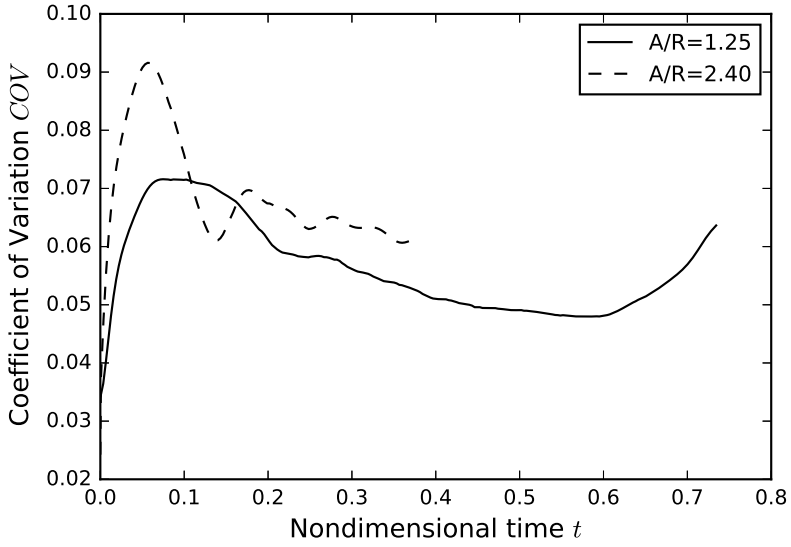

Figure 3.29. Coefficient of Variation for different aspect ratios (A/R) at constant momentum 8M.

Thus, we have analyzed the effect of variable fill times on mixing for two cases that remained *unmixed* earlier for the full fill duration cycles. Better mixing was observed for both the cases with variable fill durations. This indicates that for tanks with low inlet jet momentum and higher aspect ratios, it is possible to achieve better mixing with shorter fill cycles. Note that this may not be possible in reality because of pumping limitations, fire storage requirements or other operator constraints. Also with shorter cycles, the volume increase in the tank will be proportionate to the duration. So if the demand was high in the previous draw cycle schedule, then the operator would be required to have a much large volume increase in the tank and as we have shown in the previous sections that if the inlet momentum is low and the tank aspect ratio is high, there will be deadzone formation.

The Coefficient of Variation is plotted in Figure 3.34 for all the cases run in the isothermal chapter to obtain the visual comparison of COV values for all the cases.

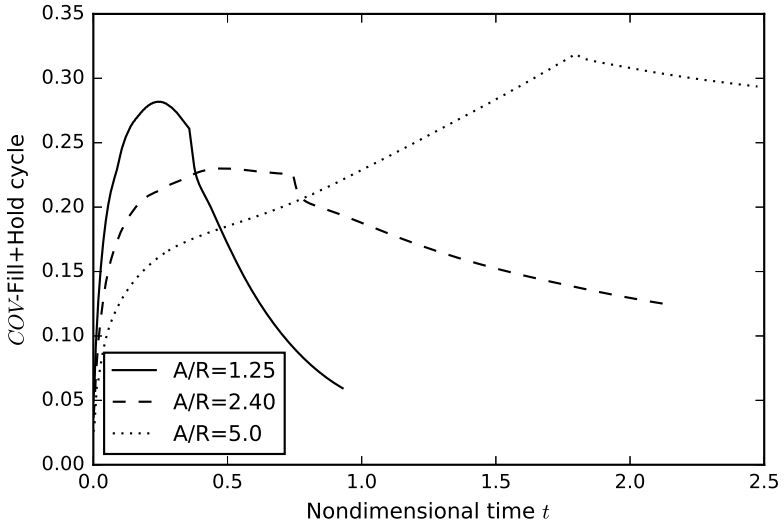

Figure 3.30. Coefficient of Variation, Fill+Hold for different aspect ratios (A/R) at constant momentum M.

3.2.5. Mixing Time Modification and Calculation. Okita and Oyama [1963] provides a formula to calculate the mixing time in drinking water storage tanks. The influence of water level is incorporated into the formula which is given by,

$$\tau_m = K\left(\frac{H^{1/2}D^{3/2}}{M^{1/2}}\right) \tag{3.47}$$

where K is a constant whose value depends on definition of complete mixing equal to 4.6 ; M is the inflow momentum flux and D is the tank diamter.

Rossman and Grayman [1999] modified this formula to estimate a new value of the experimental constant equal to 10.2. However, their data had considerable scatter with values ranging from 6.4 to 17.4. Also the experiments were conducted for vessels with H/D ratios in the range of 0.11 and 0.49.

The formula is given by

$$\tau_m = K'\left(\frac{V^{2/3}}{M^{1/2}}\right) \tag{3.48}$$

where V is the tank volume and K' is a dimensionless constant equal to 10.2

Notably, in the two tanks tested by [Rossman and Grayman, 1999]; for tank one, the ratio of the tank diameter and the jet diameter varied between 100 and 218 whereas for tank two, the variation was between 150 and 327. The essential argument of Rossman and Grayman [1999] is that, the length of the filling period τ_f should be greater than the mixing time τ_m.

Modifying Eqn.(3.48) to make it applicable to the present work, we obtain the modified equation,

$$\hat{\tau}_m = K'\left[\left(\frac{H_f^{2/3}}{d_j^{1/2}}\right)\cdot\left(\frac{\hat{D}}{\hat{u}_j}\right)\right] \tag{3.49}$$

where $\hat{\tau}_m$ is the dimensional mixing time; H_f is the dimensionless final water surface height; d_j is the dimensionless jet diamter; $\hat{D}$ is the tank width and $\hat{u}_j$ is the jet velocity.

In the above equation, K' is a constant that is determined by comparison with CFD predicted mixing time. Five isothermal cases that were mixed are chosen for calculation of mixing time. It may be recalled that the tank is considered to be mixed when the COV drops below 0.10. Hence, CFD mixing time is calculated as the time when the COV drops below 0.10. Table 3.2 shows the CFD calculated mixing times and calculated constant K' values.

In the above table, we see values of K' ranging from one to five. Similar scatter was also observed in Rossman and Grayman [1999] results. Comparison of K' values with those provided in literature indicate the same order of magnitude. This underscores

Table 3.2. CFD predicted mixing time for isothermal cases and determination of constant K' in the analytical mixing time expression

$(1/d_j)$	Aspect Ratio	τ_{cfd}, (s)	t_m	τ_{calc}, (s)	K'
25	1.25	2279.43	0.71	(K' 724.61)	3.15
50	2.40	2968.91	0.92	(K' 1146.50)	2.59
100	1.25	548.52	0.17	(K' 356.66)	1.53
	2.40	642.61	0.20	(K' 577.84)	1.18
	5.00	5303.13	1.64	(K' 914.81)	5.80

the complexity of the flow field and demonstrates a first level impact of K' on calculation of mixing times. This also illustrates that parameter B in (3.49) has captured the most significant dependance of mixing time. From this, we can infer that the term K' is not well parameterized. The complete derivation of the mixing time is shown in Appendix.

3.2.6. Conclusion. To summarize, a strong dependency of momentum on mixing was observed in the results. With everything kept the same, for unity aspect ratio tanks, increasing the momentum to eight times the baseline value caused a reduction of 67.7% value while increasing the momentum to four times the baseline value causes a 55.6% reduction in the COV maximum value compared to the baseline value. None of the cases corresponding to baseline parameters satisfied the criteria for mixing in the filling cycle. Each of the case unmixed during the fill cycle displayed a unique characteristic behavior. For the aspect ratio 1.25 vessel, the COV reaches a peak and starts to drop, for aspect ratio 2.4 vessel, the COV reaches a maximum value and becomes asymptotic, for aspect ratio 5.0 vessel, the COV is an increasing curve. Formation of deadzones *i.e.* regions of high tracer concentration inhibits mixing. With sufficient inlet momentum, even vessels of high aspect ratios (2.4,5.0) could be mixed under isothermal flow condition. The hold cycle (inflow shutoff) was found to a significant source of mixing because of the residual kinetic

energy that was dissipated when the inflow was shutoff. The case that was unmixed with an aspect ratio 1.25 during fill cycle mixed during the hold cycle. The degree of mixing in the hold cycle is proportional to the inlet jet momentum during the hold cycle. Analysis of isothermal cases with variable fill durations showed better mixing even for cases that were unmixed with complete fill duration.

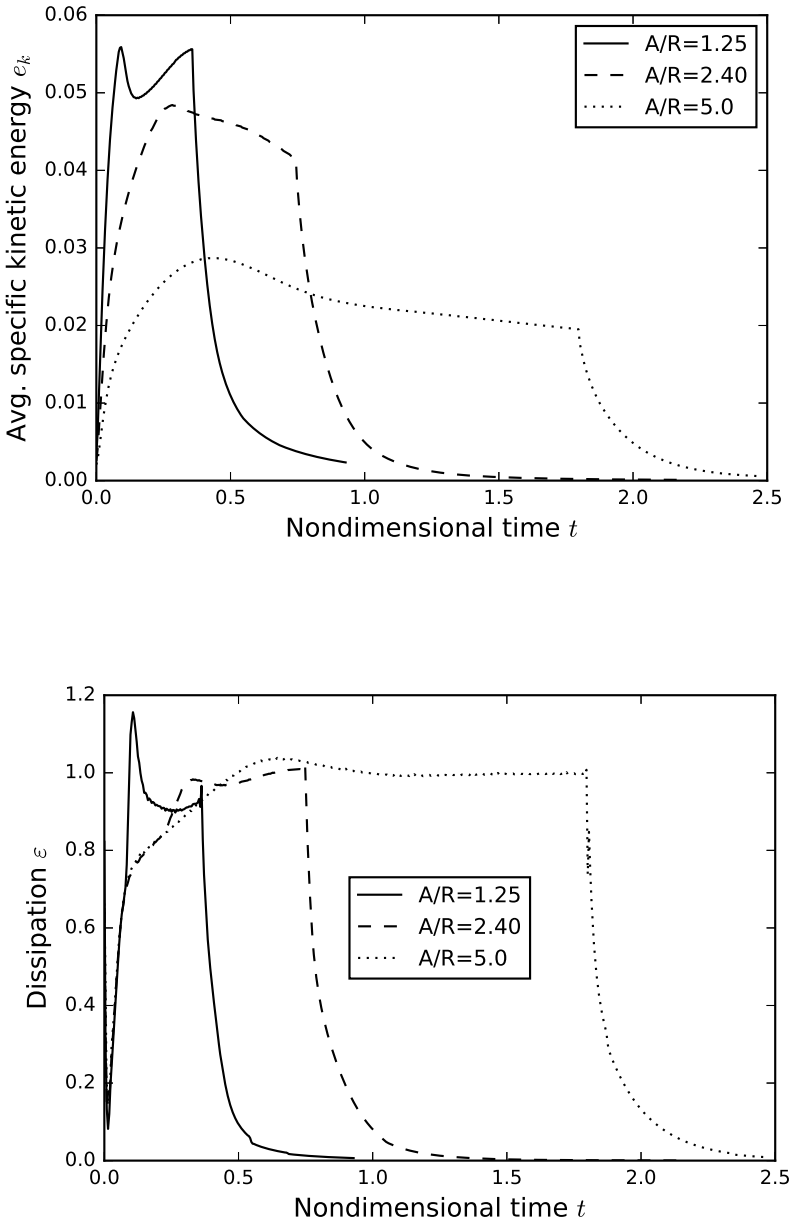

Figure 3.31. Average. specific kinetic energy and dissipation for Fill+Hold cycle (a) Decay of the average. specific kinetic energy to zero during the hold cycle (b) Dissipation ε goes to zero as all the residual kinetic energy is dissipated.

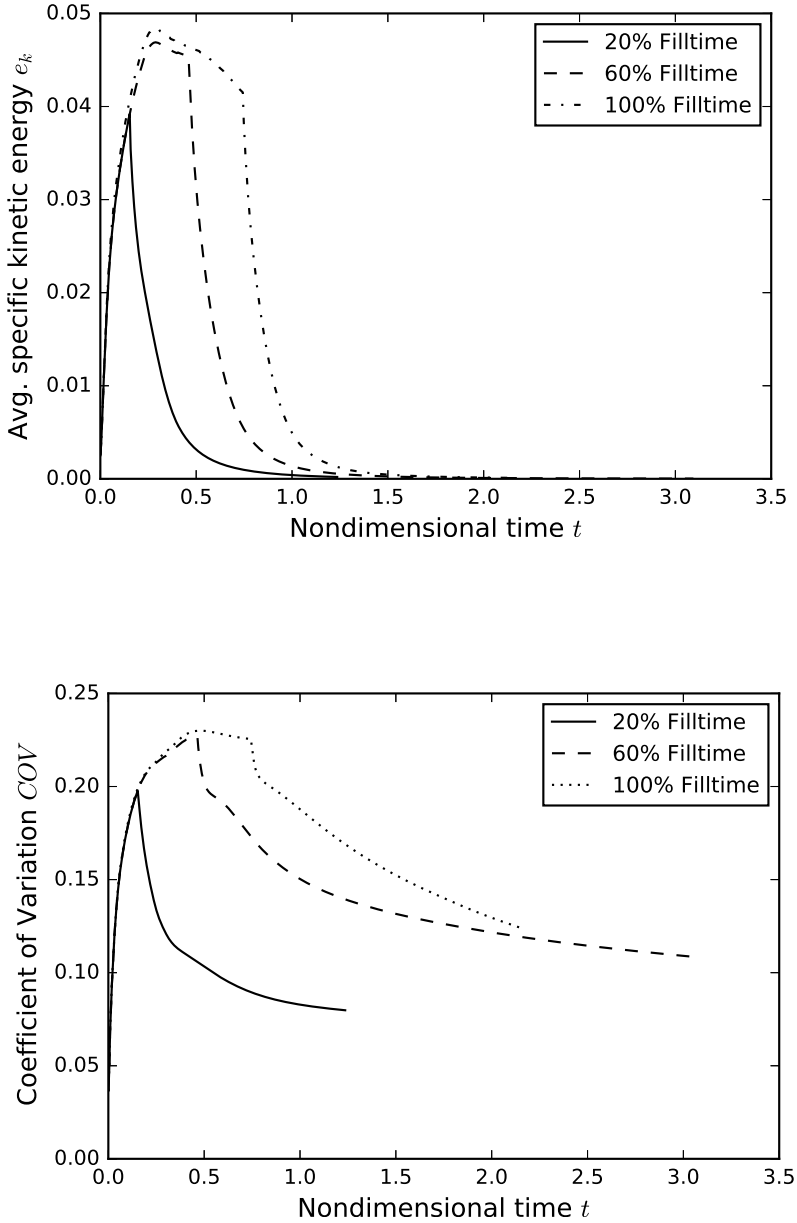

Figure 3.32. Average. Specific kinetic energy and Coefficient of Variation, Fill+Hold at different fill durations for Aspect Ratio 2.4 tank at baseline momentum M.

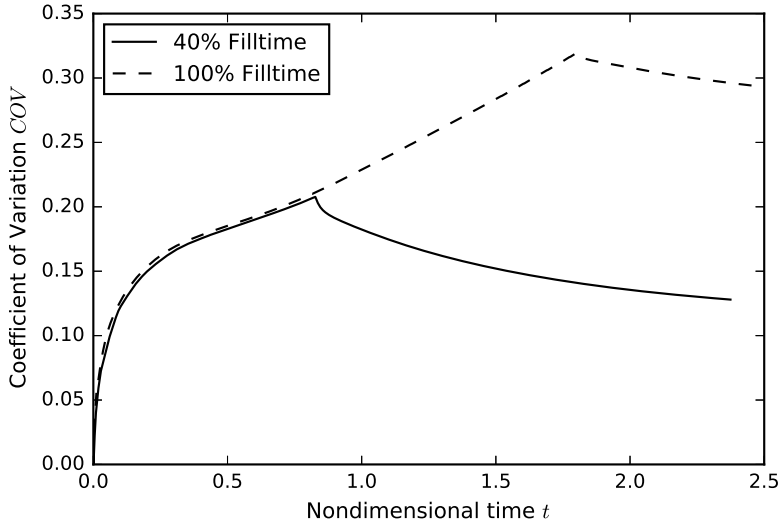

Figure 3.33. Coefficient of Variation, Fill+Hold at different fill times for aspect ratio(A/R) 5 at baseline momentum M.

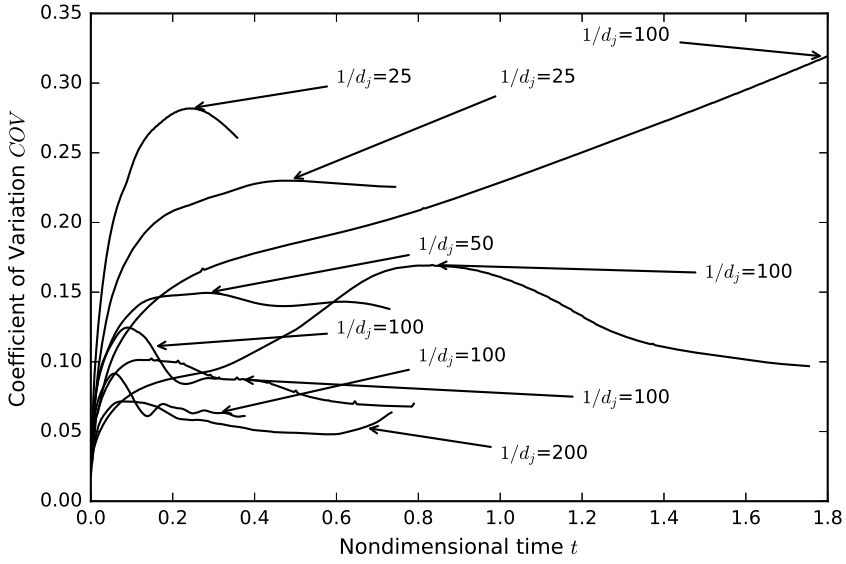

Figure 3.34. Coefficient of Variation overlay, Fill cycle for all isothermal cases with tanks with different aspect ratio and momentum.

4. NON ISOTHERMAL FLOW SIMULATIONS

In this section, simulations with buoyancy effects included are computed. Both positive buoyancy and negative buoyancy effects are considered in the simulations to cover a wide range of tank operation temperatures. The buoyancy is driven by the temperature difference between the inlet jet temperature and the bulk fluid temperature in the tank. Temperature differences between the inflow and the tank can severely affect the level of mixing. Even a temperature difference of 1 °C can lead to stratification [Grayman et al., 2000, Mahmood, 2005] in the tanks, thus leading to poor mixing characteristics. In the previous section, simulations without the buoyancy effects were considered. We have analyzed the effects of different control variables like momentum, aspect ratio on mixing for isothermal flows to establish baseline mixing behavior. However, temperature differences will exist due to seasonal variations that will affect the level of mixing.

Positive or negatively buoyant conditions are dependent on the location of the tanks and the weather patterns at that location. In the United States, positively buoyant conditions are observed during the winter months and may last up to about four months in a year while, during the rest of the year, negatively buoyant conditions are observed with the bulk fluid temperature in the tank greater than the inlet jet fluid temperature. The southern and south western regions of the US may not see winter conditions harsh enough to cause positively buoyant conditions. Different cases are run by keeping the volumetric flow rate constant and changing the jet diameter, jet velocity, temperature of the inlet and bulk water temperature in the tank. Also some cases were executed to check if the criteria to avoid Coanda attachment of the jet to the boundary is valid or not when the jet discharges parallel or near parallel to the wall. Parameters such as Coefficient of Variation along with temperature and tracer

distributions are utilized to characterize the level of mixing in the tank and analyze the impact of temperature differences on mixing.

4.1. PROBLEM FORMULATION

As in the isothermal simulations, ANSYS Fluent was used to compute the non isothermal simulations. The domain of interest is the same as that of the isothermal simulations. The simulation setup is very similar to the isothermal casesp with the exception of formulation of density. The density of air is assumed to be constant whereas for the mixture of tracer and water, the density is defined to be a function of temperature using the Bouissinesq approximation. The save strategy followed for non isothermal flows is the same as that was followed for isothermal flows *i.e.* dependent variable data such as velocity, tracer concentration and temperature were saved at every time step along the horizontal and vertical monitors defined at equal distances along the tank height and width respectively. The entire domain data was saved at every 100 timesteps. The solution methodology for non isothermal flows is also the same as that of isothermal flows with the addition of the energy equation in the solver and additional material properties like specific heat and thermal conductivity being given as inputs to the simulation.

4.1.1. Fundamental Governing Equations. The governing equations solved for the Multiphase flow CFD simulation using the Volume of Fluid (VOF) approach along with species transport and temperature input are the continuity, momentum, species transport, volume fraction and energy equations.

In this section, the temperature differences are assumed to be small so that the density term can be treated as a constant in the continuity equation and in the inertia term of the momentum equation. The density variation is included as a function of temperature in the gravity term in the momentum equation. The two dimensional momentum equation

for a Newtonian fluid with constant viscosity and variable density in vector form is given by

$$\rho\frac{D\hat{\mathbf{u}}}{Dt} = \rho\vec{g} - \nabla p + \mu\nabla^2\hat{u} + \frac{1}{3}\mu\nabla\left(\nabla\cdot\hat{\mathbf{u}}\right) \tag{4.1}$$

where ρ is variable density, $\vec{g}$ is the acceleration due to gravity

With the Boussinesq approximation, the density is treated as a constant everywhere in the Navier Stokes equations except in the gravity or the body force term in the momentum equation. Hence the equation (4.1) reduces to

$$\rho_\infty\frac{D\hat{\mathbf{u}}}{Dt} = \rho\vec{g} - \nabla p + \mu\nabla^2\hat{u} \tag{4.2}$$

where ρ_∞ is fluid density at a reference state,

The dimensional x and y components of the Navier - Stokes equation of motion are given by

$$\rho\left(\frac{\partial\hat{u}}{\partial\hat{t}} + \hat{u}\frac{\partial\hat{u}}{\partial\hat{x}} + \hat{v}\frac{\partial\hat{u}}{\partial\hat{y}}\right) = \rho\vec{g_x} - \frac{\partial\hat{p}}{\partial\hat{x}} + \mu\left(\frac{\partial^2\hat{u}}{\partial\hat{x}^2} + \frac{\partial^2\hat{u}}{\partial\hat{y}^2}\right) \tag{4.3}$$

$$\rho\left(\frac{\partial\hat{v}}{\partial\hat{t}} + \hat{u}\frac{\partial\hat{v}}{\partial\hat{x}} + \hat{v}\frac{\partial\hat{v}}{\partial\hat{y}}\right) = \rho\vec{g_y} - \frac{\partial\hat{p}}{\partial\hat{y}} + \mu\left(\frac{\partial^2\hat{v}}{\partial\hat{x}^2} + \frac{\partial^2\hat{v}}{\partial\hat{y}^2}\right) \tag{4.4}$$

At a reference state, such as far away from an object where the temperature is uniform and the fluid is either stationary or moving with uniform velocity, we have the following condition,

$$\nabla^2\vec{V}_\infty = 0. \tag{4.5}$$

Applying Eqn (4.2) at the reference state ∞ and using Eqn (4.5), gives

$$\rho_\infty \vec{g} - \nabla p_\infty = 0 \tag{4.6}$$

Subtracting Eqns. (4.6) from (4.2),

$$\rho_\infty \frac{D\hat{\mathbf{u}}}{Dt} = \Big(\rho - \rho_\infty\Big)\vec{g} - \nabla(p - p_\infty) + \mu\nabla^2\hat{u} \tag{4.7}$$

Relating the density change to temperature change with the use of coefficient of thermal conductivity β, we get the equation for the Bouissinesq approximation

$$\rho - \rho_\infty \approx -\beta\rho_\infty\Big(\ T - T_\infty\ \Big) \tag{4.8}$$

where T_∞ is the operating or the reference temperature, T is the variable temperature

Substituting the Boussinesq approximation back in Eq.(4.7), we get the final form of the momentum equation in vector form,

$$\frac{D\hat{\mathbf{u}}}{Dt} = -\beta\vec{g}\Big(T - T_\infty\Big) - \frac{1}{\rho_\infty}\nabla(p - p_\infty) + \nu\nabla^2\hat{u} \tag{4.9}$$

Assuming that for the incompressible flow, viscous dissipation is negligible, Ansys FLUENT solves the energy equation [ANSYS, 2013a] in the following form,

$$\frac{\partial}{\partial t}(\rho E) + \nabla\cdot\left(\vec{v}\Big(\rho E + p\Big)\right) = -\nabla\cdot\left(k_{eff}\nabla T - \sum_j h_j\vec{J}_j\right) \tag{4.10}$$

where k_{eff} is the effective conductivity given by $(k\ +\ k_t)$ where k_t is the turbulent thermal conductivity defined according to the turbulence mode used, $\vec{J}_i$ is the diffusion flux of species j. The first two terms in the above equation represent the energy equation due to conduction and species diffusion respectively.

In equation (4.10),

$$E = h - \frac{p}{\rho} + \frac{v^2}{2} \tag{4.11}$$

where h is the sensible enthalpy and for incompressible flow, the equation is given by

$$E = \sum_j h_j \vec{Y_j} h_j + \frac{p}{\rho} \tag{4.12}$$

where Y_j is the mass fraction of species j and h_j is the specific enthalpy for species j.

The equation for calculating the specific enthalpy for species j is given by

$$h_j = \int_{T_{ref}}^{T} C_{p,j} dT \tag{4.13}$$

where $T_{ref} = 298.15$K for the pressure-based solver.

4.1.2. Boundary and Initial Conditions. The volume change in the tank during the fill cycle is assumed to be 30%, as for the isthermal simulations. The initial condition imposed at the start of the filling cycle corresponds to 60% of the tank volume patched with a uniform distribution of water and tracer to represent old water and the remaining 40% volume patched with air. In terms of boundary conditions, the temperature at the velocity inlet is specified and the bulk fluid temperature in the tank is specificed by patching the initial volume of fluid in the tank with the required temperature. The walls are assumed to be adiabatic with no heat flux and no slip. All the other boundary conditions are similar to isothermal flows. For the initial condition, the turbulent quanitities like turbulent kinetic energy k and turbulent dissipation rate ϵ are calculated by the empirical relationships provided in the Fluent manual [ANSYS, 2013b].

4.1.3. CFD Validation. In this section, gravity current Froude number and maximum rise height of the jet calculations from negatively buoyant flow simulation results at different grid sizes are compared with analytical or established empirical behavior to demonstrate the resolution near the inlet jet region and also to validate the CFD results for non isothermal flows.

A gravity current is the flow of one fluid within another caused by the density difference between the fluids [Simpson, 1982]. An example of a gravity current would be the flow of cold water (denser) beneath warm water (lighter). The front of the current is generally observed to progress with a nearly constant speed and a characteristic shape [Benjamin, 1968] that is maintained by the gravity current until it hits the wall after which internal waves are initiated by turning of the gravity current at the wall. The preferred propagation velocity of the gravity current is the combination of propagation of velocity and height which gives the Froude number equal to one. Also the conservation of mass dictates that the product of gravity current thickness and propagation velocity is fixed. This phenonmenon has been studied extensively and empirical relationships establish show that the region just behind the leading edge of the gravity current has a Froude number of one [Simpson, 1982]. The densimetric Froude number Fr which is the ratio of the inertial forces to the buoyancy forces is given by

$$Fr = \hat{u}/\sqrt{g'h} \tag{4.14}$$

where $g' = g\left(\frac{\Delta\rho}{\rho}\right)$ is buoyancy reduced gravitational acceleration, $\hat{u}$ is averaged propagation velocity given by $\int_0^h u(y)dy$ with h being equal to the thickness of the gravity current.

From Table 4.1, we observe excellent agreement between the calculated values of the Froude number Fr at different flow times and the expected value of one. The calculations

Table 4.1. Gravity current height H, propagation velocity $\bar{U}$ and Froude number Fr calculations for three grid sizes relating to a case with $(1/d_j = 25)$ and $\Delta T = 2°C$.

	2e5 *nodes*			1.5e5 *nodes*			1e5 *nodes*		
Flowtime, (s)	H, (m)	Fr	$\bar{U}$, (m/s)	H, (m)	Fr	$\bar{U}$, (m/s)	H, (m)	Fr	$\bar{U}$, (m/s)
100	3.158	1.069	0.271	3.170	0.950	0.241	3.176	0.950	0.242
102	3.158	1.090	0.275	3.170	0.966	0.245	3.176	0.972	0.247
104	3.158	1.103	0.279	3.170	0.986	0.250	3.176	0.993	0.252
105	3.158	1.098	0.278	3.170	0.980	0.249	3.176	0.980	0.251

are made for three cases with different grid sizes relating to $1/d_j = 25$ and $\Delta T = 2°C$. Also seen from the table is that the propagation velocity $\hat{u}$ is nearly constant at different flow times that corroborates the empirical observation that the gravity current head moves with a nearly constant speed. The gravity current thickness is also constant at different flow times which also matches the empirical observation that the thickness of the gravity current behind the head is constant as it propogates. Also observed is that the Froude number for the case with the highest number of nodes is closest to the expected value of one. At all the three levels of grid resolutions, the region near the inlet and the tank floor bottom is sufficiently resolved to capture the gravity current waves and its behavior with good accuracy.

Extensive experimental studies exist in the literature [Fisher et al., 1979, Rodi, 1982, Turner, 1966] dealing with turbulent buoyant jets. The terminal rise height (z_t) for a negatively buoyant jet directed vertically upwards has been shown to satisfy a relationship of the form

$$\frac{z_t}{l_m} = constant \tag{4.15}$$

where l_m is the characteristic length scale for a plane jet, the constant has a value between 1.5 and 2.1 [Fisher et al., 1979].

Table 4.2. Terminal Rise height calculations for negatively buoyant flows.

2e5 nodes z_t (m)	1.5e5 nodes z_t (m)	1e5 nodes z_t (m)	Analytical z_t (m)
4.487	4.503	4.477	4.396

The length scale for a plane jet [Rodi, 1982] is given by

$$l_m = M/B^{2/3} \tag{4.16}$$

where M is the initial momentum specific flux given by $(u_j d_j)$ with units of m^2/s^2, B is the bouyancy flux calculated by $g\left(\frac{(\rho_f - \rho_t)}{\rho_t}(u_j d_j)\right)$ with units of m^3/s^3.
Note that for plane jets, the fluxes are per unit length of jet orifice. Also ρ_f refers to the density of feed water and ρ_t refers to initial density of tank water.

The terminal rise height was calculated from the CFD results for the same cases used in the gravity current calculations at different grid sizes. The simulated values are compared with the predicted value obtained from the analytical expression given in Eq.(4.15). From table 4.2, we observe good agreement between CFD predicted and analytical terminal rise height calculations. This also shows that the CFD simulations predict the jet behavior very well.

4.2. RESULTS AND DISCUSSION

Similar to the isothermal flows, the simulations model the filling process in a two-dimensional reactangular water storage tank which is initially filled with old water and into which new water is pumped through a inlet. The density variations due to temperature

differences between the inlet jet fluid and the bulk tank fluid are accounted for in the simulations. The aspect ratio of the tanks in the simulations varied from 1.25 to 2.40 for different variations of temperature differences and inlet jet momentum. The jet Reynolds number $\mathrm{Re_j}$ is constant for all the cases and equal to 2.88×10^5 which corresponds to a highly turbulent flow. The volumetric flow rate was assumed to be constant for all the cases and different inlet jet momentum was obtained by varying the jet diameter. The temperature difference ΔT, taken as the difference between the inlet jet temperature and the bulk tank fluid temperature, is accounted for in a dimensionless parameter called the jet Froude number Fr_j given by $\hat{u}_j / \sqrt{\left(g\beta\Delta T \hat{d}_j\right)}$. Here β is the coefficient of thermal expansion coefficient taken to be a constant equal to $207e-5$ K for water. Several cases were run for both positively and negatively buoyant conditions.

Temperature has been non-dimensionalized using the following expression so as to obtain a relative temperature whose limits lie between 0 and 1.

$$\theta = \left(\frac{T_l - T_o}{T_i - T_o}\right) \tag{4.17}$$

where T_o is tank fluid temperature assumed to be constant for the particular case, T_i is the inlet jet temperature and T_l is the local temperature.

Table 4.3 shows the values of the initial free surface height H_o, final free surface height H_f, duration of the filling cycle Δt_f, Froude number Fr_j and aspect ratio for all the simulations run with negatively buoyant conditions.

Table 4.4 shows the values of the initial free surface height H_o, final free surface height H_f, duration of the filling cycle Δt_f, Froude number Fr_j and aspect ratio for all the simulations run with positively buoyant conditions. H.

4.2.1. Positively Buoyant Simulations. Table 4.4 shows the list of cases run with positively buoyant condition. With positively buoyant inflows, the inlet jet temperature

Table 4.3. Negatively Buoyant Filling Cases with chosen control variables, Reynolds Number Re_j = constant

$(1/d_j)$	H_o	H_f	$\Delta t_f = H_f - H_o$	Froude number Fr_j	Aspect Ratio
25	0.83	1.19	0.36	1.06	1.25
	0.80	1.20	0.40	0.67	1.25
	0.83	1.20	0.37	0.47	1.25
	1.49	2.23	0.74	1.06	2.40
	1.49	2.26	0.77	0.67	2.40
	1.49	2.23	0.74	0.47	2.40
100	0.76	1.14	0.38	8.48	1.25
	0.76	1.14	0.38	5.37	1.25
	0.76	1.14	0.38	3.79	1.25
200	0.76	1.14	0.38	24.00	1.25
	0.76	1.14	0.38	15.18	1.25
	0.76	1.14	0.38	10.73	1.25

is greater than the bulk tank water temperature and hence the inflow is lighter than the tank water. This causes the inflow to rise towards the free surface water height. From a standpoint view of mixing in water storage tanks, positively buoyant conditions are desirable to achieve efficient mixing in the tanks. The parameters corresponding to $1/dj = 25$, Aspect Ratio 2.40 and $\Delta T = 2°C$ represents the baseline case. For an aspect ratio of 1.25 with $1/d_j$ equal to 25, each of the Froude number Fr_j listed in the table corresponds to a temperature difference ΔT equal to 2°C, 5°C and 10°C respectively. The temperature variations are chosen according to the average temperature fluctuations observed during the winter months where the probability of positively buoyant conditions occurring are the highest. We know that the Froude number is a dimensionless parameter given by the ratio of the inertial force and the buoyant force. With increase in ΔT, the buoyant forces become stronger and as seen from the table, we see a reduction in the Froude number with increase in ΔT which indicates that buoyant forces are more dominant than the inertial forces. One

Table 4.4. Positively Buoyant Filling Cases with chosen control variables, Reynolds Number Re_j = constant

$(1/d_j)$	H_o	H_f	$\Delta t_f = H_f - H_o$	Froude number Fr_j	Aspect Ratio
25	0.80	1.21	0.41	1.06	1.25
	0.80	1.20	0.40	0.67	1.25
	0.83	1.20	0.37	0.47	1.25
	1.49	2.23	0.74	1.06	2.40
100	0.76	1.14	0.38	8.48	1.25

case was run for an aspect ratio of 2.4 at a temperature difference equal to 2°C to study of the aspect ratio on mixing for positively buoyant flows. One case was run with inlet jet momentum equal to 4 times the baseline jet momentum at a temperature difference of 2°C to check the impact of higher momentum positively buoyant flows on mixing. In addition two cases were run with baseline parameters where the inlet location was placed at a distance of one and two jet diameters from the wall to study the impact of inlet location.

Figure 4.1 shows the Coefficient of Variation (COV) for fill-and-hold cycle for all the positively buoyant cases. We demonstrated in the isothermal flow section that the hold cycle (inlet jet is shutoff) experiences a significant amount of mixing provided there is sufficient residual kinetic energy left in the tank at the end of the fill process. From the plot, it can be observed that all the cases with positive buoyancy are well mixed at the end of the Fill and Hold cycle. As before. the tank is considered to be *mixed* when the COV value falls below a specific value, usually taken as 0.05 or 0.10. In the present work, the tank was considered to be mixed when the COV value fell below 0.10 since the entire domain data was used for the calculation of COV.

Some interesting observations can be made from the COV plot. The COV value for the case with ΔT equal to 10°C is below 0.10 for the majority of the fill cycle, but peaks to

above 0.10 towards the end of the fill cycle. This is because the jet deviates from it neutral position because of the large buoyant force that causes the jet to hit the tank bottom. Due to this, the jet momentum aiding mixing is reduced and causes the COV value to increase. However, during the hold cycle, the COV drops exponentially to zero that indicating a high degree of mixing. A similar behavior is also observed for the case with an aspect ratio of 2.4 and ΔT equal to 2°C which is also well mixed at the end of the hold cycle. The tank with ΔT equal to 2°C at baseline momentum is not mixed towards the end of the fill cycle, but has sufficient residual kinetic to become mixed in the hold cycle. The COV value drops by a maximum to a value of 0.0046 for the case with jet Froude number Fr_j of 0.47 (ΔT = 10°C) that indicates that buoyancy dominated flows are better sources of mixing in case of positively buoyant flows. In comparison, if we consider the case with higher momentum (4M), the COV value at the end of the hold cyce is 0.046. Although the tank is *well mixed*, the COV drop is not exponential nor as rapid in the hold cycle as in the case with higher Froude number.

Coanda attachment of the jet to the boundary occurs when the jet discharges parallel or near parallel to a wall. The jet attaches to the boundary due to the low pressure effects caused by its own entrainment demand [Jirka and Doneker, 1991]. This phenomenon reduces the jet's capacity to entrain ambient fluid and mix it with new inflow coming through the jet [Grayman et al., 2000].

Jirka and Doneker [1991] proposed a criterion to avoid Coanda attachment to the boundary. The criterion is given by

$$\left(\frac{h}{l_m}\right) > 0.2 \tag{4.18}$$

where h is the perpendicular distance between the jet and the wall parallel to it and l_m is length scale for a plane jet given by (4.16).

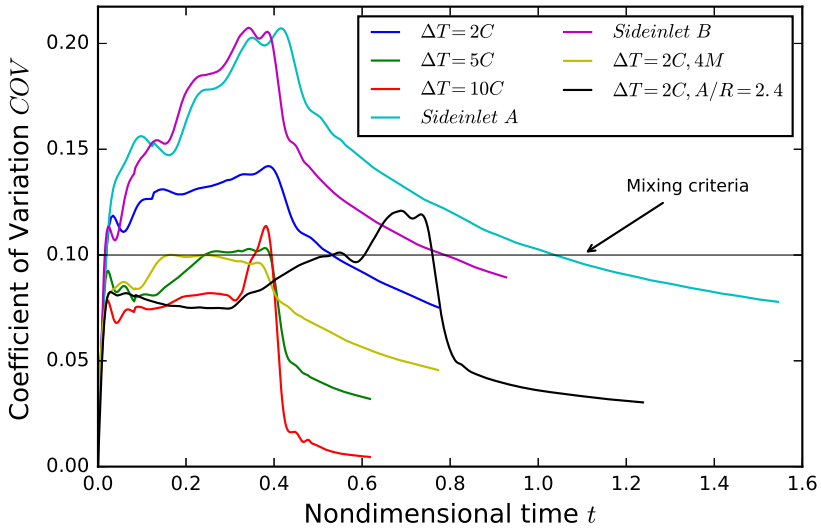

Figure 4.1. COV- Fill+ Hold cycle overlay for all positively buoyant cases. Note that, all the curves correspond to an aspect ratio of 1.25 and baseline momentum M at different ΔT except those noted on the legend. Sideinlet A refers to the case when the inlet location was kept at a distance of one jet diameter from the right wall. Sideinlet B refers to the case when the inlet location was kept at a distance of two jet diameters from the right wall.

Two simulations, one satisfying the criterion to avoid attachment and the second one not satisfying the criterion to avoid attachment were computed to study the impact of jet inlet location on mixing. Let the case not satisfying the criterion be represented by *Sideinlet A* and the case satisfying the criterion be represented by *Sideinlet B* for simplification purposes. Grayman et al. [2000] observes that thermal buoyancy effects will tend to impede mixing in the tank and suggests that thermal effects could be minimized by putting the inlet near an outer wall. *Sideinlet A* is analyzed to check the validity of this observation for rectangular water storage tanks. It was observed in the results that Coanda attachment of the jet to the boundary occurs for both the cases. From the COV plot shown in Figure 4.1, we observe that in both cases, *Sideinlet A* and *Sideinlet B* are not mixed at

the end of the fill cycle. However, both the tanks are mixed in the hold cycle although the time required for the COV to drop below 0.10 is longer for $Sideinlet\ A$ than for $Sideinlet\ B$. Compared to other cases with inlet at the tank centre, the COV values are significantly higher due to the loss of inlet momentum as the jet hits the wall and is directed towards the free surface by the wall. No reduction in thermal buoyancy effects were observed for flows with positive buoyancy when the inlet was placed near the wall which suggests that the observation by Grayman et al. [2000] is applicable only for specific cases. Tian and Roberts [2008b] recommend that positively buoyant inflows are best mixed by horizontal inlets at the bottom based on the results from experiments conducted on ground level cylindrical tanks. No mixing were observed for tests with single nozzles and only tests with multiple nozzles got mixed. In the present work, good mixing was observed for all the tanks with positively buoyant inflows with vertical inlets placed at the centre. This indicates that there is no common criteria for good mixing that could be applied for all types of tanks with different operating conditions to achieve good mixing.

Observing Figures 4.2 and 4.3, it is clear that the jet attaches to the wall irrespective of whether the criteria to avoid *coanda* attachment is satisfied or not. Since the wall serves as an impediment, the inlet jet momentum is not sufficient to cause entrainment layers to spread along the entire tank. We observe regions of relatively high concentration near the tank bottom at the end of the fill cycle for both the cases.

4.2.2. Negatively Buoyant Simulations. Table 4.3 shows the list of cases run with negatively buoyant conditions. With negative buoyant inflows, the inlet jet temperature is colder than the bulk tank water temperature and hence the inflow is denser than the tank water. This causes the inflow to rise to a terminal rise height depending on the inlet momentum before sinking towards the bottom and creating gravity currents that propagates along the width of the tank till it hits the wall. The terminal rise height is proportional to the

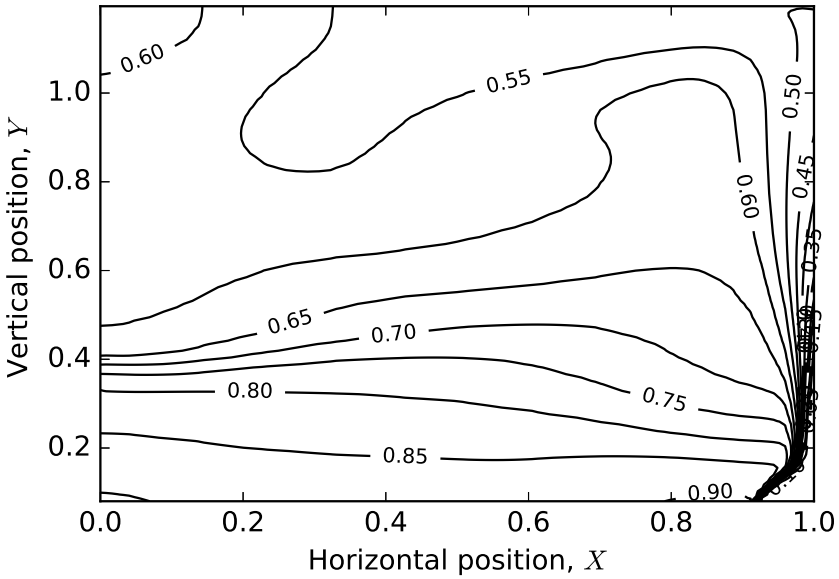

Figure 4.2. Tracer contourline plot for *Sideinlet A* where the inlet jet is at a distance of one jet diameter from the wall

velocity of the inflow and the strength of the buoyant forces. More number of simulations were performed for negatively buoyant conditions as it was thought to occur more often in reality.

The parameters corresponding to $1/d_j = 25$ and aspect ratio of 2.4 at temperature differences of 2°C, 5°C and 10°C respectively are considered to be the baseline cases. Similar to positively buoyant simulations, the temperature difference term ΔT is accounted for in the jet Froude number. From the table, we can observe that at each value of $1/d_j$ at a specific aspect ratio, the Froude number reduces. This signifies that with an increase in temperature difference between the inlet and the tank, the buoyant forces become more dominant than the inertial forces and is reflected with Froude number being less than one. The effect of lower Froude numbers at higher momentum on mixing is also investigated.

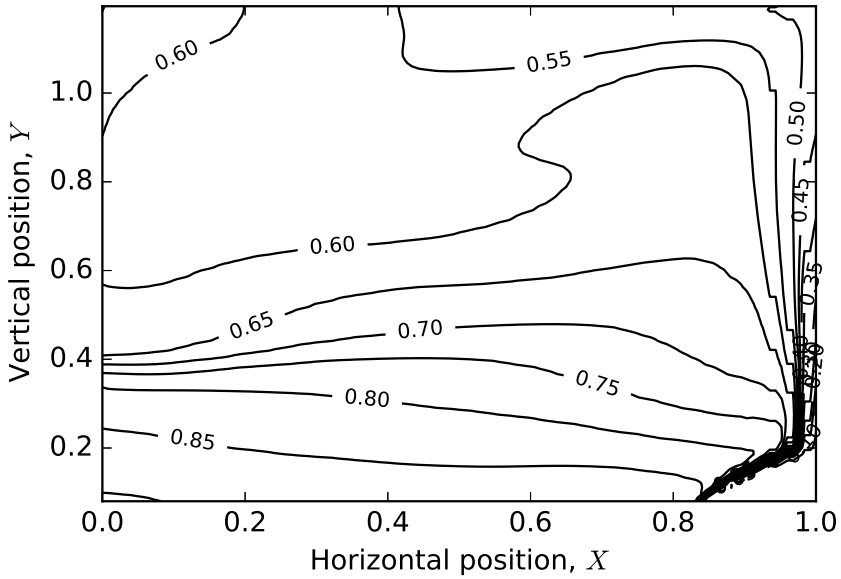

Figure 4.3. Tracer contourline plot for *Sideinlet B* where the inlet jet is at a distance of two jet diameter from the wall satisfying the criteria to avoid attachment

The cases corresponding to $1/d_j = 25$ and aspect ratio of 2.4 will be henceforth be referred to as Set A while the cases corresponding to aspect ratio of 1.25 will be referred to as Set B. Higher momentum cases ($1/d_j = 100$) and ($1/d_j = 200$) will be referred to as Set C and Set D data respectively.

Observing the filling process for negatively buoyant inflows, we can identify some common characteristics of flow behavior

1. The initial phase in which the incoming cold water with a higher density rises to a terminal rise height before it is overcome by gravity effects and falls to the tank bottom forming gravity currents that propagates along the width of the tank.

2. The second phase in which internal waves are setup by the gravity current as it turns after hitting the wall.

3. The final phase in which the internal waves setup form a gradient layer analogous to a thermocline which just gets displaced upwards by the incoming jet of water with the progression of the filling cycle. In the gradient layer, the temperature decreases rapidly from the mixed region temperature to the warm temperature of the bulk fluid in the tank. The shape and formation of the gradient layer is highly dependent on the momentum of the jet inflow and strength of the inflow buoyancy.

4.2.3. Impact of Temperature on Baseline Cases. In this section, Set A data will be analyzed for mixing. All the cases in Set A have a baseline momentum M corresponding to a baseline jet velocity of 0.236 m/s.

In the present work, Coefficient of Variation has been used to quantify mixing. The tank is considered to be mixed when the COV drops below 0.10. Figure 4.4 shows the Coefficient of variation plot for Set A data. As observed from the plot, there is almost a linear increase in COV with the progression of the fill cycle. From this we can clearly infer that none of the tanks in Set A are mixed at the end of the fill cycle by observing the high COV values. This clearly points to stratification in the tank that will be investigated with the help of temperature and tracer studies in this section. It is important to note from Figure 4.4 that there is hardly any variation in the COV values between the three cases. This would seem to suggest that buoyancy dominated inflows ($Fr_j < 1$) have no significant impact on mixing as indicated by the COV values. These cases show a somewhat similar behavior to the isothermal case corresponding to $1/d_j = 25$ with an aspect ratio of 5.0. In all of these cases, the region above the gradient layer that is not penetrated by the jet because of negative buoyancy remains unmixed throughout the fill duration.

In all of these cases, a gradient layer is formed above the terminal rise height of the jet. As mentioned in the introduction, the internal waves that are setup by the gravity current creates a gradient layer of some thickness. This gradient layer is characterized by

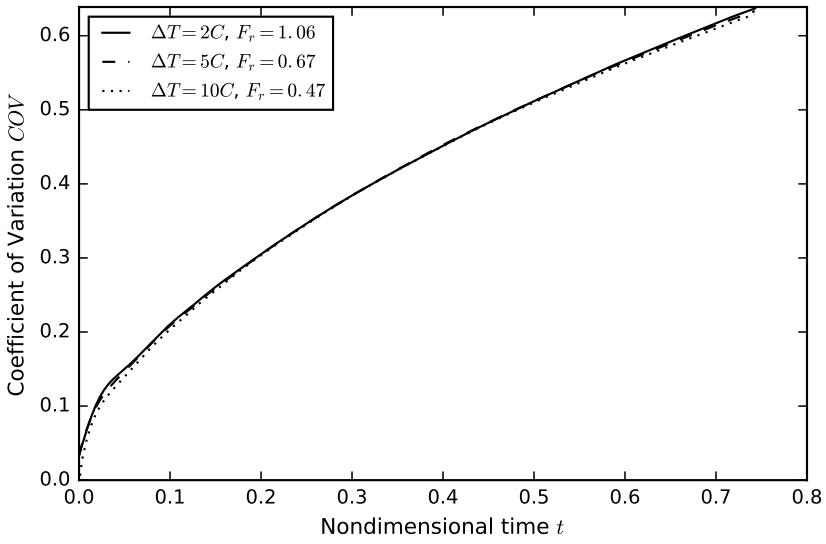

Figure 4.4. Coefficient of Variation (COV)- Fill cycle for baseline negatively buoyant cases; $1/d_j = 25$, $AspectRatio = 2.4$ at different Froude numbers.

three regions and bounded by two limits. The middle region is region that contains a tracer concentration of 0.5 which signifies uniform distribution of tracer and water. The top region has a higher concentration of tracer because of its proximity to the bulk tank fluid which has a tracer concentration of one. The bottom region has a lower concentration of tracer because of the fresh water jet inflow which has no tracer. This gradient layer keeps on getting bigger with the progression of the fill cycle and is therefore at its maximum thickness at the end of the fill cycle.

Figure 4.5 shows the tracer contour plot at t = 0.41 which is almost half the fill duration for the case with $Fr_j = 1.06$ at $\Delta T = 2°$C. We can clearly observe the formation of the gradient layer above the terminal rise height. Once the gradient layer is past the maximum rise height of the jet, the jet behaves like an isothermal inflow jet and the region below the gradient layer is very well mixed. In this region, we can infer that the gravity

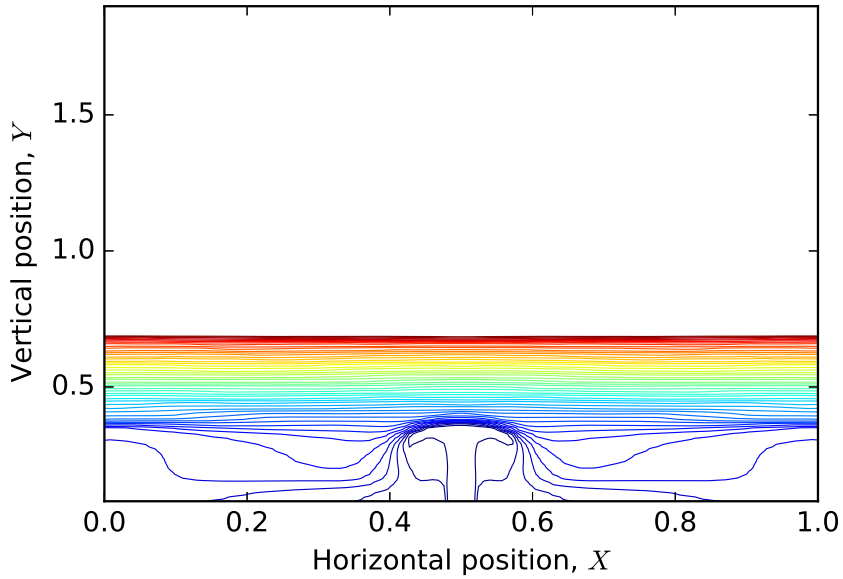

Figure 4.5. Tracer contour line plot for case with Froude number $Fr_j = 1.06$ at t = 0.41, half duration of the filling cycle
.

stabilizing effects are minimal. Higher aspect ratio tanks in this set are tall enough for the gradient layer to form completely, as evidenced by a distinct region in the tank above the jet. Thus, for a given density difference, there must be a threshold on how strong the inflow momentum should be to overcome the gradient layer and cause mixing in the region above the gradient layer. For this case however, the momentum is insufficient to overcome the gravity effects of the gradient layer which seperates the tank into three distinct regions. The formation of a distinct gradient layer is dependend on the momentum and buoyant effects.

1. The region above the gradient layer is a deadzone of high tracer concentration (old water) where jet induced mixing is non existent because of the dead zone.

2. Gradient layer which is a mixed layer region.

3. The region below the gradient layer where the jet behavior can be considered isothermal and hence rapid mixing is observed.

Thus, we have seen that even for the case with Froude number $Fr_j = 1.06$ and $\Delta T = 2°C$, the flow is gravity dominated with buoyancy strong enough to form a gradient layer that cannot be penetrated because of the low jet momentum. With lower Froude number and higher $\Delta T(5°C,\ 10°C)$, the flow will certainly be gravity dominated with higher buoyancy forces and gravity will form a gradient layer. Hence we observe the same COV trend for the other two cases at higher temperature differences. As expected, the same behavior is also seen in CFD simulation results for cases with lower Froude number Fr_j and higher temperature difference.

The terminal rise height calculations shown in Table 4.2 was calculated just before the gravity current hit the wall to compare with the analytical solution. In the simulation results, some movement of the jet above the terminal rise height was observed. This is due to the effect of the internal waves and the jet momentum that drives the jet above the terminal rise height.

Figure 4.6 shows the contour plot of tracer at the end of the fill duration for all the cases in Set A. The presence of the gradient layer can be clearly observed. The region above the gradient layer is a dead zone that remains unmixed. The jet rises to the maximum height for the case with $\Delta T = 2°C$ and $Fr_j = 1.06$ compared to the other cases since the Froude numbers shows that the inertial effects are slightly more dominant than the buoyant cases. However, the inertial effects are not strong enough to overcome the gravity stabilizing effect of the gradient layer as observed from the plot.

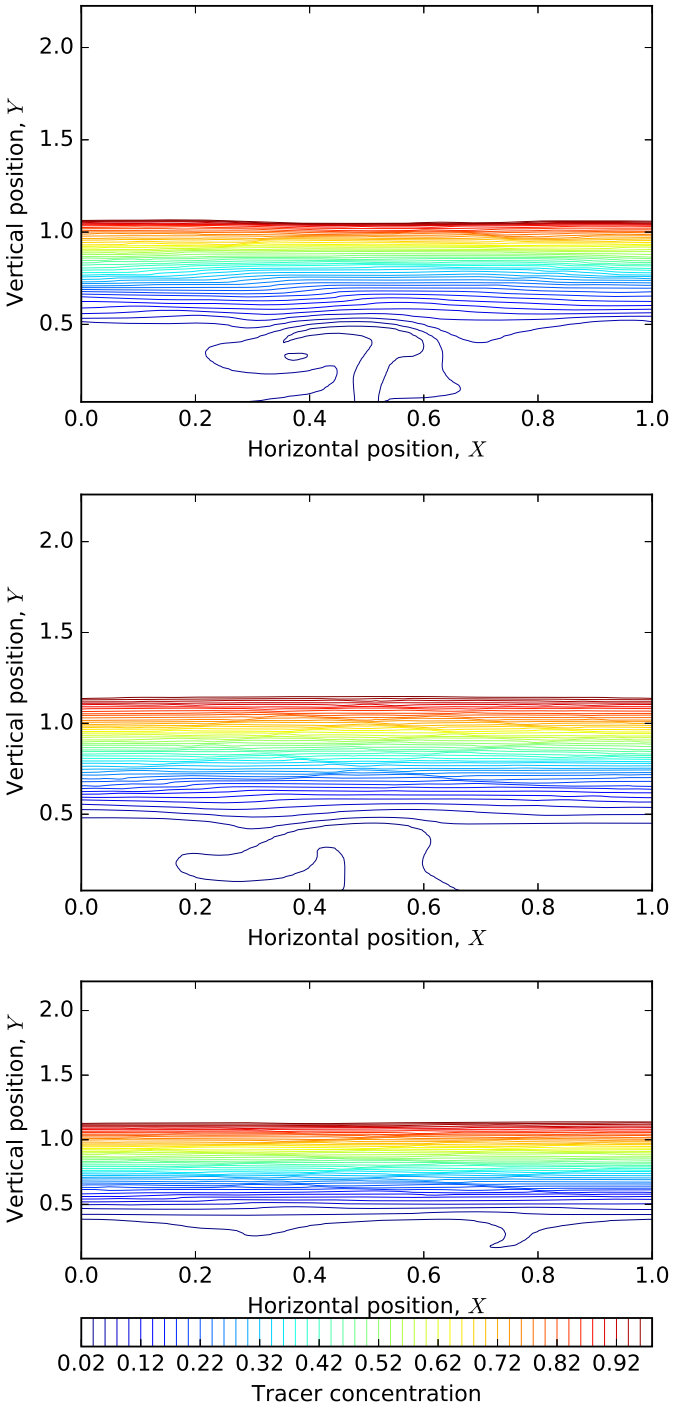

Figure 4.6. Tracer contour plot - Fill cycle end for Set A $1/d_j = 25$ at different Froude numbers and aspect ratio (a) $Fr_j = 1.06$ and aspect ratio of 2.40 (b) $Fr_j = 0.67$. (c) $Fr_j = 0.47$

Similar to isothermal flows, horizontal and vertical monitors were created at equal spacing along the tank height and width respectively for capturing dependent variable data like temperature and tracer at every time step during the simulation. This data can give key information on mixing and scope for stratification. The variation of temperature along vertical monitors is used for calculation of thickness of the gradient layer and can be used the quantify the length of the dead zone.

Figure 4.7 shows the variation of temperature along different vertical monitors defined along the tank width for Set A at fill cycle end. The thickness of the gradient layer was taken to be the difference between the free surface height at which the non-dimensional temperature is 0.95 and the height at which the non-dimensional temperature is 0.05. Some important observations can be made from the graph. In each of the plots, we see that the variation of the temperature along different monitors is almost the same *i.e.* no quantifiable difference of temperature is observed among the monitors. From this we can concur that the gradient layer is a distinct region in the tank that is preserved during the course of the fill process. Observing the free surface height at which the upper limit of the gradient layer occurs, we can conclude that the gradient layer is formed near the bottom half of the tank.

The final water surface height at the end of the fill cycle is $H_f = 2.48$. It may be recalled from Eqn.(4.18) that the scaled relative temperature will be equal to zero when the local temperature is equal to the initial bulk fluid temperature. Analyzing the three cases, the free surface height at which the non-dimensional temperature becomes zero is calculated to be 1.069, 1.155 and 1.155 corresponding to Froude numbers of 1.07, 0.67 and 0.47 respectively. It may be recalled that the difference between the final water surface height and each of these values will give the length of the deadzone for that particular case. The values are calculated to be 1.41, 1.33, and 1.33 respectively. In terms of percentage, we can infer that more than **50 %** volume of the tank becomes stratified at fill cycle end.

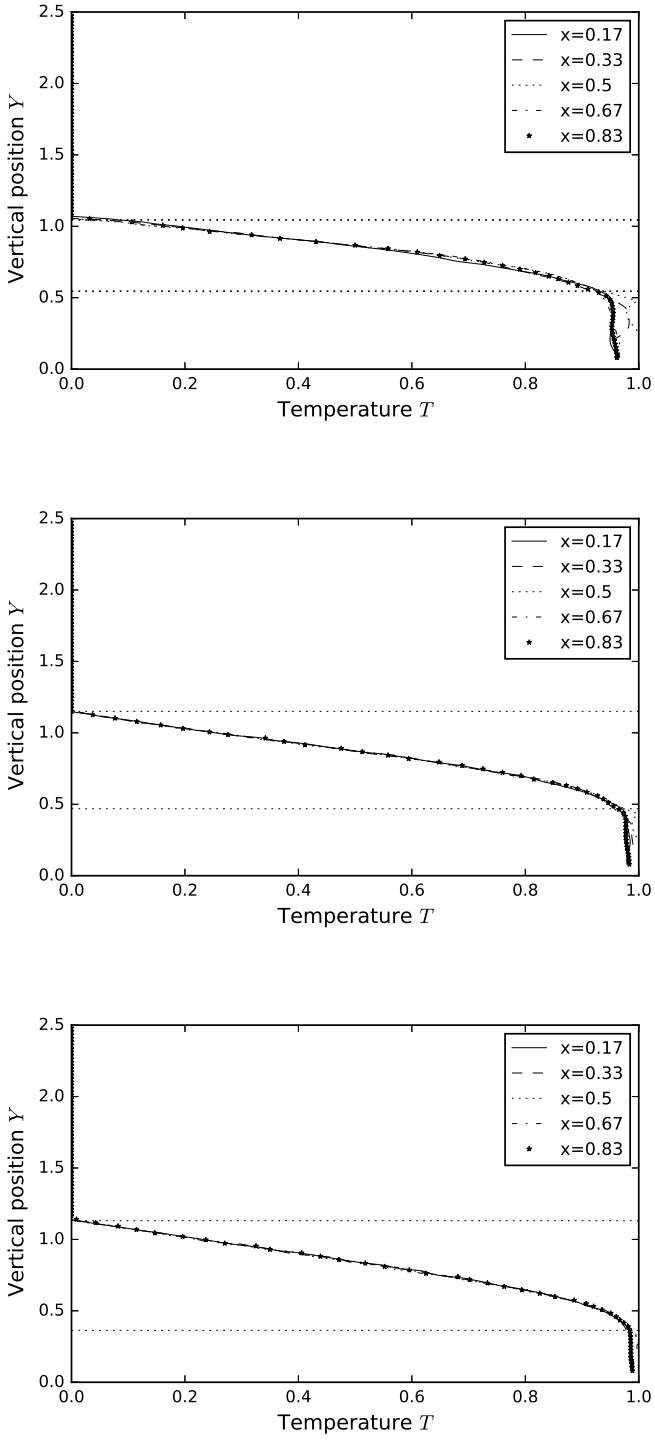

Figure 4.7. Temperature variation along vertical monitors - Fill cycle end for Set A, $1/d_j = 25$ (a) $Fr_j = 1.06$ and aspect ratio of 2.40 (b) $Fr_j = 0.67$ and aspect ratio of 2.40 (c) $Fr_j = 0.47$ and aspect ratio of 2.40. The distance between the two horizontal dotted line represent the thickness of the gradient layer.

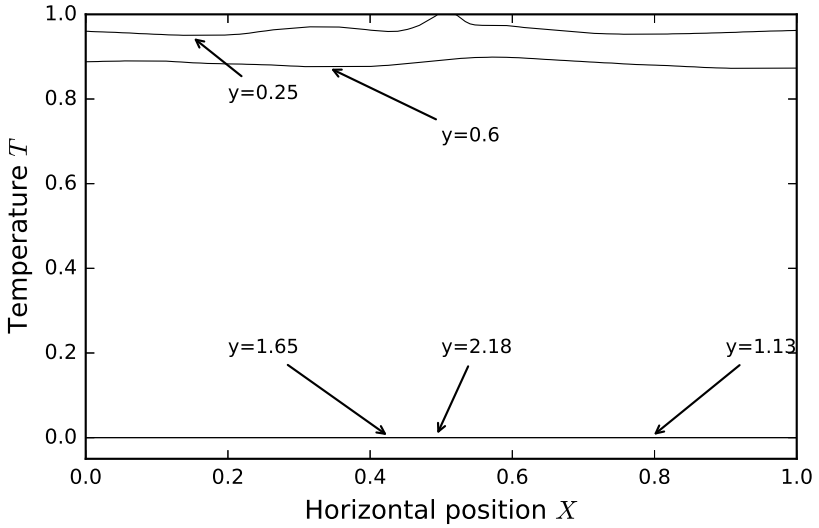

Figure 4.8. Temperature variation along 5 horizontal monitors for the case with Froude number $Fr_j = 1.07$ at the end of fill cycle.

The final step in understanding the level of mixing is consideration of temperature profiles. Many authors have reported that a temperature difference of 1°C can lead to stratification. Spatial and temporal variations in temperature can exist due to changes in inflow temperature, heat transfer from the walls and inflow-buoyancy. The variation of temperature along horizontal monitors for the case with $Fr_j = 1.07$ is shown in Figure 4.8. If the tank is $well - mixed$, we expect the convergence of temperature along all the horizontal monitors. From the plot, it is very clear that there is significant stratification in the tank. We observe no variation along monitors $y = 1.13,\ 1.65\ and\ 2.18$ with non dimensional temperature equal to zero along these monitors. This value means that the local temperature along these monitors is equal to the bulk tank fluid temperature. So the relative temperature according to the non-dimensionalization equation becomes equal to zero. This result underscores the observations in the gradient layer plots previously.

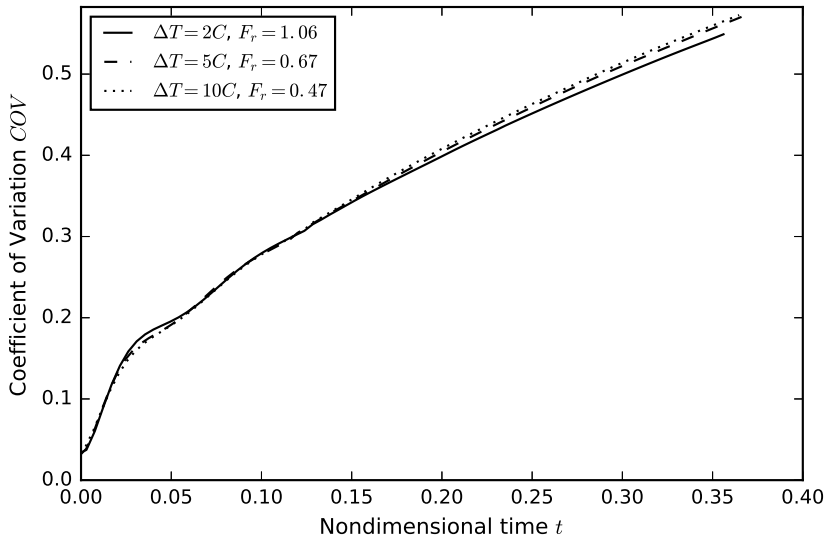

Figure 4.9. Coefficient of Variation (COV)- Fill cycle for baseline negatively buoyant cases; $1/d_j = 25$, $AspectRatio = 1.25$ at different Froude numbers.

Turning to Set B data, all tanks studied have an aspect ratio of 1.25. The significance is to identify the impact of small aspect ratio tanks on mixing for negatively buoyant inflows. The differences between the data in Set A and Set B are the aspect ratio and the initial water surface level. Since the tanks have an aspect ratio of 1.25, the initial water surface level is much lower than for 2.40 aspect ratio tanks. Figure 4.9 shows the Coefficient of variation plot for Set B data. Until half of the fill duration, we see the COV values are the same for all the three cases. Beyond the half fill duration, we see that COV curve corresponding to $Fr_j = 1.06$ slightly deviates from the other two curves with the progression of the fill cycle.

We know that some amount of fill time and therefore height is required for the gradient layer to take form and create a distinct region as observed in aspect ratio 2.4 tanks. For higher aspect ratio tanks once the gradient layer is formed, it does not have an impact on the development of the inflow jet since the tank is sufficiently tall. The maximum height

that the jet could penetrate is maximum for the case with $Fr_j = 1.07$ since the buoyancy force is the weakest for this case.

For the lower aspect ratio tanks, the gradient layer impacts the development of the jet especially for cases with Froude number greater than one. This behavior was observed in the CFD results where the bottom boundary of the gradient layer is close to the maximum rise height and hence it impacts the development of the jet. For lower Froude number cases, the inflow is gravity dominated and hence the stabilizing effect of gravity overcomes the jet momentum and causes the jet to fall back to the tank bottom. The gradient layer region is above the maximum rise height of the jet and hence does not impact the development of the jet. This can be qualitatively observed in the tracer contour plot at the end of the fill cycle for Set B data as shown in Figure 4.10. From the plot we can observe that the jet rise is maximum for case with Froude number of 1.06 and we can also clearly see that the bottom layer of the gradient layer region is very close to the jet and is not completely horizontal.

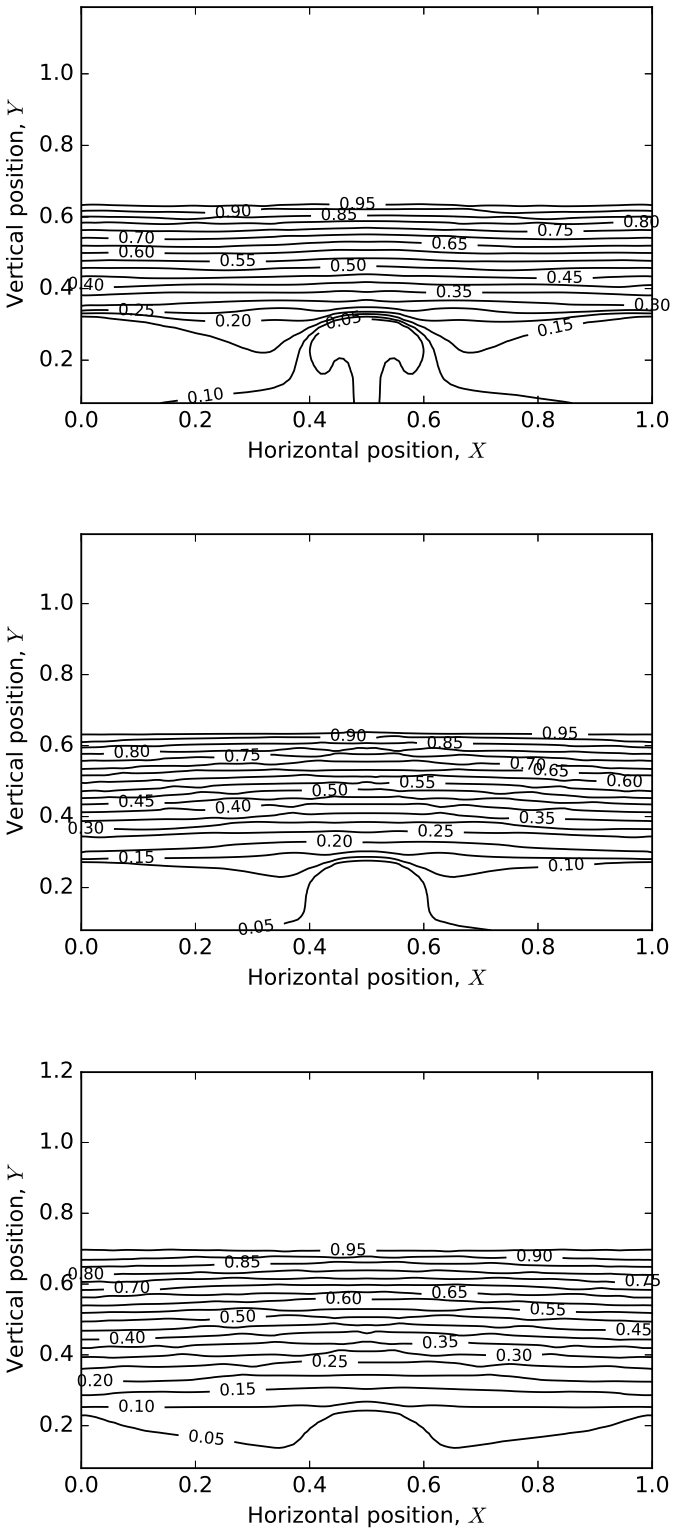

Figure 4.10. Tracer contour plot - Fill cycle end for Set B, $1/d_j = 100$ (a)$F_{rj} = 1.06$ and aspect ratio of 1.25 (b) $Fr_j = 0.67$. (c) $Fr_j = 0.47$.

As observed in the results for higher aspect ratio tanks, the inflow jet momentum is not sufficient to overcome the gradient layer and hence a deadzone is formed above the gradient that remains unmixed throughout the fill duration and hold cycle duration.

4.2.4. Higher Momentum Impact. The previous section identified the impact of baseline momentum and aspect ratio on mixing for negatively buoyant inflows. We observed that momentum was insufficient to overcome the gradient layer which leads to stratification in the tank. All of simulated conditions mixed poorly as a result of the stratification. In this section, we analyze the impact of increased jet momentum on mixing at different densities and also investigate if any threshold exists on how strong the inflow momentum should be to overcome the stabilizing gravity effect exerted by the gradient layer and cause optimum mixing in the tank. In this section, Set C and Set D data is analyzed. It may be recalled that Set C data refers to cases with $1/d_j = 100$ corresponding to four times the baseline momentum and Set D data refers to cases with $1/d_j = 200$ corresponding to eight times the baseline momentum. Here we have increased the jet velocity $\hat{u}_j$ from its baseline value of 0.236 m/s to 0.944 m/s and 1.888 m/s respectively.

Table 4.3 shows the Froude number, initial free surface height, final free surface height etc. associated with Set C and Set D. By looking at the Froude numbers, we can say that all the cases in this section are inertia dominated flows with $Fr_j > 1$. The goal is to study at what momentum and buoyancy, the jet can overcome the gradient layer and cause mixing. It is important to note that, the flows may or may not be gravity dominated by looking at the Froude numbers, but gravity is still a significant factor that impacts the mixing as observed in the results.

Figure 4.11 shows the COV plot for the fill-and-hold cycle for all the cases in Set C. A horizontal line corresponding to COV value of 0.10 is drawn to represent mixing criteria. In the plot, we see a markedly different behavior than those seen with baseline momentum

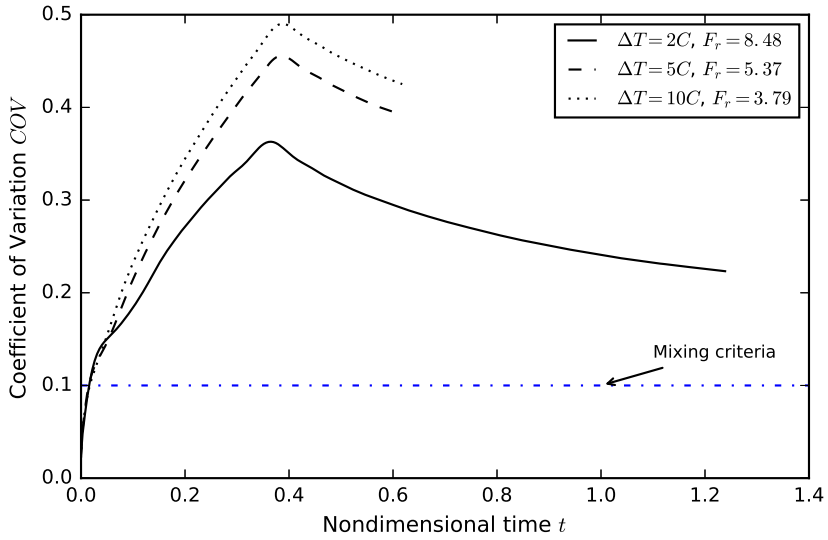

Figure 4.11. Coefficient of Variation (COV)- Fill+Hold cycle for negatively buoyant cases; $1/d_j = 100$, $AspectRatio = 1.25$ at different Froude numbers.

cases. We see a greater degree of separation between the COV plots for $\Delta T = 2°$C and $\Delta T = 5°$C than we see for $\Delta T = 5°$C and $\Delta T = 10°$C respectively. This would indicate that for the case with $Fr_j = 8.48$ and $\Delta T = 2°$C, there is enough momentum of the jet to disperse the gradient layer and cause mixing to a larger degree than for those cases with lower Froude numbers and higher temperature differences. Hold cycle was also run to determine if the residual momentum of the jet is sufficient to cause good mixing. From the plot, we can clearly observe that the COV value does not drop below 0.10 for the case with $Fr_j = 8.48$ and $\Delta T = 2°$C to consider the tank to be mixed. This points to formation of a small dead zone region in the tank that is unmixed. For lower froude number cases, as expected the Coefficient of Variation (COV) values are much higher since the buoyant forces are stronger. The highest degree of mixing is observed for the case with the highest Froude number.

It is to be noted however that compared to Set A and Set B data, the gradient layer is bigger and more dispersed because of the increased momentum, i.e. a well defined gradient layer that was observed in Set A and Set B results is not observed in Set C and Set D results.

As we have seen, the variation of non dimensional temperature along the vertical monitors can give insight into the thickness of the gradient layer, formation of deadzones etc. Figure 4.12 shows the temperature variation along vertical monitors for Set C data. Some important observations can be made from the plot. We can observe rapid variation of temperature along different vertical monitors till almost half of the free surface height for the case with $Fr_j = 8.48$ and $\Delta T = 2°C$. This indicates that the momentum of the jet is sufficient high to cause dispersion of the gradient layer along the bottom region but not sufficiently enough to completely disperse the gradient layer. This could be termed a momentum-affected gradient layer formation in which gravity is not dominant, but a significant factor.

For the case with $Fr_j = 5.37$ and $\Delta T = 5°C$, the gravity force is strong enough to form a reasonably defined gradient layer that forms a dead zone above the gradient layer, as observed in the previous section. This is the reason why we observe only minimal deviation of temperature between different vertical monitors. If gravity is already dominant at 5°C, then increasing the temperature further ($\Delta T = 10°C$) would ensure even greater dominance as the gradient layer forms. The gradient layer is more well defined because of the increased buoyancy, however, as a result of the increased dominance, the gradient layer formed for these two higher temperature differences may be termed as, gravity-dominanted gradient layer.

Figure 4.13 shows the tracer contours for case with $\Delta T = 2°C$ at the end of fill cycle. We can observe qualitively the shape of the gradient layer formation above the jet. In the analysis of the transient results, it was found that because of the high momentum and

corresponding effect of gravity, the jet position was swayed left and right by the internal waves setup by the gravity current.

Based on the results of Set A, Set B and Set C data, we observe some separation between the COV plots at higher temperature difference as the inflow momentum was increased. Based on this, we could hypothesize that "with increase in momentum, the temperature difference at which separation is observed increases". Based on this hypothesis, we would expect to see a larger separation between the COV curves at temperature differences of $\Delta T = 2°C$ and $\Delta T = 10°C$ for Set D data because momentum is eight times the baseline momentum.

Figure 4.14 shows the COV plot for the fill-and-hold cycle for all the cases in Set D. From the plot, we can see that the COV value drops to 0.1 for the case corresponding to $Fr_j = 24$ and $\Delta T = 2°C$ drops satisfying the mixing criterion. This is the only case in the negatively buoyant cases considered that is mixed during the hold cycle. So a settling time is necessary at the end of the fill cycle to let the residual energy of the jet cause the tank to get mixed.

As hypothesized, we see a larger separation in the COV plots corresponding to temperature differences of 2°C and 5°C because of increased momentum. For the case reaches a mixed state, the flow is inertia dominated as indicated by the high Froude number. The inflow jet momentum is sufficient to overcome the effects of gravity and this results in a very thin gradient layer being formed whose position is highly transient and is strongly dependent on dynamic behavior of the jet whose position swayed depending on the movement of the internal waves. This was observed in the analysis of Set D data. Observing Figure 4.15, we can identify the complexity of the internal waves created by the jet induced gravity current. The internal waves are a significant source of mixing for higher momentum and lower buoyancy cases. From this plot, we can also observe that there is no formation of

three unique regions in the tank as we have observed in the previous section. Also there is no uniquely identifiable deadzone in the tank as the jet velocity aided by the internal waves is sufficient to create circulation zones that spread through the entire tank.

Two cases with the inlet jet placed at one and two jet diameters from the wall respectively were run to investigate if thermal buoyancy effects are reduced as suggested by Grayman et al. [2000]. Both cases were run at baseline momentum. No quantifiable difference was observed in the COV values when compared with the case with inlet at the center.

COV values are plotted in Figure 4.16 for all the negatively buoyant cases with an aspect ratio of 1.25. We can observe qualitatively compare the level of mixing for cases with different momentum.

In Section One, we had modified the mixing time correlation of Okita and Oyama [1963] to make it applicable to our work. The modified expression is given in (3.49). From the results of negatively buoyant cases, we have observed that buoyancy has a major effect on formation of stratified regions in tanks. From (3.49), we can also observe that the mixing time correlation does not have any buoyancy dependecy term to account for temperature differences between inlet and outlet. Since buoyancy is a significant factor to achieve mixing in non-isothermal flows, we can infer that the existing mixing time correlation is unsuitable for non-isothermal flows. No attempt has been made in this work to modify the mixing time correlation to include a buoyancy term.

4.2.5. Conclusion. To summarize, positively buoyant conditions were found to be desirable to achieve good mixing in the tank. A number of cases were run to study the dependence of different control variables on mixing. All the tanks with postively buoyant inflow were mixed at the end of simulation. It was also found that buoyancy dominated flows are better sources of mixing than inertia dominated flows *i.e.* higher the temperature

difference between the inlet and the tank, stronger is the buoyant force that results in stronger circulation patterns that mix the tank more efficiently. Placing inlets near the side wall caused the attachment of the jet to the side and resulted in formation of deadzone during the filling procees. It is to be pointed out that a settling time at the end of the fill cycle is necessary to achieve the highest possible degree of mixing for a tank at a given condition. Placing inlets at the tank center resulted in good mixing even for tanks with lower momentum and higher aspect ratio.

To summarize, negatively buoyant inflow conditions were found to be undesirable to achieve good mixing in the tanks. Of all the simulations conducted with negatively buoyant flows, only one case satisfied the COV mixing criterion. The Higher the density difference between inflow fluid and bulk tank fluid, stronger the negative buoyancy and the higher the probability of stratified regions being left in the tanks. At lower jet momentum, very poor mixing was observed with the formation of a gradient layer that caused rapid mixing only below the gradient layer. Mixing was observed only when the jet velocity was increased to eight times its baseline value at a baseline temperature difference of two degree Celsius. With increase in temperature difference, even at high inlet jet velocity, the vessel was unmixed. This shows that to there is a strong dependency of buoyancy on mixing. With isothermal flows, jet momentum was found to be the most important factor to achieve mixing whereas with negatively buoyant flows, buoyancy is also a very important factor along with jet momentum.

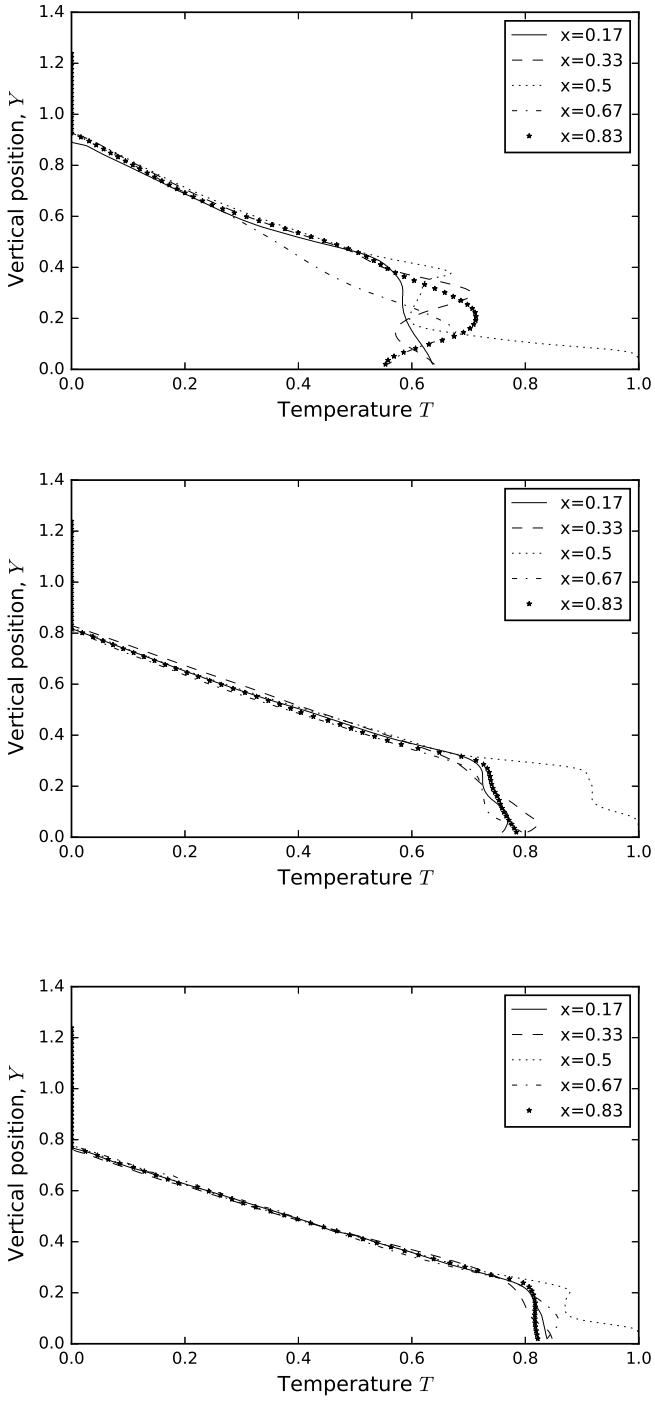

Figure 4.12. Temperature variation along vertical monitors- Fill cycle end for Set B, $1/d_j = 100$. (a)$Fr_j = 8.48$ and aspect ratio of 1.25 (b) $Fr_j = 5.37$ (c) $Fr_j = 3.79$.

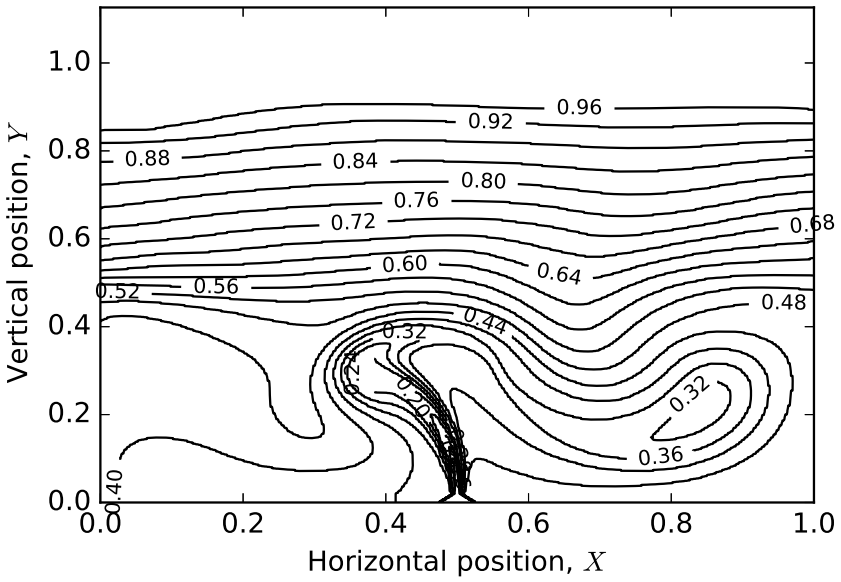

Figure 4.13. Tracer contour plot - Fill cycle end for Set C; Case with $Fr_j = 8.48$ and $\Delta T = 2°\text{C}$ - Negativey Buoyant Flows

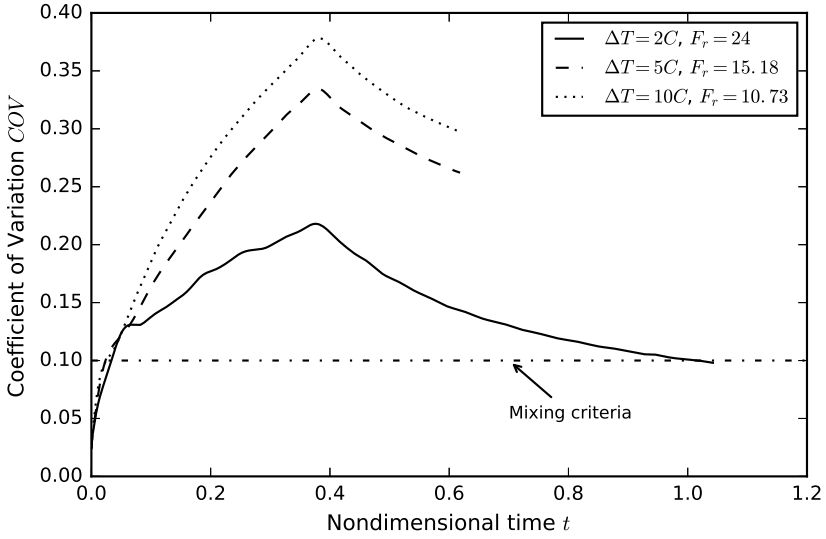

Figure 4.14. Coefficient of Variation (COV)- Fill+Hold cycle for negatively buoyant cases; $1/d_j = 200$, $AspectRatio = 1.25$ at different Froude numbers.

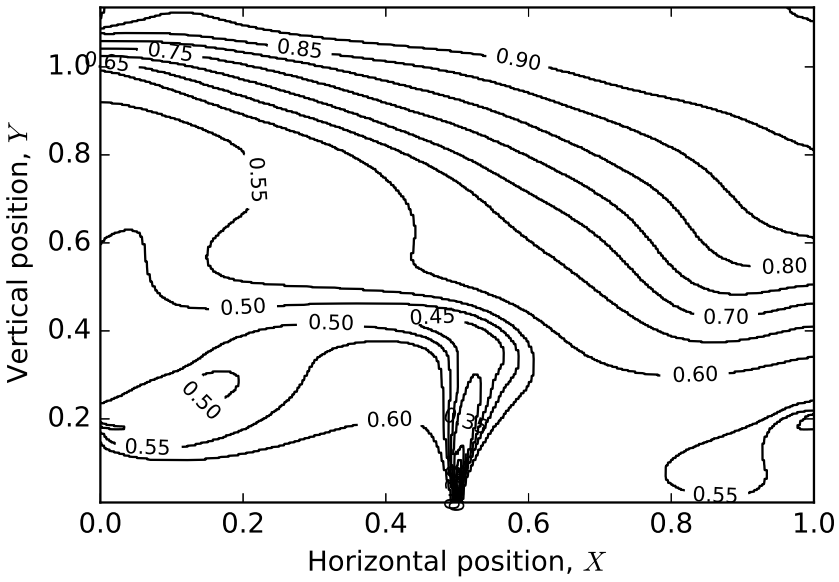

Figure 4.15. Tracer contour plot - Fill cycle end for Set D; Case with $Fr_j = 24$; Case is mixed during hold cycle

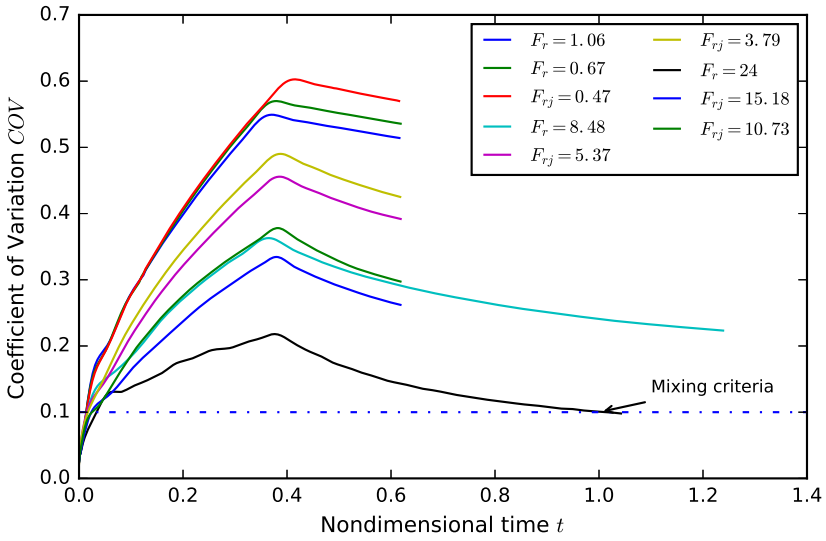

Figure 4.16. COV for negatively buoyant cases with aspect ratio 1.25; at different Froude numbers

5. SUMMARY AND RECOMMENDATIONS

5.1. SUMMARY

This section provides a brief overall summary of the work and recommendations for future work.

In this thesis, CFD simulations of the filling cycle for municipal water storage tanks were conducted to study mixing patterns which impacts water quality. The CFD model was adequate to resolve the complex mixing patterns setup by the inflow turbulent jet that greatly affects mixing in water storage tanks.

Coefficient of Variation was used to quantify the level of mixing. Inlet momentum was found to be the most important parameter to achieve mixing for isothermal flows. With increase in momentum, a very significant improvement was observed in mixing. The degree of stratification is high for vessels with high aspect ratio and low momentum. Of particular significance is the fact that a vessel with aspect ratio 5.0 which was unmixed with baseline inlet momentum got mixed when the inlet jet velocity was increased to four times its baseline value. With sufficient inlet momentum, even vessels of high aspect ratios could be mixed under isothermal condition. Analysis of isothermal cases with variable fill durations showed better mixing even for cases that were unmixed with complete fill duration.

Positively buoyant conditions were found to be desirable to achieve uniform mixing in tanks. All the cases were mixed with positively buoyant inflows. Placing inlet at one and two jet diameter distance from th side wall caused the jet to attach to the boundary and caused a significant increase in COV compared to other positively buoyant cases. However, these cases still mixed in the hold cycle. An interesting observation of positively buoyant

results is that the case with baseline jet momentum and a temperature difference of 10°C showed a higher degree of mixing than the case with four times the baseline jet momentum and a temperature difference of 2C. From this, we can infer that buoyancy is a better source of mixing than inertial effects for positively buoyant cases. However, postively buoyant conditions occur only during a few months in a year and in limited geographic locations.

Negatively buoyant conditions were found to be undesirable to achieve uniform mixing in tanks. Of all the simulations conducted with negatively buoyant inflows, only one case satisfied the usual criteria for mixing in the hold cycle. The probability of stratification occuring with negatively buoyant inflows is higher with taller vessels. With increases in temperature difference, even at high inlet jet velocities, the vessels remained unmixed with the formation of significant deadzones. Existing tanks should be analyzed for water quality issues since negatively buoyant conditions occurence are more common in tank operation. One potential remedy would be use a heat exchanger situated near the inlet to reduce the negative buoyancy effects. Filling process could also be done during the evening/night to reduce the temperature difference.

The hold cycle (inflow shutoff) was found to be a significant source of mixing. Previously it was thought that majority of the mixing takes place only in the fill cycle, but in the present results, it was observed that hold cycle generally improved mixing for all cases as the residual kinetic energy of the tank is dissipated. The degree of mixing during the hold cycle was found to be proportional to the inlet jet velocity in the filling cycle and strength of buoyancy if applicable. In this work, some of the cases (isothermal, positively and negatively buoyant) which did not mix in the fill cycle did achieve conditions in the hold cycle. Hence it is important to have a settling time at the end of each fill cycle to achieve the highest possible degree of mixing for that tank at a given aspect ratio, momentum and buoyancy if applicable.

5.2. RECOMMENDATIONS FOR FUTURE WORK

There were some gaps in CFD modeling of Storage water tanks field that this work could not address. Some of these gaps that could be addressed in the future work are

1. Simulation of multiple Fill-and-Draw cycles. This would give good insight into how typical tank operations affect mixing.

2. Three dimensional CFD simulation of filling cycles. Although this would be computationally expensive, it would be able to predict more accurately the complex flow patterns that impact mixing. Two dimensional simulations are expected to overpredict mixing.

3. CFD simulation with multiple inlet nozzles to study potential for improved mixing. Also simulations with multiple horizontal inlets could reduce thermal buoyancy effects.

4. Inclusion of surface energy transfer effects on the internal mixing dynamics in municipal water storage tanks. In this work, the tank walls are considered to be adiabatic. Energy transfer through walls could be a source of mixing.

5. Additional studies are required to reduce the wide band of values for the constant K' in the modified mixing time correlation. Also further analysis is required to incorporate the buoyancy term in the mixing time correlation in case of non-isothermal flows.

APPENDIX

MIXING TIME CORRELATION

[Rossman and Grayman, 1999] formulated a simplified mixing time correlation after modification of formula proposed by [Okita and Oyama, 1963]. The expression is given by

$$\hat{\tau}_m = K'\left(\frac{V^{2/3}}{M^{1/2}}\right) \tag{6.1}$$

where V is the tank volume, M is the momentum flux, $\hat{\tau}_m$ is the dimensional mixing time and K' is an experimental constant.

Substituting for the terms applicable to this work,

$$\hat{\tau}_m = K'\frac{(HDZ)^{2/3}}{(\dot{V}u_j)^{1/2}} \tag{6.2}$$

Substituting for the volumetric flow rate,

$$\hat{\tau}_m = K'\frac{(HDZ)^{2/3}}{(u_j d_j Z u_j)^{1/2}} \tag{6.3}$$

$$\hat{\tau}_m = K'\frac{(HDZ)^{4/6}}{(u_j d_j Z u_j)^{3/6}} \tag{6.4}$$

$$\hat{\tau}_m = K'\left[\frac{(H^4 D^4 Z^4)}{(u_j^6 d_j^3 Z^3)}\right]^{1/6} \tag{6.5}$$

Examining the quantity in square brackets, we get

$$\left[\frac{(H^4D^4Z^4)}{(u_j^6d_j^3Z^3)}\right]^{1/6} = \left(\frac{H^4D^4}{u_j^6d_j^3}\right)Z \tag{6.6}$$

$$= \left(\frac{H}{D}\right)^4\left(\frac{D^8}{u_j^6d_j^3}\right)Z \tag{6.7}$$

$$= \left(\frac{H}{D}\right)^4\left(\frac{Z}{D}\right)\left(\frac{D^9}{u_j^6d_j^3}\right) \tag{6.8}$$

$$= \left(\frac{H}{D}\right)^4\left(\frac{Z}{D}\right)\left(\frac{D}{d_j}\right)^3\left(\frac{D^6}{u_j^6}\right) \tag{6.9}$$

$$= \left(\frac{H}{D}\right)^4\left(\frac{Z}{D}\right)\left(\frac{d_j}{D}\right)^{-3}\left(\frac{D}{u_j}\right)^6 \tag{6.10}$$

Then using the notation for dimensional terms,

$$\hat{\tau}_m = K'\left[\left(\frac{\hat{Z}}{\hat{D}}\right)\left(\frac{\hat{H}}{\hat{D}}\right)^4\left(\frac{\hat{d}_j}{\hat{D}}\right)^{-3}\left(\frac{\hat{D}}{\hat{u}_j}\right)^6\right]^{1/6} \tag{6.11}$$

Presuming that, $\hat{Z}/\hat{D} \simeq 1$,

$$\hat{\tau}_m = K'\left(\frac{\hat{H}}{\hat{D}}\right)^{2/3}\left(\frac{\hat{d}_j}{\hat{D}}\right)^{-1/2}\left(\frac{\hat{D}}{\hat{u}_j}\right) \tag{6.12}$$

Hence, for a two dimensional domain (Rectangular $\hat{Z}/\hat{D} \simeq 1$)

$$\hat{\tau}_m = K'\left(\frac{\hat{H}}{\hat{D}}\right)^{2/3}\left(\frac{\hat{d}_j}{\hat{D}}\right)^{-1/2}\left(\frac{\hat{D}}{\hat{u}_j}\right) \tag{6.13}$$

$$\hat{\tau}_m = K'\left(\frac{H^{2/3}}{d_j^{1/2}}\right)\cdot\left(\frac{\hat{D}}{\hat{u}_j}\right) \tag{6.14}$$

A key observation from the mixing time correlation,

$$\hat{\tau}_m \propto \frac{\hat{D}}{\hat{u}_j} \tag{6.15}$$

Thus, an inverse relationship exists between the mixing time and the jet velocity. This would imply that by keeping the tank width as constant, by increasing the jet velocity to eight times the baseline value, the mixing time would reduce by a factor of eight.

BIBLIOGRAPHY

ANSYS. *ANSYS Fluent Theory Guides*. ANSYS Inc., 275 Technology Drive, Canonsburg, PA 15317, 15.0 edition, November 2013a.

ANSYS. *ANSYS Fluent User's Guide*. ANSYS, Inc., 275 Technology Drive Canonsburg, PA 15317, 15.0 edition, November 2013b.

AWWA. Finished water storage facilities. Technical report, U.S. Environmental Protection Agency, 2002.

T. Brooke Benjamin. Gravity currents and related phenomena. *J . Fluid Mech*, 31(2): 209–248, 1968.

P F Boulos, W M Grayman, R Bowcock, et al. hydraulic mixing and free chlorine residual in reservoirs. *American Water Works Association*, 1996.

Kaushik Das and Debashis Basu. Software validation test plan and report for ansys-fluent version 12.1. Technical report, U.S. Nuclear Regulatory Commission, November 2010.

J.T Davies. *Turbulence Phenomena: An Introduction to the Eddy Transfer of Momentum, Mass, and Heat, Particularly at Interfaces*. Academic Press, January 1972.

Hugo B. Fisher, E John List, Robert C.Y. KOH, Jorg Imberger, and Norman H. Brooks. *Mixing in Inland and Coastal Waters*. Academic Press, San Diego, CA, 1979.

Walter M Grayman and Robert M Clark. Using computer models to determine the effect of storage on water quality. *American Water Works Association*, 1993.

Walter M Grayman and Rossman. Mixing and aging of water in distribution system storage facilities. *American Water Works Association*, 2004.

Walter M. Grayman, Lewis A. Rossman, Clifford Arnold, Rolf A. Oeininger, Charlotte Smith, James F. Smith, and Rita Schnipke. Water quality modeling of distribution system storage facilities. Research report, American Water Works Association, AWWA Research Foundation 6666 West Quincy Avenue Denver, CO 80235-3098, 2000.

Peter D. Hoffman. Mixing in a large storage tank. *AIChE SYMPOSIUM SERIES*, 1996.

S. Jayanti. Hydrodynamics of jet mixing in vessels. *Chemical Engineering Science*, 2001.

Gerhard H. Jirka and Robert L. Doneker. Hydrodynamic classification of submerged single-port discharges. *J. Hydraul. Eng.,*, 117(9):1095–1112, September 1991.

Mark S Kennedy, Scott Moegling, Simsek Sarikelle, and Khis Suravallop. Assessing the effects of storage tank design on water quality. *American Water Works Association*, 1993.

Mahmood. Evaluation of water mixing characterisctics in distribution system storage tanks. *American Water Works Association*, 2005.

Michael Marek. Cfd modeling of turbulent jet mixing in a water storage tank. In *32nd IAHR Int. Association for Hydraulic Research*. International Association for Hydro-Environment Engineering and Research, July 2007.

K. D. Martel, G. J. Kirmeyer, B. M. Murphy, and P. F. Noran. Preventing water quality deterioration in finished water storage facilities. *American Water Works Association*, 94: 139–148, 2002.

N. Okita and Y. Oyama. Mixing characteristics in jet mixing. *Chemical engineering*, 27 (4):252–260, 1963.

Suhas Patankar. *Numerical Heat Transfer and Fluid Flow*. Hemisphere Publishing Corporation, 1980.

A. W. Patwardhan. Cfd modeling of jet mixed tanks. *Chemical Engineering Science*, 2002.

N. Rajaratnam. *Developments in Water Science*, chapter The Plane Turbulent Free Jet, pages 1–26. Elsevier Scientific Publishing Agency, 1976.

Wolfgang Rodi. Turbulent buoyant jets and plumes. In Wolfgang Rodi, editor, *Turbulent buoyant jets and plumes*, pages 1–68. Pergamon Press, 1st edition, 1982.

L. A. Rossman and W. M. Grayman. Scale-model studies of mixing in drinking water storage tanks. *J Environ Eng*, 125:755–761, 1999.

H. Schlichting. *Boundary-Layer Theory*. Springer, 8th edition, March 2000.

John E. Simpson. Gravity currents in the laboratory, atmosphere, and ocean. *Ann. Rev. Fluid Mech.*, 14:213–234, 1982.

Xiaodong Tian and Philip J. W. Roberts. Mixing in water storage tanks. i: No buoyancy effects. *Journal of Environmental Engineering*, 2008a.

Xiaodong Tian and Philip J. W. Roberts. Mixing in water storage tanks. ii: With buoyancy effects. *Journal of Environmental Engineering*, 2008b.

William W. Liou Tsan-Hsing Shih. A new k-e eddy viscosity model for high reynolds number turbulent flows. *Computers and Fluids*, 24(3):227–238, February 1994.

J.T. Turner. Jets and plumes with negative or reversing buoyancy. *Journal of Fluid Mechanics*, 26(04):779–792, December 1966.

Kailas L. Wasewar and J. Vijay Sarathi. Cfd modelling and simulation of jet mixed tanks. *Engineering Applications of Computational Fluid Mechanics*, 2(2), 2008.

VITA

Pramod Narayan Bangalore was born in Bengaluru (previously Bangalore), Karnataka. He graduated with a Bachelor's degree in Mechanical Engineering from Bangalore Institute of Technology in July 2012.

In Fall 2013, he enrolled for a Master's degree in Mechanical Engineering at Missouri University of Science and Technology, Rolla. At Missouri S&T, he carried out thesis research work under the guidance of Dr. Kelly Homan, on Mixing Dynamics in Municipal Water Storage Tanks. He also served as a department representative for Council of Graduate Students during the duration of his Master's degree. He worked as a Simulation Project Co-Op at MYNAH Technologies, LLC during Spring and Summer, 2015.

In July, 2016, he received his MS degree in Mechanical Engineering from Missouri University of Science and Technology.